Thèse

Pour obtenir le grade de

Docteur de l'Université Louis Pasteur de Strasbourg

Discipline : Chimie

Présentée par :

Evgeniy S. SALNIKOV

CNRS UMR 7177

Laboratoire de RMN et biophysique des membranes

Etudes structurales de peptides antibiotiques de type peptaibol provoquant des modifications membranaires par spectroscopies RPE pulsée et RMN de l'état solide

---

Soutenance prévue le 30-10-2007 devant la commission d'examen :

Prof. Derek MARSH:	**Rapporteur externe**
Prof. Erick DUFOURC:	**Rapporteur interne**
Dr. Martial PIOTTO:	**Rapporteur interne**
Prof. Gerd KOTHE:	**Examinateur**
Dr. Jan RAAP:	**Examinateur**
Prof. Sergey A. DZUBA:	**Directeur de thèse**
Prof. Burkhard BECHINGER:	**Directeur de thèse**

To my parents

Acknowledgements

I gratefully thank my thesis directors, Prof. Sergey Andreevich Dzuba and Prof. Burkhard Bechinger for their endless optimism and wise supervision, which gives me an opportunity to progress as a scientist. I am indebted to Dr. Jan Raap, who introduces me into the wonderful world of membrane-modifying peptides and actually made this thesis project possible. I also sincerely thank "SupraChem" project and his head Alexandre Varnek for the financial support during my stay in Strasbourg.

I would like to extend my appreciation to my committee members: Prof. Derek Marsh, Prof. Gerd Kothe, Prof. Erick Dufourc and Dr. Martial Piotto for their useful comments and warm atmosphere during thesis defense. I'm especially grateful to Prof. Derek Marsh who agreed to revise the manuscript in such a short time period.

I would like to express my gratitude to Dr. Philippe Bertani, who guided me in the field of solid-state NMR of oriented samples and always helped me during my stay in France. I thank Dr. Alexandre Milov for critical discussions of EPR experiments and Denis Erilov, James Mason, Jesus Raya, Roland Graff and Lionel Allouche who also participate in this work. I greatly appreciate the friendship of Svetlana Nedelkina and my interactions with Jesus Raya, Alexandre Milov and Leonid Kulik. I also thank the rest members of both laboratories, the laboratory of NMR of condensed matter (Strasbourg, France) and the laboratory of chemistry and physics of free radicals (Novosibirsk, Russia), where I had luck to work. I would like to especially mention my brazilian friends Jarbas Magalhães Resende and Cléria Mendonça de Moraes for their cheerfulness.

Finally, I am most grateful to my family who was always supporting me. I dedicate my doctoral thesis to my parents.

Contents

Abstract 3

Abbreviations 4

1. Introduction 5

2. Theory

2.1 *Structure and properties of lipid membranes* 13

2.2 *Basic theory of Magnetic Resonance* 19

Relaxation 19

EPR. Conventional Hahn echo pulse sequence 20

NMR. Chemical shift 21

3. Materials and Methods

3.1 *Materials* 22

3.2 *EPR of membrane-modifying peptides*:

Preparation of MLVs samples 24

ESEEM - access to peptide topology 24

CW EPR spectra simulation - access to peptide oligomerization 29

3.3 *Solid-state NMR of oriented samples*

Preparation of oriented membrane samples 33

Control of the orientation of lipid bilayer by ^{31}P NMR-spectroscopy 34

Determination of the orientation of a helix by ^{15}N NMR-spectroscopy 35

Cross-Polarization NMR measurements 39

PISEMA and peptide secondary structure 41

Simulation of NMR experiments 44

3.4. *Solid-state NMR of lipid vesicles*

Preparation of MLV samples 47

^{2}H NMR of Labeled Phospholipids 48

4. Location of Trichogin GA IV in lipid membrane by ESEEM

Introduction 50

Results 52

Discussion 56

5. Alamethicin topology in a phospholipid membrane by Solid State NMR of oriented samples and EPR. Low and cryo temperatures versus room temperature: critical comparative study.

Introduction 59

Results 61

Discussion 77

6. Structure and alignment of the membrane-associated peptaibols ampullosporin A and alamethicin by oriented ^{15}N and ^{31}P solid-state NMR spectroscopy

Introduction 81

Results 82

Discussion 97

7. Lipid membrane disturbance by the presence of alamethicin and ampullosporin A peptides. Perspective.

Introduction 102

Results 103

Discussion 106

8. Summary 108

Appendix. Preparation of ^{15}N uniformly labelled ampullosporin A. 112

Bibliography. 115

Publications and Conference Abstracts 127

Abstract

The structure, dynamics and topology of selected peptaibols when associated with biological membranes were characterized by magnetic resonance methods. Investigations were focused on the three members: trichogin GA IV, ampullosporin A and alamethicin, which are different in length and vary in their intensity of biological activity.

Using ^{15}N uniformly labeled alamethicin and ampullosporin A, solid-state NMR of oriented samples allows to obtain information on the structure, dynamics and topology of peptides in their membrane bound state. Using TOAC (2,2,6,6-tetramethylpiperidine-1-oxyl-4-amino-4-carboxylic acid) labeled analogs of peptides alamethicin and trichogin GA IV, newly developed ESEEM (electron spin echo envelope modulation) approach allows to access peptide topology. In addition, CW (continuous wave) EPR of these TOAC labeled analogs gives information on peptide oligomerization.

Studies suggest some common properties for the peptaibols when bound to membranes, suggesting similar mode of action. Namely: hydrophobic match / mismatch between peptide hydrophobic length and membrane apolar core was shown to play a key role on peptide orientation; a high 3_{10} helical content in both alamethicin and ampullosporin A, when in a transmembrane state, was detected; and to the best of our knowledge, herein is the first time that oligomerization of transmembrane alamethicin molecules was directly observed.

Another important aspect of this thesis work is the investigation of exactly the same peptaibol molecule, e.g. alamethicin, when bound to membranes using EPR and oriented solid-state NMR to obtain information on both the alignment and the oligomerization of the peptides in membranes. This approach using two complementary techniques allows not only the gathering of more information about peptide/membrane interactions but also the direct comparison of these different magnetic resonance methods.

Abbreviations:

Lipids:

PC: phosphatidylcholine

POPC: 1-palmitoyl-2-oleoyl-sn-glycero-3-phosphocholine

DPPC: di-palmitoyl-phosphatidylcholine

POPG: 1-palmitoyl-2-oleoyl-sn-glycero-3-[phospho-rac-(1-glycerol)]

POPE: 1-palmitoyl-2-oleoyl-sn-glycero-3-phosphoethanolamine

POPS: 1-palmitoyl-2-oleoyl-sn-glycero-3-phospho-L-serine

DOPC: 1,2-dioleoyl-sn-glycero-3-phosphocholine

Other:

NMR: Nuclear Magnetic Resonance

EPR: Electron Paramagnetic Resonance

CW EPR: Continuous Wave EPR

ESEEM: Electron Spin Echo Envelope Modulation

MLV: multilamellar vesicle

TOAC: 2,2,6,6-tetramethylpiperidine-1-oxyl-4-amino-4-carboxylic acid

PELDOR: pulsed electron–electron double resonance

DQC: double quantum coherence

CP: cross-polarization

CD: Circular Dichroism

Aib: Amino*IsoB*utiryc acid

Fmoc: 9-Fluorenylmethoxycarbonyl

HPLC: high performance liquid chromatography

CSA: Chemical Shift Anisotropy

CS: Chemical Shift

Chapter 1

Introduction

Peptaibols are linear antibiotic peptides of fungal origin, ranging in length from 5 to 20 residues. Their name derives from their chemical composition: "Pept" is the abbreviation of peptide, "Aib" indicates a high content of the unusual aminoacid Aib (aminoisobutiryc acid), and "ol" is due to the presence of a C-terminal 1,2-amino alcohol; they also contain an N-terminal acetyl group. (Chugh et al., 2001). Presently this family of peptides encompasses more than 300 members (alamethicins, suzukacilins, zervamicins, antiamoebins, ampullosporins, trichogins, etc), whose sequences are collected in the Peptaibol database (http://www.cryst.bbk.ac.uk/peptaibol) (Whitmore et al., 2003).

Aib is a well-known helix-inducing amino acid, since the presence of the second methyl group on the C_α atom imposes strong stereochemical restrictions on the peptide backbone (Karle and Balaram, 1990; Pispisa et al., 2000a and 2000b), which exhibits a high tendency to adopt 3_{10} or α-helical conformations. Indeed all peptaibol structures determined so far are largely helical (Rebuffat et al., 1999).

Peptaibols are potent antimicrobial agents, many of which appear to permeate biomembranes. Their activity potency is strongly biased towards the longest ones, e.g. alamethicin (for review, see e.g. Woolley and Wallace, 1992; Duclohier and Wroblewski, 2001). When added to lipid bilayers alamethicin exhibits a well-defined pattern of successive increases in conductance levels, each of a duration of a few milliseconds (Gordon and Haydon, 1972; Boheim, 1974) which resemble those seen in the presence of large voltage- or ligand-gated channel proteins (reviewed in (Woolley and Wallace, 1992; Sansom, 1993; Bechinger, 1997)). There is presently a consensus for the mode of action of the long peptaibols whose helical length matches the standard bilayer thickness with the "barrel stave" model. In addition, the understanding of their action could provide valuable information on membrane channel proteins, which are difficult to purify in quantitative amounts sufficient for structural studies.

The “barrel stave” model (Fig. 1.1) describes the formation of transmembrane pores/channels by bundles of amphipathic helices, which oligomerize like the staves of a barrel, so that their hydrophobic surfaces interact with the lipid core of the membrane and their hydrophilic surfaces point towards the interior of the pore, which is filled with water. Since this model requires peptide insertion into the hydrophobic core of the lipid bilayer, it is reasonable to assume that in this case peptide association with the target membrane is driven predominantly by hydrophobic interactions. The best-studied peptide for which this model seems to hold is alamethicin, which we will talk a lot in the present thesis.

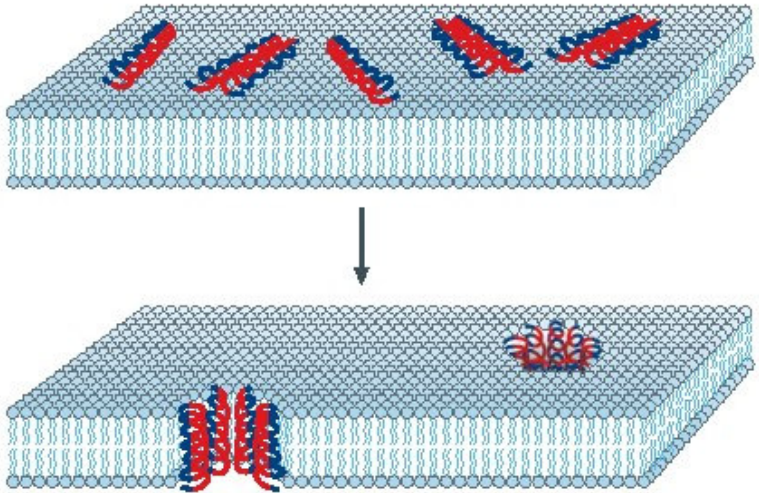

Figure 1.1. *The barrel-stave model of antimicrobial-peptide-induced killing. In this model, the attached peptides oligomerize and insert into the membrane bilayer so that the hydrophobic peptide regions align with the lipid core region and the hydrophilic peptide regions form the interior region of the pore. Hydrophilic regions of the peptide are shown in red, hydrophobic regions of the peptide are shown in blue. (taken from Brogden, 2005)*

Peptaibols, especially those with helix length shorter than 18 residues, are not capable to completely span the lipid bilayer of normal thickness. Herein the situation is much less clear and several mechanisms of membrane activity have been proposed. Employing the parallel with cationic peptides, which also adopt surface orientation, the “carpet-like” and “toroidal pore” models have been proposed to explain the membrane disruption activity of short peptaibols.

In the “carpet-like” model (Fig. 1.2), peptides are in contact with the phospholipid head groups throughout the entire process of membrane permeation and do not penetrate into the lipid hydrophobic core neither do oligomerize, in contrast to the barrel-stave mechanism. Peptides lay parallel to the membrane surface (with the hydrophobic face pointing towards the lipid core, and the hydrophilic face to water). Membrane permeation occurs only if there is a high local concentration of membrane-bound peptides (so that they form a “carpet”). In this case, the surface tension caused by peptide insertion in the headgroup region is released by the formation of transient membrane spanning pores, made up of dynamic peptide-lipid supramolecular complexes (Gazit et al., 1995; Matsuzaki, 2001). In these holes, the lipid bilayer bends back onto itself forming a toroidal structure. As a consequence, a fraction of peptide molecules translocates into the inner leaflet of the membrane, significantly reducing the peptide density in the outer layer, and leading to the closing of the pore. Furthermore, at higher concentrations, the peptide causes the disintegration of the membrane and the formation of micelles (micellization). In this mechanism, as the peptide interacts strongly with the phospholipid head groups, electrostatic interactions presumably play a crucial role. This model explains the activity of antimicrobial peptides such as ovispirin that orientate parallel (“in-plane”) to the membrane surface (Yamaguchi et al., 2004).

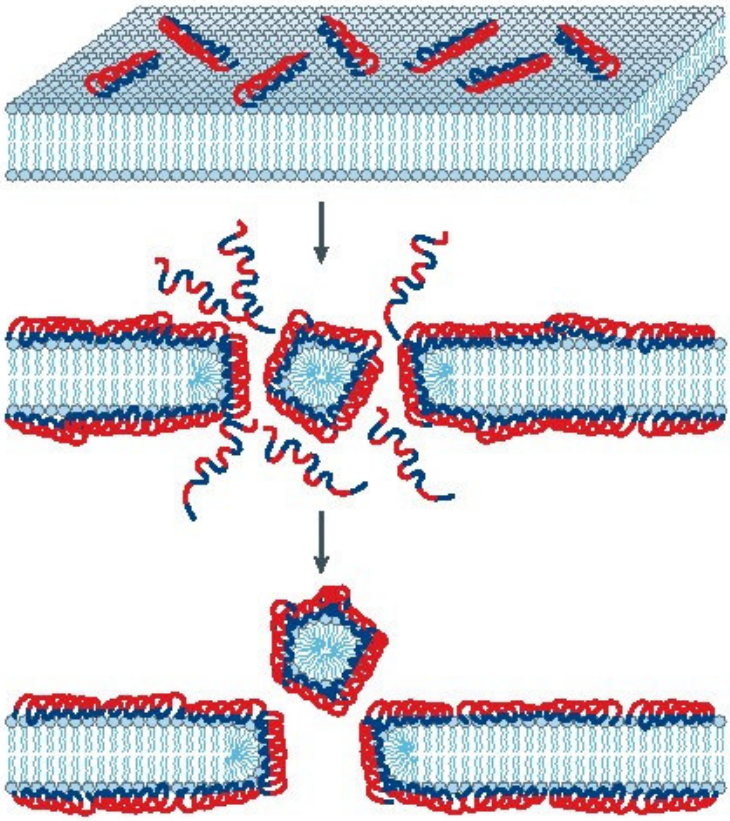

Figure 1.2. *The carpet model of antimicrobial-induced killing. In this model, the peptides disrupt the membrane by orienting parallel to the surface of the lipid bilayer and forming an extensive layer or carpet. Hydrophilic regions of the peptide are shown in red, hydrophobic regions of the peptide are shown in blue (taken from Brogden, 2005).*

In the "toroidal-pore" model (Fig. 1.3), antimicrobial peptide helices insert into the membrane and induce the lipid monolayers to bend continuously through the pore so that the water core is lined by both the inserted peptides and the lipid head groups. This type of transmembrane pore is supposed to be induced by magainins, protegrins and melittin (Yang et al., 2001, Matsuzaki et al., 1996, Hallock et al., 2003). In forming a toroidal pore, the polar faces of the peptides associate with the polar head groups of the lipids. The lipids in these openings then tilt from the lamellar normal and connect the two leaflets of the membrane, forming a continuous bend from the top to the bottom in the fashion of a toroidal hole; the pore is lined by both the peptides and the lipid head groups. The toroidal model differs from the barrel-stave model as the peptides are always associated

with the lipid head groups even when they are perpendicularly inserted in the lipid bilayer.

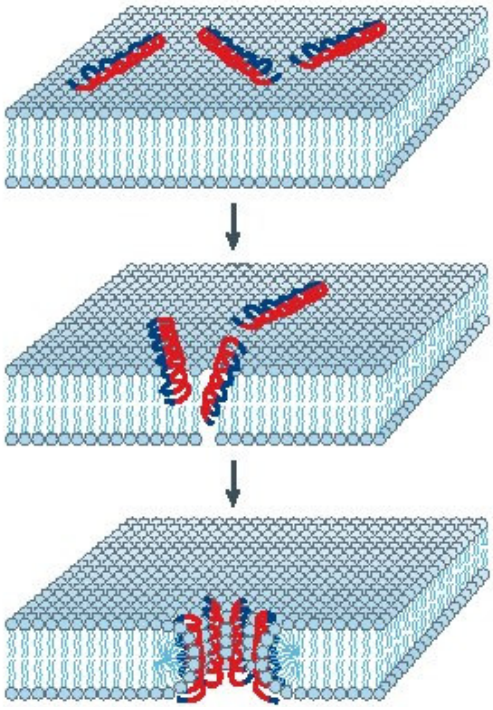

Figure 1.3. *The toroidal model of antimicrobial peptide-induced killing. In this model the attached peptides oligomerize and induce the lipid monolayers to bend continuously through the pore so that the water core is lined by both the inserted peptides and the lipid head groups. Hydrophilic regions of the peptide are shown in red, hydrophobic regions of the peptide are shown in blue. (taken from Brogden, 2005)*

Although descriptions of membrane damage seem to vary, they are likely to be related. It has been suggested that ion channels, transmembrane pores and extensive membrane rupture do not represent three completely different modes of action, but instead are a continuous graduation between them (Dathe and Wieprecht, 1999 and also Bechinger and Lohner, 2006). It was combined in “detergent-like” model (Bechinger and Lohner, 2006), which represents the most generally applicable explanation for the membrane-activities of amphiphiles. A complete description of the peptide–membrane interactions and the resulting membrane morphologies would need to take into account a wide variety of parameters and conditions. These include the peptide-to-lipid ratio, the

detailed membrane composition, temperature, hydration and buffer composition. As with detergents this can be done by establishing phase diagrams (Fig. 1.4).

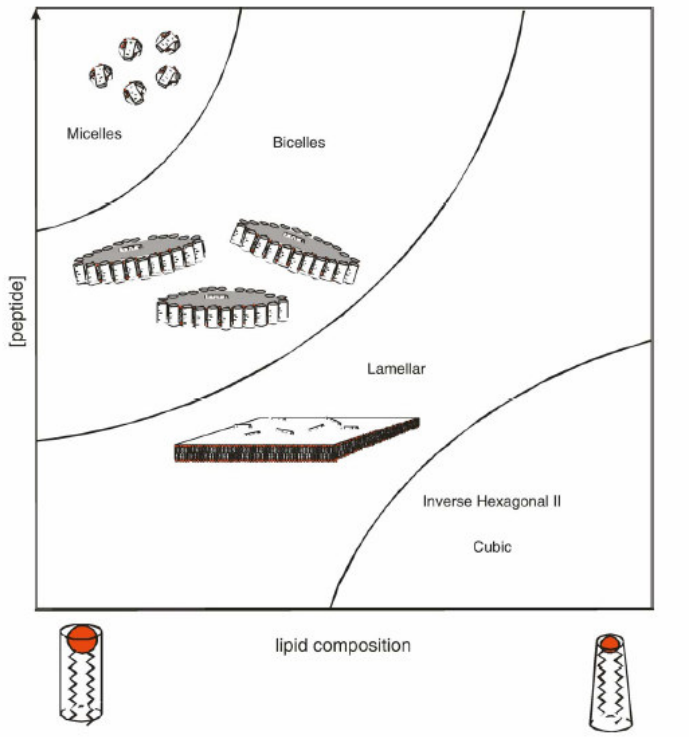

Figure 1.4. *This figure shows a schematic phase diagram of antibiotic peptide/phospholipid mixtures. A variety of macroscopic phases are obtained as a function of peptide / lipid ratios and lipid composition. Here two lipids with different molecular shapes are mixed and their effect on the macroscopic phase transition in the presence of antibiotic peptides is shown. For a complete description of antibiotic activities other parameters such as temperature, pH, or cholesterol concentration would have to be considered. (taken from Bechinger and Lohner, 2006)*

Notably, the detergent-like properties of amphipathic peptides are not in contradiction but include the above mentioned toroidal pore and carpet models, in fact these latter models should be considered 'special cases' where the conditions are such that these kind of supramolecular structures are observed within a much more complex phase diagram. It therefore seems tedious to argue about the 'correct model' as all of them might occur depending on the detailed conditions. Notably, the extensive plasticity of peptide/detergent–lipid complexes opens up the possibility that a peptide induces a certain macromolecular structure when interacting with the membranes of one organism,

but a different one when interacting with another species. On the other hand the mutagenesis of the peptide sequence causes shifts in the phase diagram and therefore also affects the biological mechanisms.

The aim of the thesis is the characterization of the structure, dynamics, topology and self-assembly of peptaibols when associated with biological membranes. We focused our investigations on the three members: trichogin GA IV (11 amino acids), ampullosporin A (15 amino acids) and alamethicin (20 amino acids), which are different in length and vary in their intensity of biological activity.

*n*Oct-*Aib*^{1}-Gly-Leu-*Aib*^{4}-Gly-Gly-Leu-*Aib*^{8}-Gly-Ile-Lol (trichogin GA IV)

Ac-Trp-Ala-*Aib*^{3}-*Aib*^{4}-Leu-*Aib*^{6}-Gln-*Aib*^{8}-*Aib*^{9}-*Aib*^{10}-Gln-Leu-*Aib*^{13}-Gln-Lol (ampullosporin A)

Ac-*Aib*^{1}-Pro-*Aib*^{3}-Ala-*Aib*^{5}-*Aib*^{6}-Gln-*Aib*^{8}-Val-*Aib*^{10}-Gly-Leu-*Aib*^{13}-Pro-Val-*Aib*^{16}-*Aib*^{17}-Gln-Gln-Phol (alamethicin)

where *n*Oct is n-octanoyl, Lol is leucinol and Phol is phenylalaninol.

Alamethicin is the best-studied peptaibol. It produces voltage-dependent pore formation in PC membranes (Duclohier and Wroblewski, 2001). The topology and structure of alamethicin in the membrane has been demonstrated to be a function of a number of parameters describing the environmental conditions (concentration, pH, etc…). CD data was obtained for the existence of two forms of membrane bound alamethicin that interconvert as a function of alamethicin concentration (Woolley and Wallace, 1993). As a consequence the two state model has been also proposed by Huang (Huang, 2006) based on a large amount of experimental studies by oriented CD, neutron in-plane scattering and x-ray diffraction techniques (Huang and Wu, 1991, He et al., 1996, Chen et al, 2003, Lee et al., 2004). At low peptide-to-lipid ratios the peptide associates with the surface of a membrane; however, above a threshold concentration the peptide orients transmembrane (Huang and Wu, 1991). Correspondingly, a minimal peptide concentration is required in the medium for antibiotic activity. Moreover, well-defined water-filled pores were detected by neutron in-plane scattering in bilayers containing transmembrane alamethicin (He et al., 1996).

Much less is known for membrane bound ampullosporin A and trichogin GA IV peptaibols. Ampullosporin A induces K^+ leakage across egg PC membranes (Kropacheva et al., 2005) and trichogin GA IV induced leakage of carboxyfluorescein entrapped inside large unilamellar vesicles formed by POPC (Mazzuca et al., 2005) even without transmembrane potential.

To access the topology of peptide bound to membranes solid-state NMR spectroscopy on oriented bilayers is highly efficient (Bechinger, 1999). Proton-decoupled ^{15}N spectra of uniformly ^{15}N labeled peptides immediately provide key information that allows to deduce the approximate peptide orientation relative to oriented lipid bilayer in a straightforward and direct manner. The comparison of such spectra at different membrane orientations relative to external magnetic field provides information also on peptide dynamics. Two-dimensional PISEMA experiments allow one to derive more accurate information and more details on the structural conformation of the peptide bound to membrane. In an ideal case it can even provide the structure of transmembrane peptide (Ketchem et al., 1996). These techniques will be applied to ^{15}N uniformly labeled peptaibols ampullosporin A and alamethicin.

The formation of transmembrane pores occurs through oligomerization of peptide monomers and can be monitored by different approaches of Electron Paramagnetic Resonance (EPR). The Electron Spin Echo Envelope Modulation (ESEEM) approach monitors the water exposure of labels and could therefore be used to delineate the depth of the label with respect to the membrane surface. X-band EPR study will be performed on membrane-bound state of spin-labeled analogs of trichogin GA IV and alamethicin.

The techniques are highly complementary. Pulsed EPR applying to the peptides in membranes needs low temperature and introducing of relatively big spin labels. Both these restrictions could dramatically affect native peptide-membrane interactions. Fortunately, NMR is free of these particular restrictions. On the other hand, solid-state NMR of oriented samples requires macroscopically oriented membranes. Preparation of well-aligned samples is of particular importance for deducing peptide helix orientation, which immediately moves these experiments to the field of the art. The main goal of this thesis is the investigation of exactly the same peptaibol molecule, e.g. alamethicin, when bound to membranes using EPR and solid-state NMR to obtain information on alignment and oligomerization in membranes. It will allow both gathering more information about peptide/membrane interactions and also direct comparison of these different magnetic resonance approaches.

Chapter 2

Theory

2.1 Structure and properties of lipid membranes

Lipid membranes are essential for any kind of living cell. Lipid membranes separate the cell from its environment and in the case of eukaryotic cells lipid membranes also separate the organelles from the cytosome of the cells.

Lipid bilayers are (in the liquid cristaline phase) very flexible and they allow the controlled insertion of proteins, peptides and polysacharides. Bilayers spontaneously form of lipids with the right properties in an aqueous environment. This results in stable membranes with self-healing properties and a high degree of flexibility.

Lipids are amphiphilic molecules, consisting of a polar head-group and two hydrophobic hydrocarbonhydrate chains linked by a glycerol group. The hydrophobic hydrocarbon sidechains can vary in length and in saturation. It is also possible that the sidechains contain other groups (i.e.: sphingolipids). The headgroup consists mostly of a phosphate group linked to a polar group (i.e.: Choline, Serine, Ethanolamine, Innositol). The structures of POPC (1-Palmitoyl-2-Oleoyl-*sn*-Glycero-3-Phosphocholine) and POPG (1-Palmitoyl-2-Oleoyl-*sn*-Glycero-3-[Phospho-*rac*-(1-glycerol)]) are given in Fig. 2.1. Whereas the headgroup of POPG consists of Glycerol, the headgroup of POPC consists of Choline. The negatively charged phosphate group gives together with the positively charged Coline the zwitterionic headgroup of POPC. The neutral glycerol group of POPG forms together with the negative charge of the phosphate group an anionic headgroup. These properties allow to generate lipid bilayers with a negative surface charge. This is insofar of special interest as many proteins need a negative surface charge to interact with the membrane (i.e Colicines (Zakharov et al. 1996, Lakey et al., 1991)). The glycerol group links the headgroup with the fatty acid chains. The fatty acids consist of palmitoyl (hexadecanoic) with 16 carbons at the glycerol position 1 and of oleoyl (9-cis-

octadecenoic) with 18 carbons and an unsaturated bond between the 9 and 10 position. With this chain length the hydrophobic thickness of the bilayers is in the range of about 27 Å (Harzer and Bechinger, 2000).

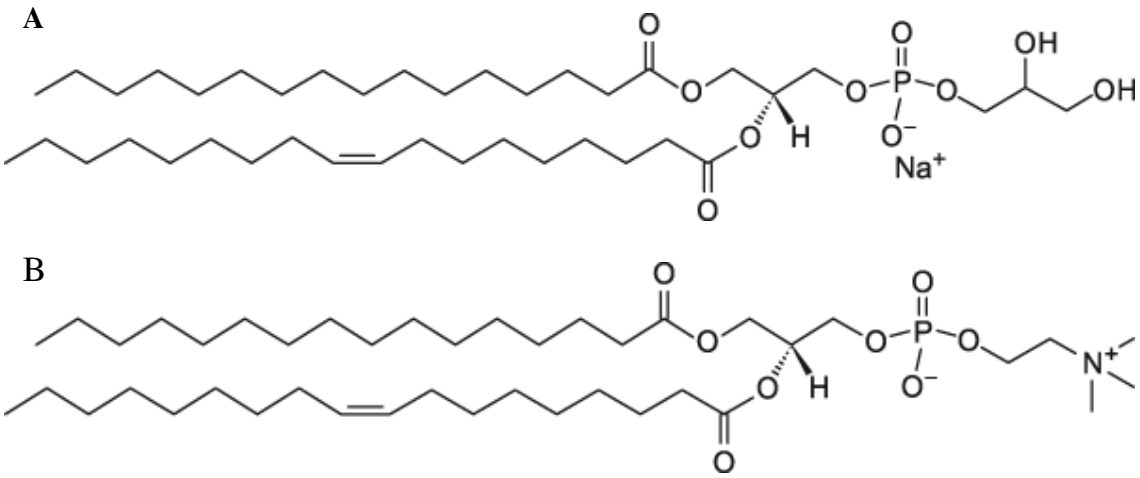

Figure 2.1. *Structure of A: POPG (sodium salt) and B: POPC. The headgroup (glycerol for POPG and choline for POPC) is linked by a phosphate to the glycerol group. The hydrocarbonate chains are attached to the 1- and 2- position of the glycerol group.*

Lipids can have different geometrical properties. An important factor is the relation between the cross-sectional area of the hydrocarbon portion (v/l) to the optimal surface area required by the polar headgroup (S_0) (Gennis, 1989). If the relation v/S_0l is between 0.5 and 1 (i.e. phosphatidylcholine, phosphatidylserine…) the shape of the lipid is cylindrical and lipid bilayers are formed (Fig 2.2 A, L_α phase). For $v/S_0l>1$ (i.e. phosphatidylethanomine, phosphatic acid…) the lipids are considered to have a cone shape and an inverted hexagonal phase can be formed (Fig. 2.2 C: H_{II} phase). For $½>v/S_0l$ (i.e. lysophospholipids or detergents) the lipids have the shape of an inverted cone and form either rods which can arrange in a hexagonal shape (H_I phase) for $½>v/S_0l>1/3$ or micelles for $1/3>v/S_0l$ (B). However it has to be noted that the most lipids for micelle formation have only one hydrocarbonate chain.

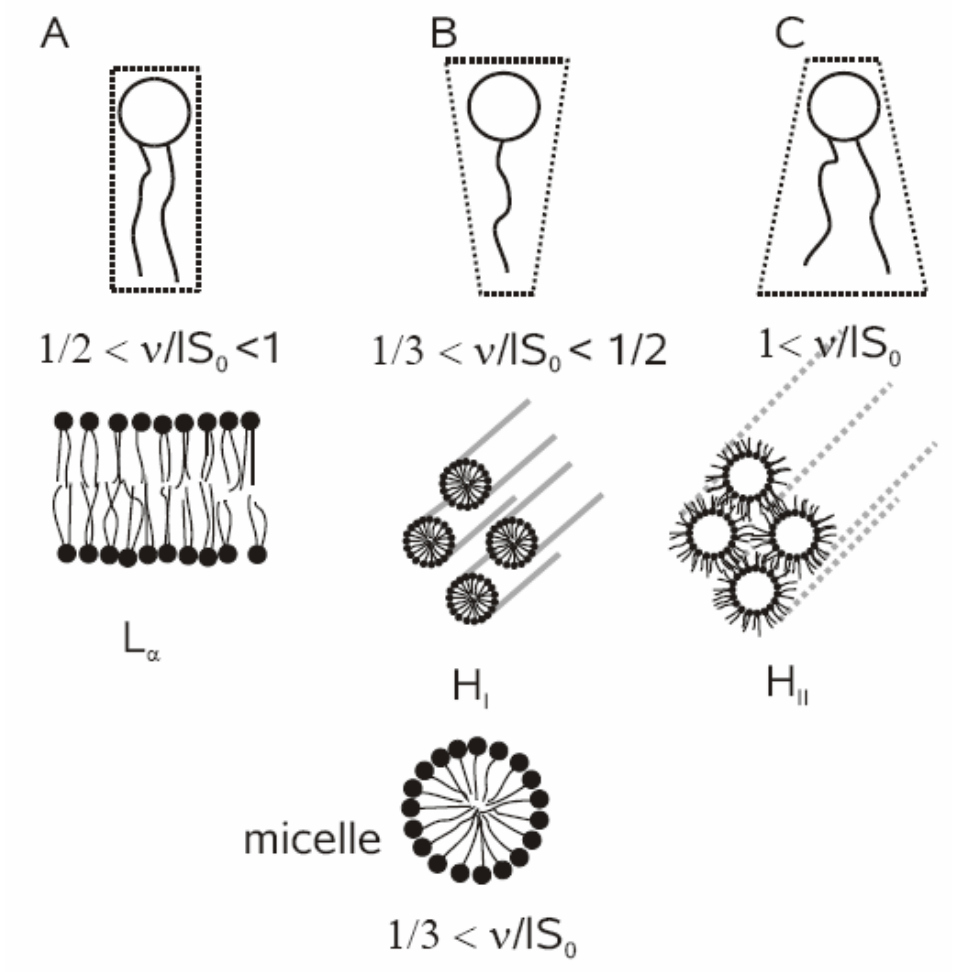

Figure 2.2 *The different geometric properties of different lipids lead to different aggregates in aqueous solution. If the headgroups fill the same area like the tails the lamellar phase L_α is formed. If the headgroups fill much more space than the tails, the hexagonal phase H_I or micelles are formed. If the headgroup fills a much smaller area, the inverted hexagonal phase H_{II} can be formed.*

The temperature plays an important role for the structure of lipid bilayers. At low temperatures a gel phase (L_β or $L_{\beta'}$) is observed, in which the lipids are arranged in a hexagonal lattice in absence of any lateral diffusion. At high temperatures the lipids become liquid crystalline (L_α). The lipids can diffuse laterally across the membrane and the system behaves like a liquid in two dimensions. Membranes of phosphatidylcholine with twice the same carbohydrate sidechain can adopt an intermediate state (rippled phase $P_{\beta'}$)(Hicks et al. 1987) and the gel phase of these lipids exhibits a tilt of the carbohydrate

chains ($L_{\beta'}$ phase). The liquid crystalline state provides the membrane proteins and polypeptides the mobility, they need to fulfill their functions. The membrane allows mobility in two dimensions (inplanar) and blocks effectively all uncontrolled exchange in the third dimension (flip-flop across the membrane). The liquid crystalline phase can be considered as a 2-D liquid.

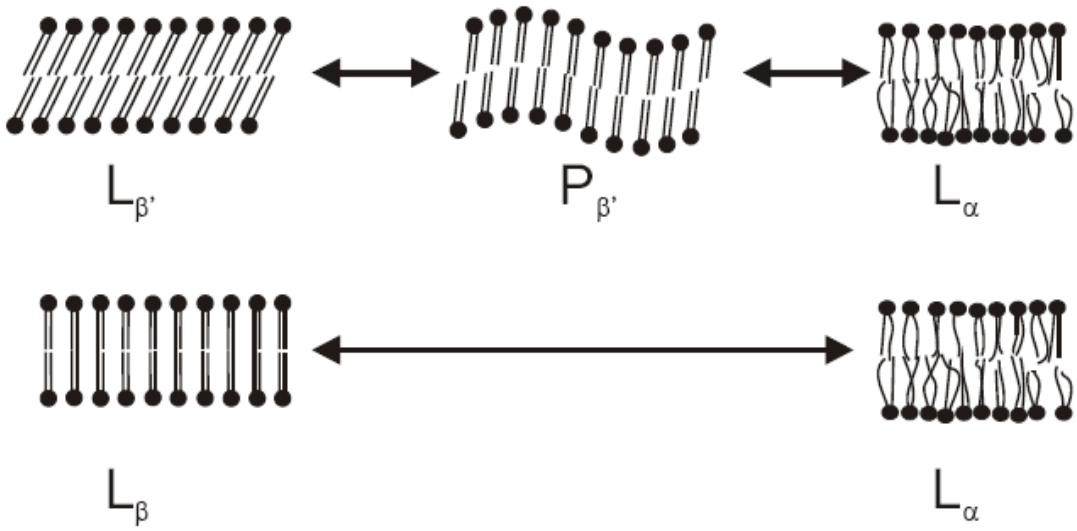

Figure 2.3. *Schematic model of the molecular organization of lipids as a function of temperature. In the gel phase (L_β) at low temperature the lipids are arranged in a 2-D crystal whereas the lipids can diffuse in the plane at higher temperatures in the liquid crystalline phase (L_α). Some lipids (i.e. Phosphatidylcholine) exhibit an intermediate state called the ripple phase (P_β).*

The melting transition temperature is strongly affected by the lipid chain length. For example, T_m = 298 K for DMPC, and 314.6 K for DPPC, the latter having two more methylene groups per chain. It is also strongly dependent on the degree (and positions) of lipid insaturations: for example, the T_m for 1-palmitoyl-2-steroyl phosphatidylcholine and 1-palmitoyl-2-oleyl-phosphatydilcholine, which differ for one double bond only, are 44° C and 2°C, respectively (Szoka and Papahadjiopoulos, 1980; Sackman, 1995).

In addition, phosphatidylcholine membrane of DPPC has more than three different phases (see Fig. 2.4).

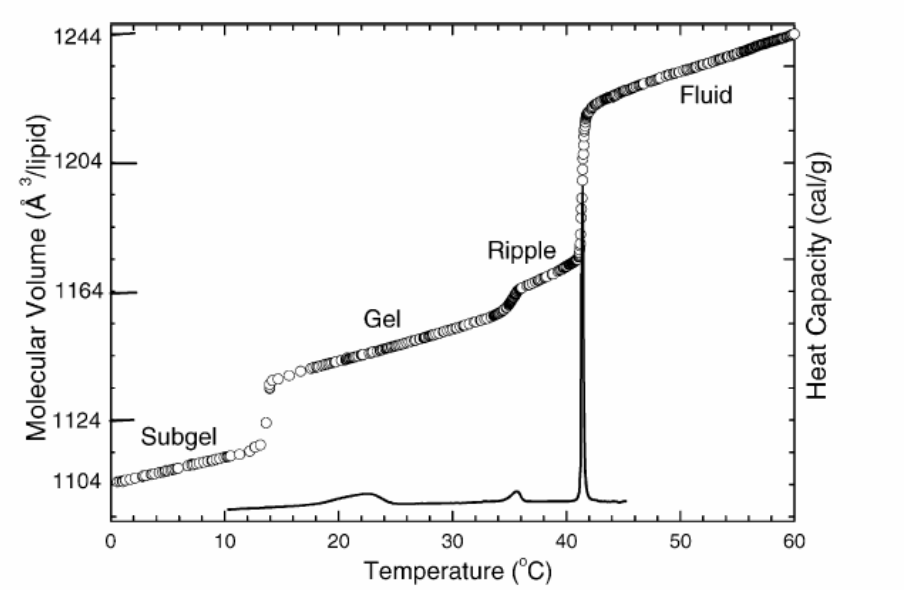

Figure 2.4. *Molecular volume (open circles) and heat capacity (solid line) vs. temperature for DPPC bilayers in excess water (taken from (Tristram-Nagle and Nagle, 2004)).*

The most important properties of phosphatidylcholine lipid bilayers, which were used in the present thesis work, are collected in the table 2.1.

Table 2.1. Physical Characteristics of the Lipids Used during This Investigation

Phospholipid (abbreviation and full name)		№. of carbons	Hydrophobic thickness (Å)		Tm (K)
			fluid phase	gel phase	
DCPC	1,2-dicapryl-*sn*-glycero-3-phosphocholine	10:0	15.5[a]		240.4[d]
DLPC	1,2-dilauroyl-*sn*-glycero-3-phosphocholine	12:0	19.5[a]		273[g]
	1,2-dimyristoleoyl-*sn*-glycero-3-phosphocholine	14:1 Δ9cis	20.0[b]		
DMPC	1,2-dimyristoyl-*sn*-glycero-3-phosphocholine	14:0	26.2[c]	30.3[e]	298[e]
DPPC	1,2-dipalmitoyl-sn-glycero-3-phosphocholine	16:0	28.5[c]	34.4[c]	287.6/ 314.6[c]
POPC	1-palmitoyl-2-oleoyl-*sn*-glycero-3-phosphocholine	16:0/18:1 Δ9cis	28.5/27.1[h]		271[f]

[a] *from (Lewis and Engelman, 1983)*

[b] *from (Harzer and Bechinger, 2000)*

[c] *from (Nagle and Tristram-Nagle, 2000)*

[d] *from (Huang et al., 1994)*

[e] *from (Tristram-Nagle et al., 2002)*

[f] *from (Silvius, 1982)*

[g] *from (Caffrey and Feigenson, 1981).*

[h] *The corresponding chain lengths of di-acyl-sn-glycerophosphocholines were used (Nagle and Tristram-Nagle, 2000).*

2.2 Basic theory of Magnetic Resonance

The magnetic moment can interact with an external magnetic field. This is used to manipulate the spin system in magnetic resonance experiments. Whereas the methodological principles for the manipulation of the spin system (electron spin S in EPR, nuclear spin I in NMR) are very similar in NMR and EPR spectroscopy, the technical requirements and therefore the practical realization is quite different in both fields. Owing to the much larger magnetic moment of the electron spin S (a factor of 768 larger compared with a proton nuclear spin) the technical requirements (resonance frequency, detecting times, pulse lengths) for EPR are much more demanding as compared with NMR spectroscopy. Nevertheless, most of the technical restrictions have been overcome by the development of specific pulse methods and techniques.

Relaxation

The relaxation is an effect of the coupling of the magnetic moment to other magnetic moment (spin-spin-relaxation) and to the lattice (spin-lattice-relaxation). The spin-lattice-relaxation (also called T_1 relaxation) is the result of loss of energy towards other degrees of freedom of the system. The spin-spin-relaxation (also called T_2 relaxation) is the loss of coherence of the individual spins by spin-spin-interactions. It is notable that the spin-spin-relaxation does not affect the energy of the spin-system. Phenomenologically the relaxation can be described by rate equations

$$\begin{aligned} \frac{d}{dt}M_x &= -\frac{M_x}{T_2} \\ \frac{d}{dt}M_y &= -\frac{M_y}{T_2} \\ \frac{d}{dt}M_z &= -\frac{(M_z - M_0)}{T_1} \end{aligned} \qquad (2.1)$$

Relaxation effects can be measured to gain information mainly about the dynamics of a system. These effects have to be taken into account in the planning of an experiment. In general a delay of about $5T_1$ is required after an acquisition for the system to relax to the thermal equilibrium. The next acquisition should start after this delay unless the sequence design explicit intends to work with a steady state magnetization instead of thermal equilibrium magnetization at the beginning of an acquisition.

EPR

EPR, is a spectroscopic technique, which detects species that have unpaired electrons. It is also often called ESR, Electron Spin Resonance. A surprisingly large number of materials have unpaired electrons. These include free radicals, many transition metal ions, and defects in materials. Free electrons are often short-lived, but still play crucial roles in many processes such as photosynthesis, oxidation, catalysis, and polymerization reactions.

Conventional Hahn echo pulse sequence

In principle acquiring of a spectrum needs an applying a π/2 pulse followed by the acquisition of the Free Induction Decay (FID). But between the π/2 pulse and the data acquisition there is a time gap. This time gap ("dead-time") is necessary for the switch between irradiation and acquisition but also to avoid artefacts like acoustic ringing. During this dead-time gap the system evolves, the system relaxes (T_1 and T_2 relaxation). In the case of Pulsed EPR of nitroxide radicals the dephasing is so fast that it's even impossible to detect FID after a dead-time period. Luckily, the spins can be rephrased by application of an additional π pulse (Hahn, 1950).

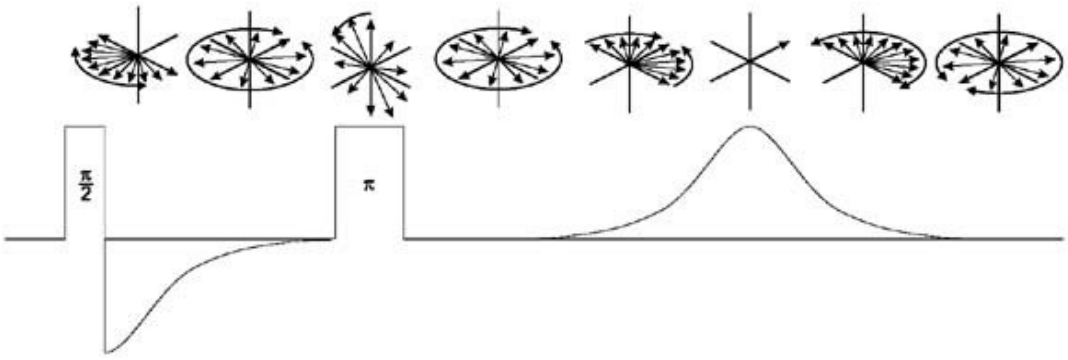

Figure 2.5: *Magnetization behavior during an echo experiment (taken from http://www.bruker-biospin.com/pulsetheory.html)*

Mainly, the decay of the FID is due to the different frequencies in the spectrum causing the magnetization to fan out in the x-y plane of the rotating frame. When we apply the π pulse, we flip the magnetization about the x axis. This almost has the effect of running the FID backwards in time. The higher frequency spin packets will have traveled further than the lower frequency spin packets after the first pulse. However, because the higher frequency spin packets are rotating more quickly, they will eventually catch up

with the lower frequency spin packets along the +y axis after the second pulse. The conventional two-pulse sequence is shown in Fig. 2.5. It forms so-called Hahn-echo, which is actually consists of one inverted and one straight FID.

NMR

Chemical shift

The chemical environment of a nucleus causes a local magnetic field, which slightly differs from the global magnetic field. It can be written as

$$\omega = \gamma B_{local} = \gamma B_0(1-\sigma) \qquad (2.2)$$

where B_0 is the ground magnetic field and σ is the shielding constant. As the chemical shift is proportional to the ground magnetic field the chemical shift is specified by

$$\frac{\delta - \delta_0}{\delta_0} = \frac{\Delta\omega}{\gamma B_0} \qquad (2.3)$$

Usually the chemical shift is given in parts per million (ppm). The electron distribution is in general not spherical around the nucleus. Therefore the shielding depends on the direction of the electron distribution with respect to the magnetic field. This effect is called the chemical shift anisotropy (CSA). In a first approach the CSA can be described by a tensor.

$$\Delta\omega = \gamma \frac{B_0^i(\delta_{ij} - \delta_0)B_0^j}{|B_0| \cdot \delta_0} \qquad (2.4)$$

For fast rotating molecules the anisotropic effect of the chemical shift is averaged out and a residual isotropic chemical shift is left over. The isotropic chemical shift dispersion is generally in the range of several ppm. The isotropic chemical shift can be used to identify the nuclei of different atoms in the molecule. For a big molecule or immobilized molecules the averaging doesn't occur anymore and anisotropic effects overlay the isotropic chemical shifts of the individual sites, thereby hampering their assignment.

Chapter 3

Materials and Methods

3.1 Materials

The solid-state synthesis of the spin-labeled trichogin GA IV analogues FTOAC1, FTOAC4, FTOAC8, *n*Oct-TOAC1, and *n*Oct-TOAC4 was done at the University of Padova, Italy, by C. Peggion, F. Formaggio and C. Toniolo as described (Monaco et al., 1999a).

*n*Oct -**TOAC**[1]-Gly-Leu-Aib[4]-Gly-Gly-Leu-Aib[8]-Gly-Ile-Leu-OMe (*n*Oct-TOAC1)
*n*Oct-Aib[1]-Gly-Leu-**TOAC**[4]-Gly-Gly-Leu-Aib[8]-Gly-Ile-Leu-OMe (*n*Oct-TOAC4)
Fmoc-**TOAC**[1]-Gly-Leu-Aib[4]-Gly-Gly-Leu-Aib[8]-Gly-Ile-Leu-OMe (FTOAC1)
Fmoc-Aib[1]-Gly-Leu-**TOAC**[4]-Gly-Gly-Leu-Aib[8]-Gly-Ile-Leu-OMe (FTOAC4)
Fmoc-Aib[1]-Gly-Leu-Aib[4]-Gly-Gly-Leu-**TOAC**[8]-Gly-Ile-Leu-OMe (FTOAC8)

In all these peptide analogues the C-terminal leucinol (Lol) is replaced by its synthetic precursor L-leucine methyl ester (Leu-OMe). In three analogues the N-terminal *n*-octanoyl (*n*Oct) group is substituted by the 9-fluorenylmethyloxycarbonyl (Fmoc) group.

The solid-state synthesis and characterization of the spin-labelled Alamethicin F50 analogues Alm1, Alm8, Alm16 were described in (Peggion, Coin, and Toniolo, 2004).

Ac-**TOAC**[1]-Pro-Aib-Ala-*Aib*-Ala-Glu(OMe)-*Aib*-Val-*Aib*-Gly-Leu-*Aib*-Pro-Val-*Aib*-*Aib*-Glu(OMe)-Glu(OMe)-Phol (Alm1)
Ac-*Aib*-Pro-Aib-Ala-*Aib*-Ala-Glu(OMe)-**TOAC**[8]-Val-*Aib*-Gly-Leu-*Aib*-Pro-Val-*Aib*-*Aib*-Glu(OMe)-Glu(OMe)-Phol (Alm8)
Ac-*Aib*-Pro-Aib-Ala-*Aib*-Ala-Glu(OMe)-*Aib*-Val-*Aib*-Gly-Leu-*Aib*-Pro-Val-**TOAC**[16]-*Aib*-Glu(OMe)-Glu(OMe)-Phol (Alm16)

Unlabeled alamethicin was from Sigma (A4665-10 mg). ^{15}N uniformly labelled alamethicin is a gift of J. D. O'Neil. It was prepared as described previously and is more than 92% uniformly labeled with ^{15}N (Yee and O'Neil, 1992).

Ac-*Aib*-Pro-*Aib*-Ala-*Aib*-*Aib*-Gln-*Aib*-Val-*Aib*-Gly-Leu-*Aib*-Pro-Val-*Aib*-*Aib*-Gln-Gln-Phol (^{15}N uniformly labelled alamethicin)

^{15}N uniformly labelled and unlabelled ampullosporin A was prepared by Herdis Friedrich, Jena and described in details in Appendix 1.

Ac-Trp-Ala-*Aib*-*Aib*-Leu-*Aib*-Gln-*Aib*-*Aib*-*Aib*-Gln-Leu-*Aib*-Gln-Lol
(^{15}N uniformly labelled ampullosporin A)

All lipids, including 1-palmitoyl$_{d31}$-2-oleoyl*sn*- glycero-3-phosphatidylcholine (POPC-d31) and 1-palmitoyl$_{d31}$-2-oleoyl*sn*- glycero-3-phosphatidylglycerol (POPG-d31), were from Avanti Polar Lipids, Inc. (Alabaster, AL). For the preparation of a 10 mM D_2O phosphate buffer solution (PBS) at pH 7.4 and a 10 mM Tris buffer solution at pH 7.5, reagent grade salts and deuterated water (D_2O) were obtained from Sigma-Aldrich. All commercial materials were used without further purification.

3.2 EPR of membrane-modifying peptides.

Preparation of multilamellar vesicles (MLVs) samples.

Lipids and peptides were co-dissolved in chloroform in order to mix properly all components. The solvent was first evaporated with a stream of nitrogen gas. Residual traces of solvent were removed by drying the mixture under vacuum for at least 3 hours. The mixture was dispersed in buffer solution by vortex mixing if necessary with heating well-above the phase transition temperature of lipid membrane (i.e. at 328 K for DPPC membranes and room temperature for POPC membranes). The hydrated lipid bilayers were briefly sonicated in a bath sonicator and subjected to five rapid freeze-thaw cycles and then centrifuged and concentrated by pelletting in a benchtop centrifuge. After removal of the excess buffer the final water concentration was about 50 % w/w.

Following this procedure non-oriented MLVs were obtained (see Fig. 3.1.)

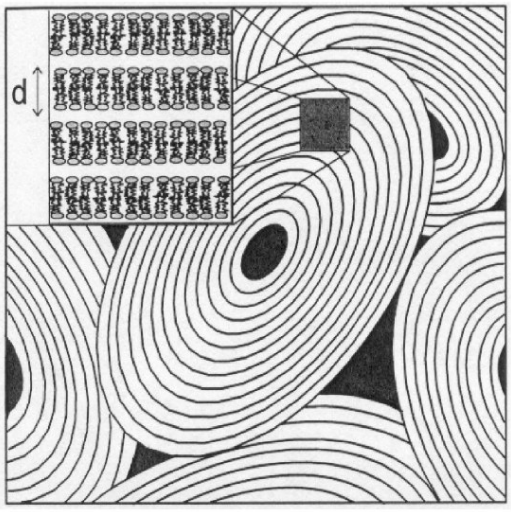

Figure 3.1. *Schematic view of MLVs with defect regions of excess water (taken from Koenig et al., 1997).*

ESEEM - access to peptide topology.

The ESEEM (Electron Spin Echo Envelope Modulation) phenomenon originates from the dependence of anisotropic hyperfine interaction (hfi) constants of electron spins on the presence of nearby magnetic nuclei. The frequency of modulation is a function of the magnetic moment of the coupled nucleus and can therefore be used to recognize this nucleon. The amplitude of the modulation is directly proportional to the coupling constant. Therefore, the more nuclei of one type and the closer they are, the bigger the amplitude of modulation with this characteristic frequency. The ESEEM technique is

widely used for structural investigations (for a review see (Schweiger and Jeschke, 2001)). For example, it was extensively used for the study of photosynthetic complexes and the process of electron transfer during photosynthesis.

The ESEEM technique (Dikanov and Tsvetkov, 1992) is suitable to study the orientation and immersion depth of peptide molecules in the membrane. An analogous approach was employed previously (Kurshev and Kevan, 1995), wherein the location of a doxylstearic acid spin probe in lipid bilayers was studied by ESEEM induced by its interaction with ^{31}P of phospholipids.

ESEEM technique has been used to determine the immersion depth of spin-probes in lipid membrane. For this purpose deuterated water was used to distinguish hydrogen atoms of water from those of lipid molecules and to increase the amplitude of the ESEEM that is known to be much larger for deuterons at the X-band. The amplitude of the modulation on the frequency of deuterium reflects the proximity of electron spin label to water molecules. It is clear that the membrane hydrophobic core doesn't contain water and therefore the bigger the deuterium amplitude of modulation the closer the spin-probe has to be to water and the shallower the immersion depth (fig. 3.2).

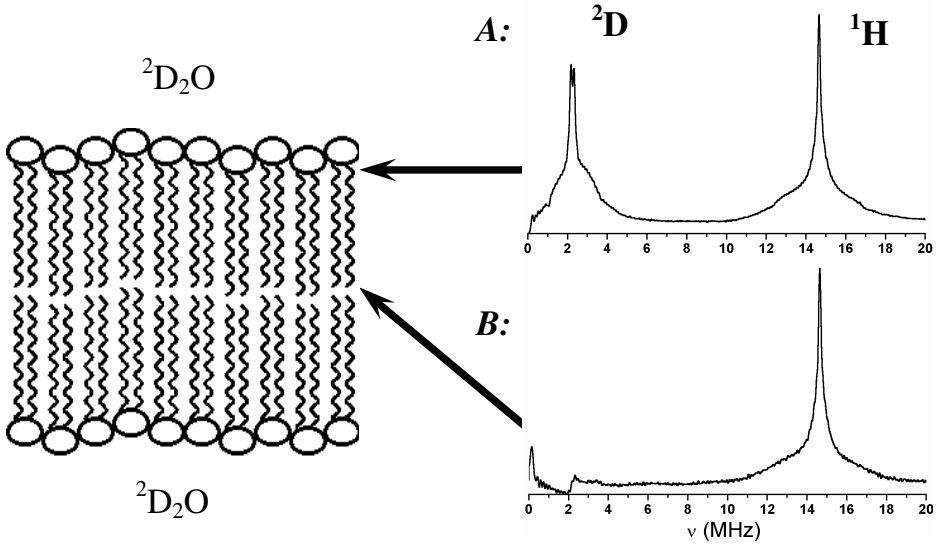

Figure 3.2. *Schematic representation of two cases:* ***A****: radical close to heavy water results in the high intensity 2D peak in ESEEM spectrum,* ***B****: radical deep inside the membrane far away from 2D atoms results in no peak at 2.2 MHz in ESEEM spectrum.*

The detailed investigation of the dependence of the amplitude of modulation on the position of spin label along DPPC lipid side chain is shown in Fig. 3.3 (adapted from Erilov et al., 2004). The profile reveals a sigmoidal, trough-like dependence on chain position, in which a transition takes place from a high-polarity region adjacent to the lipid headgroups to a low-polarity region at the center of the membrane (Erilov et al., 2004; see fig. 3.3). Please note, that the position, width and magnitude of the transition region depend on the membrane lipid composition, particularly on cholesterol content, and on the lipid phase.

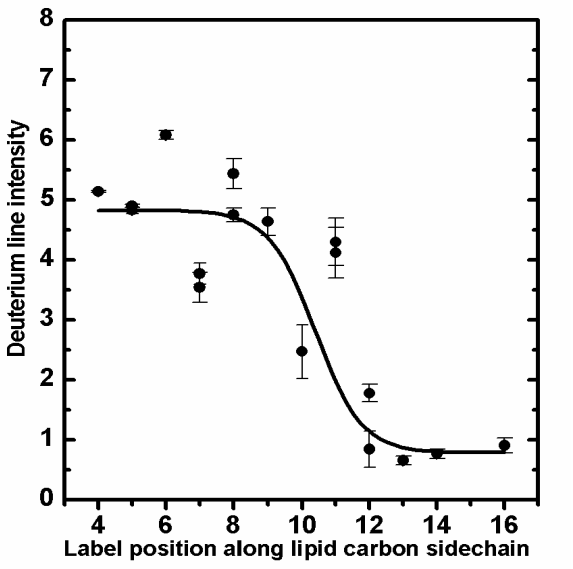

Figure 3.3. *The dependence of the ^{2}D amplitude of modulation on the position of spin label along DPPC lipid side chain (circles). Solid line shows the fit with sigmoidal function. (adapted from Erilov et al., 2004).*

To determine peptide topology within the membrane by this method, a number of peptide analogs labeled at different positions by a stable paramagnetic radical is necessary. Comparison of deuterium peak intensities obtained for these peptide analogs will allow us to determine relative immersion depth of different parts of the peptide, which could be used to deduce peptide orientation.

In the present study the 2,2,6,6-tetramethylpiperidine-1-oxyl-4-amino-4-carboxylic acid (TOAC) stable radical was used as a spin label. It is known that replacement of *Aib* by this label has only minor effects on the peptide structure and antimicrobial function. However, this question always needs to be asked.

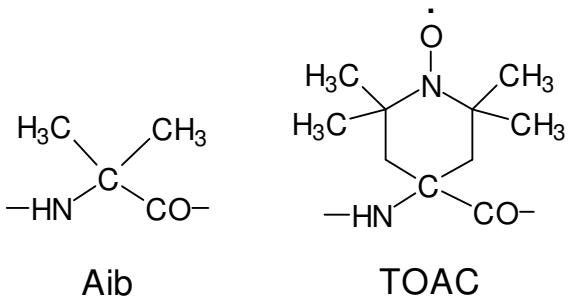

The determination of the immersion depth of the label using a calibration curve (Fig. 3.3) must be performed taking into account the possible influence of the embedded peptide on the water penetration profile. Indeed, TOAC label exposed inside of the water filled pore could give additional modulation similar to TOAC labels exposed to the membrane surface.

ESEEM EPR experiment. ESEEM experiments were performed on a Bruker ESP 380E pulse X-band EPR spectrometer. A home-made rectangular resonator was used, with a quartz Dewar containing liquid nitrogen. The resonator was overcoupled to obtain a dead time of 100 ns. To improve the signal to noise ratio the three pulse – stimulated echo ($\pi/2$-τ-$\pi/2$-t_1-$\pi/2$-τ-echo) with microwave pulse widths of 16 ns and the microwave power adjusted accordingly was used. The time delay t_1 between the second and the third pulse was incremented while maintaining the separation τ between the first and the second pulse constant at 200 ns to maximize the deuterium modulation. A Hahn echo decays with a time constant of T_2 whereas the stimulated echo decays with a time constant of approximately T_1. (Spin and spectral diffusion contributions cause the stimulated echo to decay somewhat faster than T_1.) T_2 is generally much shorter than T_1, so the ESEEM decays more slowly in a stimulated echo than in a Hahn echo experiment. Therefore, a three pulse ESEEM experiment usually gives superior resolution than a two pulse ESEEM experiment.

Hahn or two pulse echoes are not the only echoes to occur. If we apply three $\pi/2$ pulses we obtain five echoes. Three of the echoes are simply two pulse echoes produced by the three pulses. The stimulated and refocused echoes only occur when you have applied more than two pulses (Fig. 3.4).

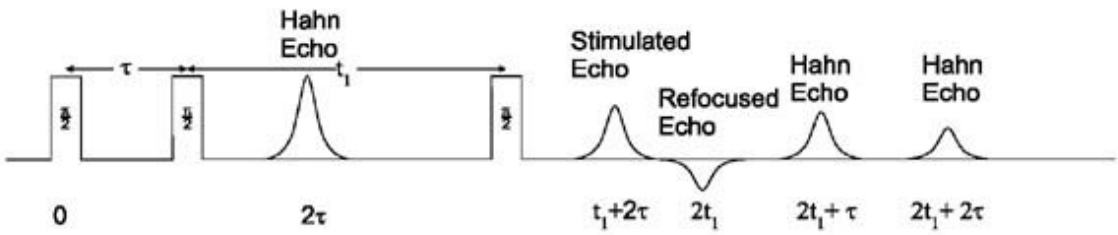

Figure 3.4. *Echoes and timing in a three pulse experiment (taken from http://www.bruker-biospin.com/pulsetheory.html)*

In a three pulse ESEEM experiment, we are only interested in the stimulated echo. The other echoes result in artefacts as they run through our stimulated echo. A four-step phase-cycling program was employed to eliminate unwanted echoes (see Fig. 3.5).

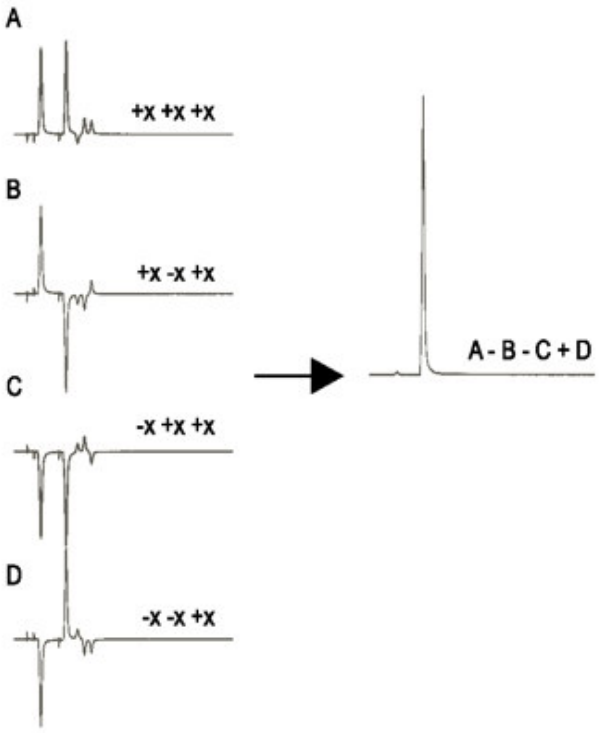

Figure 3.5. *Cancellation of unwanted echoes by phase cycling(taken from http://www.bruker-biospin.com/pulsepractice.html)*

The ESEEM-data were treated as follows (Erilov et al., 2005; Salnikov et al., 2006): (1) the experimental echo decay was approximated with a bi-exponential function; (2) the data were then divided by this function, so that only oscillations around the unity

remained; (3) the unit level was subtracted from the signal; (4) the array of the ESEEM data was zero filled to increase the total number of points up to 4K; (5) a numerical Fourier transformation was performed. Note that, in case different samples are compared, such procedure allows one to obtain the relative contribution of the modulated ESE signal (the unity in step (2) represents a non-modulated contribution) from which quantitative information about the relative positions of nearby nuclei can be provided.

CW EPR spectra simulation - access to peptide oligomerization

The dipolar interaction of unpaired electrons leads to considerable line broadening when motional averaging effects are absent. This is the case at the temperature of 77 K. Simulation of the broadened EPR spectra could give an idea of spin-spin distance. Herein we employed two different ways to account for dipolar broadening.

The first one was successfully used for the analysis of oligomerized spin-labeled insulin (Steinhoff et al., 1997). It takes the undisturbed monomer spectrum and additionally broadens it to account for dipolar spin interactions. It uses a simplified formula, which takes relatively little of machine time and takes into account possible interspin distance distributions, but assumes the orientational distribution to be isotropic. This is certainly the case for homogeneous spin solutions and works nicely for the spin-labeled insulin protein (Steinhoff et al., 1997).

The second method simulates the whole EPR spectrum of two coupled electron spins directly from Hamiltonian. It is rather time-consuming, but orientational anisotropy can be introduced easily. This method works for the simulation of EPR spectra for biradicals. Relative molecular frame orientations for two coupled radicals is the essential difference between these methods.

In frozen solution, the diffusive residual motion of protein side chains is strongly restricted for temperatures below 200 K. The EPR spectral line shape of a frozen protein solution or polycrystalline sample is adequately described by a powder spectrum. The shape of a powder spectrum of nitroxide spin labels randomly oriented in space is simulated on the grounds of the eigenvalues of the spin Hamiltonian:

$$H = \beta_e S\mathbf{g}B_0 + S\mathbf{A}I \qquad (3.1)$$

where B_o is the external magnetic field vector, β_e the Bohr magneton, S and I are the electron and the nuclear spin operators, respectively, **g** is the electron g value tensor, and **A** is the electron nuclear hyperfine tensor. The eigenvalues of the Hamiltonian are given to a good approximation by (Libertini and Griffith, 1970)

$$\begin{aligned} E &= g(\theta,\varphi)\beta_e B_0 + A(\theta,\varphi)M_S M_I \\ g(\theta,\varphi) &= g_{xx}l_{zx} + g_{yy}l_{zy} + g_{zz}l_{zz} \\ A(\theta,\varphi) &= (A_{xx}^2 l_{zx} + A_{yy}^2 l_{zy} + A_{zz}^2 l_{zz})^{1/2} \end{aligned} \qquad (3.2)$$

where g_{ii} and A_{ii} are the principle values of the tensors **g** and **A**, respectively, and I_{ij} are the squared direction cosines between the corresponding nitroxide molecular axes i and the magnetic field directions z. M_S and M_I are the eigenvalues of S_z and I_z, respectively. The EPR line positions are calculated from Eq. 3.2 in steps of 1.5° for θ and φ. The intensity $\boldsymbol{I\,d\Omega}$ of each absorption line is proportional to the number of molecules dN with their z molecular axis pointing into the space angle $\boldsymbol{d\Omega}$. The intensity is given for a random distribution of nitroxide orientations by

$$Id\Omega \propto \sin\theta \cdot d\theta \cdot d\varphi \qquad (3.3)$$

The procedure described above yields a stick spectrum that is convoluted by a superposition of a Gaussian and a Lorenzian to account for the natural line-broadening mechanisms. Here, the line width is assumed to be independent of the orientation of the nitroxides.

Simplest pair model.

The dipolar interaction of two unpaired electrons leads to considerable line broadening when motional averaging effects are absent. The absorption lines of a pair of interacting spins are shifted from the points without interaction by the amount of ΔB, which is given to a good approximation by (Ciecierska-Tworek et al., 1973; Likhtenshtein, 1976)

$$\Delta B = \pm\frac{3g\beta_e(3\cos^2\theta - 1)}{4\rho^3} \qquad (3.4)$$

where θ is the angle between the magnetic field B_o and the distance vector ρ between the two interacting spins. Here, the effect of anisotropic magnetic tensors is

neglected. The resulting dipolar line shape function G(ΔB) is calculated using Eq. 3.4 with discrete steps for θ of 1.5°. In a frozen solution or powder sample, the orientation distribution of the distance vector between the interacting spins may be assumed to be isotropic. Thus, the line intensity for each angle interval is determined from Eq. 3.3. To account for a range of distances expected to arise from a distribution of conformations of the protein or of the spin label side chain, a Gaussian distribution of interspin distances with a mean distance r_0 and width σ is permitted. The EPR spectrum F(B) is calculated by convoluting the non-interacting spectrum f(B) with the line shape function G(ΔB) (Steinhoff et al., 1991):

$$F(B) = \int f(B')G(B - B')dB' \qquad (3.5)$$

When the interspin distance becomes very small, the electron orbitals overlap and the EPR line shape is modulated due to J coupling. A separation between line shape effects due to dipolar interaction and exchange interaction seems to be difficult for immobilized samples. However, if we take the values reported by Closs and co-workers (1992) as a first approximation for our systems, the exchange interaction frequency J falls below the value of the dipolar splitting for interspin distances larger than 10 Å. The analysis with this method is thus restricted to distances exceeding 10 Å.

CW EPR spectra dipolar broadened with described pair-model were simulated using MATLAB 7.0 software package (http://www.mathworks.com/products/matlab/).

Simulation of CW EPR spectra for biradical.

In the case of two coupled electron spins Hamiltonian has a form:

$$H = \beta_e \mathbf{g_1} S_1 B_0 + \beta_n g_n I_1 B_0 + S_1 \mathbf{A_1} I_1 + \beta_e \mathbf{g_2} S_2 B_0 + \beta_n g_n I_2 B_0 + S_2 \mathbf{A_2} I_2 + S_1 \mathbf{J} S_2 \qquad (3.6)$$

where β_n is the nuclear Bohr magneton, g_n is the nuclear g value tensor and **J** is a coupling tensor between two unpaired electrons, which consists of dipolar coupling tensor and scalar J-coupling. Different relative orientations of two coupled radicals were permeated, which was set by three Euler angles for the orientation of each radical.

CW EPR spectrum for biradical was simulated with Easyspin software package (Stoll and Schweiger, 2006). As an advantage it calculates resonance field directly from Hamiltonian.

CW EPR experiment. Conventional, continuous-wave EPR spectra were recorded on a Bruker ESP 380E X-band EPR spectrometer with 100 kHz field modulation and 1 G modulation amplitude. A Bruker rectangular resonator was used, with a quartz Dewar containing liquid nitrogen (77 K).

3.3 *Solid-state NMR spectroscopy of oriented samples*

Solid-state NMR spectroscopy is a powerful tool for determining the structure of membrane-active peptides and proteins, because it allows the study of amorphous and partly mobile biological solids directly in the liquid-crystalline lipid bilayers (Bechinger, 1999; Fu and Cross, 1999; Marassi and Opella, 1998). Orientation-dependent nuclear spin interactions such as ^{15}N chemical shift and ^{15}N-^{1}H dipolar coupling provide exquisite probes of the orientation of membrane peptides relative to the bilayer normal. Correlation of the N-H dipolar coupling and the ^{15}N chemical shift in a two-dimensional (2D) spectrum (Wu et al., 1994) further allows the determination of the orientational topology of membrane peptides with multiple ^{15}N labels and even with multiple helical segments (Kim et al., 1998; Marassi et al., 1997).

Preparation of oriented membrane samples.

Lipid and peptide were co-dissolved in appropriate solvent in order to mix properly all components. The solution was spread onto ultrathin cover glasses (9 × 22 mm, Marienfeld, Lauda-Königshofen, Germany). All organic solvent was removed by exposure to a high vacuum overnight and the membranes were equilibrated at 93% relative humidity. Before the glass slides were stacked on top of each other, if necessary, the hydration at higher temperature and 100% relative humidity for 2 hours was performed (328 K for DPPC membrane and 310 K for DMPC membrane to turn it to fluid phase). The result of this preparation is shown schematically in Fig. 3.6. The degree of alignment could be checked by ^{31}P NMR of the lipid headgroups. Note, that addition of salt as well as high bound peptide / protein content could disturb the formation of oriented bilayers.

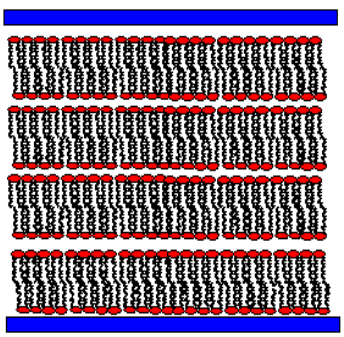

Fig. 3.6. Schematic view of oriented lipid bilayers between two glass plates.

Control of the orientation of lipid bilayer by ^{31}P-NMR-spectroscopy

The big class of phospholipids contains a phosphate group realizing the binding between the glycerol hydroxyl and the head group (i.e.: choline, ethanolamine) of the lipid. The phosphorous atom is well suitable to measure the orientation (or the orientational distribution) of the lipids in a sample. The measured ^{31}P isotope has a natural abundance of 100%, thus no labeling is needed. The high gyromagnetic ratio (μ_P / μ_H = 0.4) makes the nucleus very sensitive and makes control of sample orientation possible within minutes.

It is possible to determine a static CSA tensor of phosphorous in phospholipids at low temperature. In hydrated samples at in the room temperature the head group and the whole lipid undergo a fast rotational diffusion and the chemical shift anisotropy is averaged to a residual axialsymmetric tensor. Referenced to Phosphoric acid (= 0 ppm) the CSA tensor of POPC is approximately: (Seelig and Seelig, 1980)

$$\hat{\delta} = \begin{pmatrix} -19 & 0 & 0 \\ 0 & -19 & 0 \\ 0 & 0 & 28 \end{pmatrix}$$

This tensor makes the evaluation measured phospholipid bilayer sample relatively easy. The contribution of the spectrum at 28 ppm is related to the ratio of lipid with a bilayer normal parallel to the magnetic field. Other contributions to the spectrum represent other orientations. The spectrum of an unoriented lipid sample (powder) consists of dominant contribution at -19 ppm and a shoulder at 28 ppm.

The ^{31}P-NMR measurement provides a fast control of the quality of an oriented sample. Not only the orientation can be controlled but also lipids degradation can be detected. Lipids with different headgroups (Choline, Etanolamine …) have slightly different values in the CSA tensor and give rise to separate intensities.

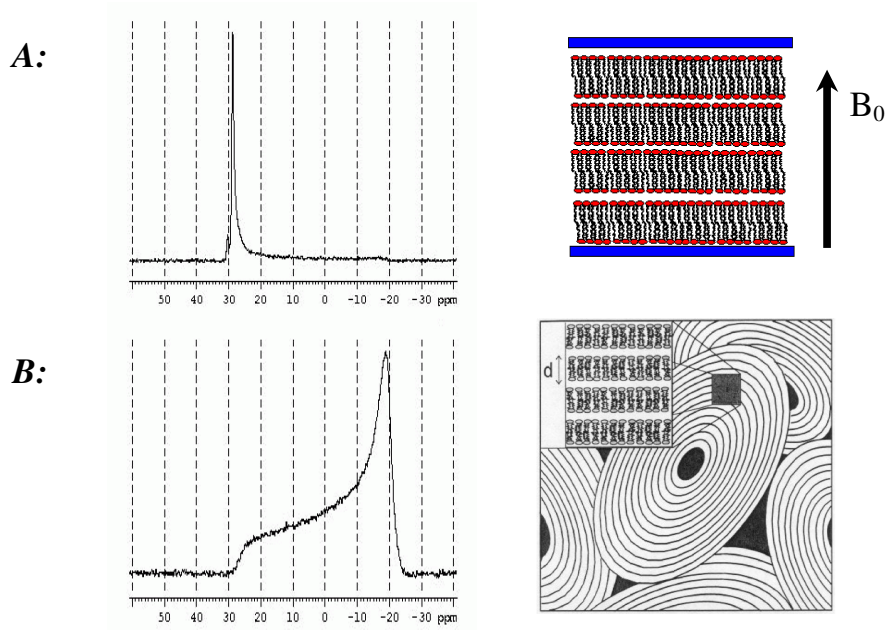

Figure 3.7. A: *proton-decoupled ^{31}P NMR spectrum of an oriented lipid bilayer sample containing a fraction of unoriented bilayers, the bilayer normal is oriented parallel to the magnetic field,* ***B****: proton-decoupled ^{31}P NMR spectrum of unoriented MLVs ("powder").*

^{31}P experimental parameters. Proton-decoupled ^{31}P solid-state NMR spectra were acquired at 161.953 MHz on a Bruker Avance widebore 400 NMR spectrometer equipped with a double resonance flat-coil probe. Proton decoupled ^{31}P spectra were acquired using a Hahn-echo pulse sequence with $\pi/2$ pulse 2.5 µs. The spectral width was 75 kHz. The echo and recycle delays were 40 µs and 3 s, respectively. The temperature was maintained at 295 K. Spectra were referenced externally to 85% H_3PO_4 at 0 ppm.

Determination of the orientation of a polypeptide helix by ^{15}N-NMR-spectroscopy

The orientation of a helix can be determined by ^{15}N-NMR-spectroscopy of the ^{15}N nitrogens of the peptide backbone. Since the natural abundance of ^{15}N is very low it has to be introduced artificially by labeling methods. The necessity of labeling implies some efforts to gain suitable samples.

Labeled amino acids for the synthesis are commercially available for many different amino acids (e.g. Alanine, Leucine), but relatively expensive. For proteins over-expressed in bacteria the labeling of all sites is straightforward but single-site labeling is more difficult.

Referenced to ammoniumchloride ($^{15}NH_4Cl \equiv 41.5$ ppm) the CSA tensor of the nitrogen atom of the peptide backbone has the following form:

$$\hat{\delta} = \begin{pmatrix} \delta_{11} & 0 & 0 \\ 0 & \delta_{22} & 0 \\ 0 & 0 & \delta_{33} \end{pmatrix}$$

where δ_{11} is in the range of 37-65 ppm, δ_{22} – 58-94 ppm and δ_{33} – 204-235 ppm (see Table 3.1).

Table 3.1 *^{15}N chemical shift tensor principal values from solid-state NMR measurements. The information for this table was taken from Korzhnev (Korzhnev et al., 2001) and Lee (Lee et al., 2001). See legend below for more information*

Sample	δ_{xx} [a]	δ_{yy} [a]	δ_{zz} [a]	δ_{iso} [b]	β [c]
Ala*Ala	65.3	78.1	215.5	119.6	12.6°
AcGly*AlaNH2	44.6	85.1	229.4	119.7	17.6° ± 2°
$(*Ala)_n$ α -helix	47.7	64.1	213.7	108.5	
$(*Ala)_n$ -5 β -sheet	53.7	71.4	210.7	111.9	
$(*Ala,Leu)_n$ α -helix	44.7	66.6	213.7	108.3	
$(*Ala,Asp\ (OBzl))_n$ α -helix	47.7	68.4	217.7	111.3	
$(*Ala,Glu\ (OBzl))_n$ α -helix	48.7	66.4	215.7	110.3	
$(*Ala,Glu\ (Ome))_n$ α -helix	46.7	67.8	214.7	109.7	
$(*Ala, Val)_n$ β-sheet	44.7	72.1	211.7	109.5	
$(*Ala, Ile)_n$ β -sheet	49.7	72.7	209.7	110.7	
$(*Asp\ (OBzl))_n$ -1 α_R –helix	48.7	62.5	214.7	108.6	
$(*Asp\ (OBzl))_n$ -2 α_L-helix	50.7	58	210.7	106.5	
$(*Asp\ (OBzl))_n$ -2 α_L-helix	49.7	57.1	211.7	106	
$(*Asp\ (OBzl))_n$ -2 α_L-helix	50.7	66.1	212.7	109.7	
N-Ac*Gly	37.0	82.8	220.4	113.4	25.5° ± 1°
(*Gly) collagen powder	42.3	67.0	223.4	110.9	24.5° ± 1°
(*Gly) collagen oriented	42.3	67.0	223.4	110.9	24.5° ± 2°
(*Gly) collagen	45.6	67.6	216.8	110.0	23°

(*Gly) maganine	42.0	73.2	215.0	110.1	22° ± 2°
Boc-$(Gly)_2$ *Gly-OBzl	55.1	62.1	223.0	113.4	22° ± 1°
Boc-$(Gly)_2$ *Gly-OBzl	36.4	83.4	220.4	113.4	24° ± 1°
Gly*Gly	46.8	79.7	220.8	115.8	
Gly *Gly·HCL	57.3	59.8	210.0	109.0	18.6° ± 2°
AcGly *$GlyNH_2$	40.7	64.2	210.0	105.0	17.6° ± 2°
Gly *Gly·HCL·H_2O (powder)	58.5	64.1	209.5	110.7	25° ± 5°
Gly *Gly·HCL·H_2O (crystal)	60.3	70.9	215.9	115.7	21.3°
$(*Gly)_n$ β-sheet	45.7	61.4	205.7	104.3	
$(*Gly)_n$ -helix	49.7	62.8	214.7	109.1	
$(*Gly, Ala)_n$ α -helix	44.7	57.6	212.7	105.0	
$(*Gly,Ala)_n$ β -sheet	39.7	66.0	206.7	104.1	
$(*Gly,Leu)_n$ α -helix	45.7	61.7	210.7	106.0	
$(*Gly,Leu)_n$ β -sheet	40.7	66.2	206.7	104.5	
$(*Gly, Val)_n$ β -sheet	39.7	74.6	203.7	106.0	
$(*Gly, Ile)_n$ β -sheet	45.8	68.3	209.7	108.6	
$(*Gly,Lys(Z))_n$ α -helix	40.7	69.2	208.7	106.2	
$(*Gly,Glu(OBzl))_n$ α -helix	47.7	61.2	210.7	106.5	
$(*Gly,Sar)_n$	38.7	65.8	204.7	103.1	
(*Phe) maganine	55.0	80.0	220.0	118.3	22° ± 3°
AcGly *TyrNH2	52.1	77.1	209.3	112.8	19.6° ± 2°
n-Ac-L-*Val-L-Leu (powder)	60.2	87.1	230.1	125.8	20° ± 2°
n-Ac-L-Val-L-*Leu (powder)	58.7	93.7	232.8	128.4	18° ± 2°
n-Ac-D,L-*Val (powder) site I	59.6	80.5	235.3	125.1	21° ± 2°
n-Ac-D,L-*Val (powder) site II	57.5	81.0	227.0	121.8	21° ± 2°

[a] Here $\delta_{zz} > \delta_{yy} > \delta_{xx}$ are the frequency ordered principal values of the chemical shift tensor. [b] The isotropic chemical shift $\delta_{iso}=(\delta_{xx+} \delta_{yy+} \delta_{zz})/3$. [c] The angle between the least shielded axis, δ_{zz}, of the CSA tensor and the N-H bond.

The orientation of the principal axis of the CSA-tensor is displayed in Fig. 3.8

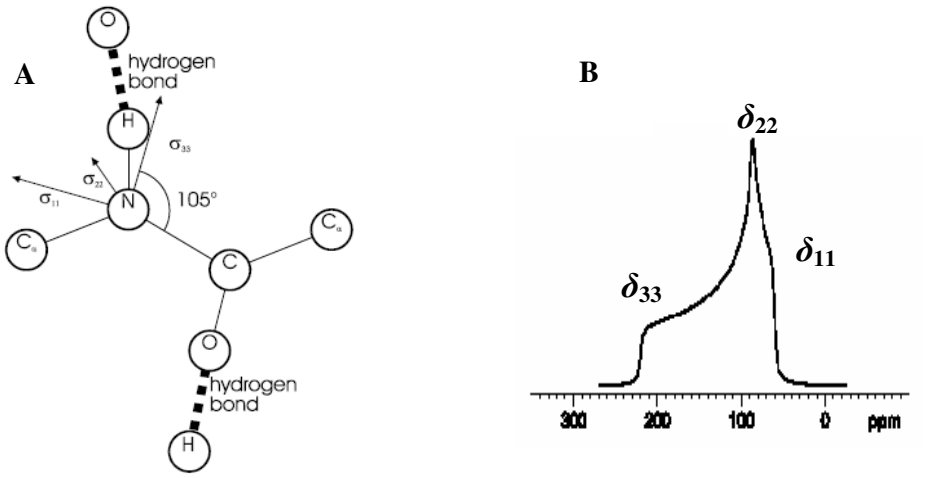

***Figure 3.8. A**: Hydrogen bonds between the backbone hydrogens and the backbone oxygen of other aminoacids are essential stabilizing forces in a helix conformation. The δ_{33} component of the CSA tensor of amid ^{15}N is on average 17º away of the hydrogen bond of the helix and subsequently roughly parallel to the helix axis. The δ_{11} and δ_{22} components are nearly perpendicular to the helix axis and have about the same size. **B**: ^{15}N powder spectrum of a peptide bond.*

For many applications the tilt angle of a helix within the lipid bilayer is of particular interest. The interpretation of the measured data is simplified by the fact that the principal axis of the dominant contribution (δ_{33}) to the CSA tensor is nearly parallel to the helix axis. The hydrogen bond is a consequence of the charge distribution within the molecule (positive partial charge at the hydrogen and negative partial charge at the oxygen atom). It suggests itself that the hydrogen bond is closely related to shielding tensor and the CSA tensor. The resonance of inplanar polypeptides is dominated by δ_{11} and δ_{22} and in the range between 37 ppm and 94 ppm (Fig. 3.9 A). The resonance of transmembrane polypeptides is dominated by δ_{33} and peak appears in the range between 204 ppm and 235 ppm (Fig. 3.9 B).

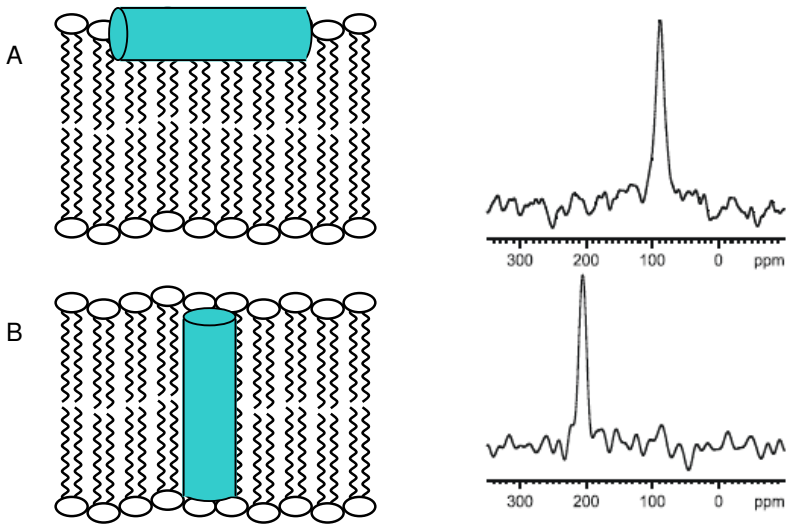

Figure 3.9. *^{15}N solid-state NMR spectrum of a helical polypeptide reconstituted in oriented lipid bilayers.* ***A****: polypeptide is oriented inplanar on the membrane surface.* ***B****: polypeptide is oriented transmembrane.*

For a more detailed description of the orientation of a helix in the bilayer further calculations considering the CSA-tensor within the molecular frame are necessary. However, the result is in general not a unique orientation but a set of orientations, which are consistent with the measured frequency.

Cross-Polarization NMR measurements

Due to the low sensitivity of the ^{15}N nucleus (μ_P / μ_H = -0.1) and long T_1 relaxation times experiments like a Hahn-echo would not give signal in reasonable time. Therefore the signal has to be enhanced. This is under certain conditions possible by Hartmann-Hahn Cross-Polarization. The basic idea of cross-polarization is the induction of transversal magnetization to protons (by a 90° pulse) and the transfer of this transversal magnetization to the nitrogen nuclei. This transfer of magnetization can be archived by locking both the proton and the nitrogen nuclear spin by irradiation with an electromagnetic field, which satisfies the Hartmann-Hahn condition.

At the Hartmann-Hahn condition

$$\gamma_H B_1^H = \gamma_N B_1^N$$

the precession velocity of both proton and nitrogen are the same.

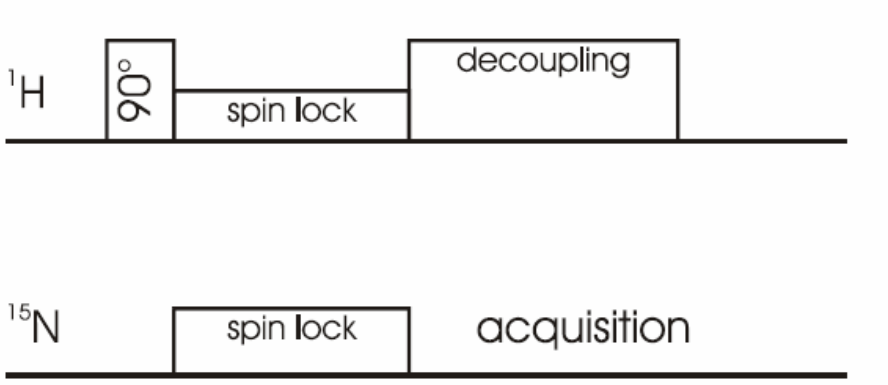

Figure 3.10. *Schematic representation of the cross-polarization (CP) experiment.*

Using the cross polarization experiment the critical factor for relaxation of the system to the thermal equilibrium is T_1 of the protons and not T_1 of the nitrogens. Protons in oriented lipid samples have a $T_1 \approx 1$s whereas nitrogens have a $T_1 \approx 10$s. Therefore cross polarization experiments can be performed with a much shorter repetition time than NMR-experiments using directly ^{15}N.

During Mismatch-Optimized IS transfer (MOIST) simultaneous π phase shifts are introduced for the spin-locking field, on both channels, at intervals long enough to allow the system to attain equilibrium before the next phase shift. This resembles normal Hartmann-Hahn cross polarization except for the synchronous phase reversals of the two spin-locking radio frequency fields. This has a strong beneficial effect on the efficiency of cross polarization away from the perfect match. Thus, the sequence involving repeated simultaneous π phase shifts of the two channels allows efficient cross polarization even under Hartmann-Hahn mismatch conditions as they occur under real experimental conditions (Levitt et al., 1986.).

^{15}N 1D experimental parameters. Proton-decoupled ^{15}N cross polarization (CP) spectra of static aligned samples were acquired at 40.54 MHz on a Bruker Avance widebore 400 NMR spectrometer equipped with a double resonance flat-coil probe (Bechinger and Opella, 1991). An adiabatic CP pulse sequence was used with a spectral width, acquisition time, CP contact time and recycle delay time of 75 kHz, 3.5 ms, 0.5 ms and 3 s, respectively. The ^{1}H π/2 pulse and spinal64 heteronuclear decoupling field strengths was 42 kHz. 40 k scans were accumulated and the spectra were zero filled to 4 k points. A 100 Hz exponential line-broadening was applied before Fourier transformation.

Spectra were externally referenced to $^{15}NH_4Cl$ at 41.5 ppm. An Oxford temperature control unit was used to set the temperature.

PISEMA and peptide secondary structure

In order to get insight to the structure of peptide bound to lipid bilayers 2D ^{15}N -^{1}H dipolar coupling - ^{15}N chemical shift correlation experiment spectra are highly efficient.

Transient dipolar oscillations during the CP transfer have been observed in various systems that exhibit a relatively weak proton–proton coupling network. However, the dipolar oscillation is primarily damped by the proton–proton spin diffusion due to the strong coupling of the directly bonded protons to remote protons. With the use of a frequency-switched Lee–Goldburg (FSLG) pulse sequence (Lee and Goldburg, 1965) to sufficiently suppress proton homonuclear dipolar coupling, PISEMA (Polarization Inversion Spin Exchange at Magic Angle) (Wu et al., 1994) has dramatically improved the resolution of static solid-state anisotropic dipolar and chemical shift correlation spectra.

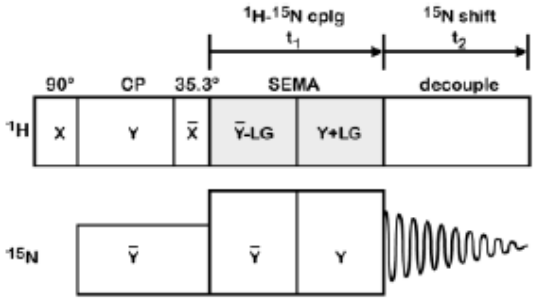

Figure 3.11. *The 2-dimensional PISEMA pulse sequence for high-resolution solid-state NMR ^{1}H–^{15}N dipolar coupling / ^{15}N chemical shift correlation spectroscopy.*

The 2-dimensional pulse sequence for the PISEMA experiment is shown in Fig. 3.11. Cross-polarization is obtained after the 90° pulse in the preparation period. A 35.3° pulse rotates the ^{1}H magnetization to the magic angle, and the ^{1}H–^{15}N dipolar coupling frequencies evolve during the SEMA period in t_1 while the ^{1}H–^{1}H homonuclear dipolar interactions are decoupled using flip-flop, FSLG irradiation. The ^{15}N magnetization is observed during the t_2 period with continuous ^{1}H frequency irradiation for heteronuclear ^{1}H–^{15}N decoupling.

The PISEMA experiments have been widely used to obtain orientational constraints from uniformly labeled membrane proteins in a lamellar lipid phases (for a review see

Marassi, 2002). Complete resonance assignment would provide information for 3D structure calculations of the protein in the membrane-bound state, but the similarity of chemical shift tensors for all residues makes this analysis too complicated. The problem was partially solved by the production of proteins labeled at single site ^{15}N. However, the resonance patterns in the two-dimensional PISEMA spectra form the so-called PISA wheels (Polarity Index Slant Angle), which uniquely define the helical tilt with respect to the bilayer normal without a need for resonance assignments provided that the polypeptide adopts an α-helical conformation.

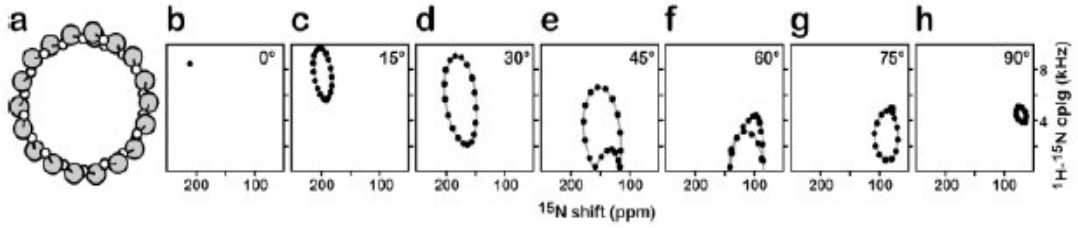

Figure 3.12. *The ^{1}H-^{15}N dipolar coupling / ^{15}N chemical shift PISA wheel PISEMA spectra calculated for 20-residue α helix with uniform dihedral angles (φ/ψ = -65º/-40º) at different helix tilts relative to the magnetic field direction and subsequently the membrane normal: (b) 0º, (c) 15º, (d) 30º, (e) 45º, (f) 60º, (g) 75º, (h) 90º. The gray lines trace out the PISA wheels that are characteristic of helices associated with membranes. (a) A view of the α helix down its helix axis is shown. (taken from Marassi, 2002)*

These characteristic patterns result from the orientation of the amide NH bond vectors relative to the α-helix and from the noncoincidence of the δ_{33} component of the ^{15}N chemical shift tensor and the N–H bond vector (see Fig. 3.8). The resonance frequencies in the PISEMA spectra of oriented proteins depend on helix or strand orientation, as well as on the backbone dihedral angles, the magnitudes and orientations of the principal elements of the amide ^{15}N chemical shift tensor, and the N-H bond length. Therefore, it is possible to calculate solid-state NMR spectra for specific structural models of proteins, as shown in Fig. 3.12 for the case of an ideal α-helix with uniform dihedral angles (φ/ψ = -65°/-40°). When the helix axis is parallel to the lipid bilayer normal and the magnetic field direction, all of the amide sites have an identical orientation relative to the direction of the applied magnetic field; therefore, all of the resonances overlap with the same dipolar coupling and chemical shift frequencies (Fig. 3.12 (b)). For all helix orientations other than parallel to the field (0°), the spectra have

Pisa wheels that reflect the helix tilt and rotation in the membrane. Tilting the helix away from the membrane normal introduces variations in the orientations of the amide NH bond vectors in the magnetic field and leads to dispersion of the $^{1}H–^{15}N$ dipolar coupling and ^{15}N chemical shift frequencies (Fig. 3.12 (c–h)), which are manifest in the appearance of ellipsoid resonance patterns (or Pisa wheels) in the spectra. Because a modest helix tilt of about 15° aligns the NH bond from one amide site and the δ_{33} amide ^{15}N chemical shift tensor element of another amide site with the magnetic field, the maximum values of chemical shift and dipolar coupling are observed in the spectrum, albeit from different resonances. This is a direct consequence of the δ_{33} of the amide shift tensor being rotated approximately 17° from the N-H bond vector. Many transmembrane helices are tilted with respect to the bilayer normal. The combination of tilt and the noncoincidence of the δ_{33} and NH bond vectors makes it possible to resolve many resonances from residues in otherwise uniform helices and is responsible for the wheel-like pattern observed in 2-dimensional PISEMA spectra of uniformly ^{15}N labeled proteins.

For helices with tilts greater than 40° some amide NH bonds adopt orientations near the magic angle (55°) and have resonances with dipolar couplings close to 0 kHz. Other amide NH bonds are oriented with angles greater than 55° and have resonances with dipolar couplings of opposite sign, which results in a portion of the Pisa wheel being reflected through the 0-kHz frequency axis. Helices oriented parallel to the membrane surface (90°) have amide N-H bonds and ^{15}N chemical shift δ_{33} vectors nearly orthogonal to the field. As a result, they give highly overlapped spectra with the resonance frequencies at around 5 kHz and 75 ppm. The spectra in Fig. 3.12 demonstrate that it is possible to determine the approximate tilt of a helix in lipid bilayers without resonance assignments.

Calculation of PISEMA spectra for uniformly ^{15}N labeled helices of α, 3_{10} and π type reveals that PISA wheel is sensitive to peptide secondary structure (see Fig. 3.13).

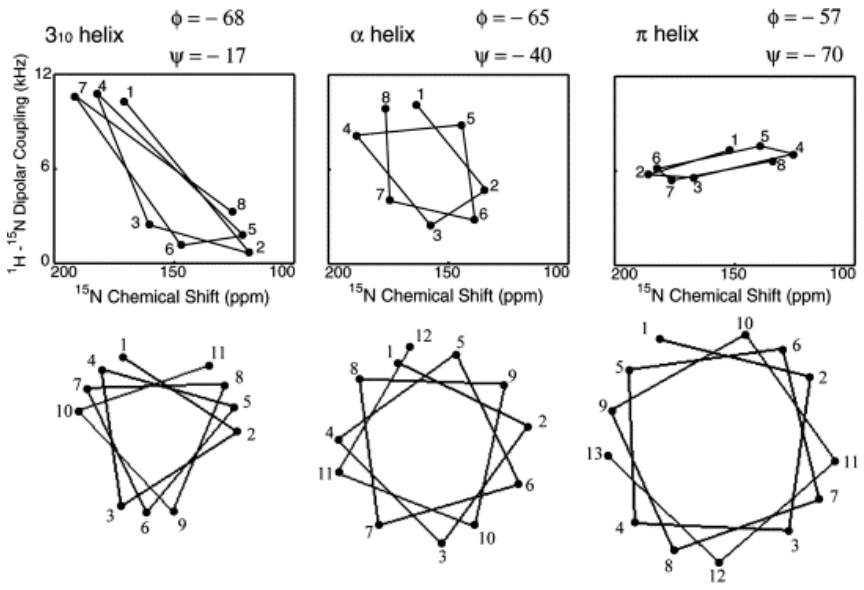

Figure 3.13 *The relationship between helical wheel projections, and PISA wheel patterns for 3_{10}, α, and π-helices. Note that the same scale of bond lengths is used for the helical wheel projections so that their relative size is illustrated. Helical tilt (τ) of 30º was used for the simulation of PISEMA spectra. (taken from Kim and Cross, 2004)*

PISEMA experimental parameters. The two-dimensional PISEMA experiment was used to correlate the ^{15}N-^{1}H dipolar coupling with the ^{15}N chemical shift of the same nitrogen (Wu et al., 1994). PISEMA spectra of static aligned samples were acquired at 40.54 MHz on a Bruker Avance widebore 400 NMR spectrometer equipped with a double resonance flat-coil probe (Bechinger, 1991). The effective ^{1}H RF spin-lock amplitude was 45 kHz. During the spin exchange period the ^{1}H RF amplitude was decreased to 36.8 kHz in order to maintain the Hartmann– Hahn match condition with an effective field along the magic angle of 45 kHz. Experiments used a 3 s relaxation delay, 0.5 ms Hartman–Hahn contact period for CP, and a 3.5 ms acquisition period with ^{1}H decoupling. Samples were cooled with a stream of air at a temperature of 295 K. Spectra were externally referenced to $^{15}NH_4Cl$ at 41.5 ppm. For the experimental set-up a fully ^{15}N, ^{13}C labeled NAL single crystal was used.

Simulation of NMR experiments.

All numerical simulations were accomplished on a 3,4-GHz Pentium(R) D workstation operating under Windows XP Professional using the SIMPSON / SIMMOL solid-state NMR simulation package (Bak et al., 2002). Calculated PISEMA spectra were

visualized using the GSim software, version 0.12.0. (http://www.dur.ac.uk/vadim.zorin/soft.htm).

Chemical shift tensor is important for correct deriving of peptide tilt angle. The amide ^{15}N CS tensor values of normal amino acids exhibits rather small deviation, depending however on the polypeptide secondary structure and environment (see Table 3.1).

Alamethicin and ampullosporin A peptides contain a high percentage of unusual Aib residues (8 of 20 and 7 of 15, correspondingly). The lack of H_α in these residues could dramatically affect ^{15}N chemical shift tensor principal values, it could even result in a valuable decrease in tensor anisotropy. Note, that isotropic CS value is rather similar to that for other aminoacids, as it was clearly shown by NMR analysis of ^{15}N perlabeled alamethicin in solution (Yee and O'Neil, 1992). Rather small experimental information is available on Aib amid ^{15}N CSA tensor. To refine this question Ac-Aib labeled by ^{15}N at a single site was investigated (see Fig. 3.14). As a result (see Fig. 3.14), amide CSA tensor values of Aib were found to be of about (70 ppm, 106 ppm and 249 ppm). Chemical shift anisotropy parameter $((\delta_{xx+}\ \delta_{yy})/2 - \delta_{zz})$ exhibits similar value to that is generally observed (see Table 3.1), while the isotropic value of 142 ppm is noticeably higher. There is a strong experimental support on the similar CS isotropic values for usual amino acids and Aib when it's a part of a peptide (see HSQC spectrum of ampullosporin A in Fig. 6.1).

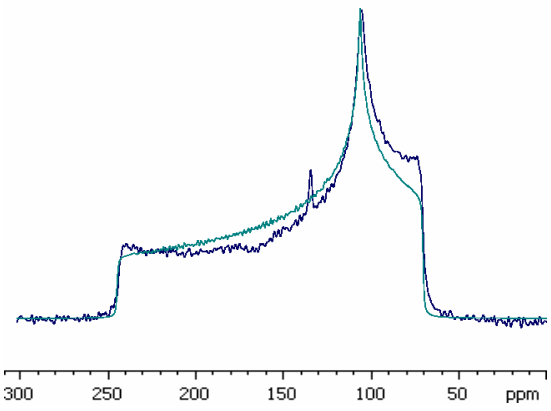

Figure 3.14. *Proton-decoupled ^{15}N solid-state NMR spectrum of dry powder of Ac-Aib (noisy line) and its SIMPSON simulation (smooth line) with the CS tensor of (70 ppm, 106 ppm and 249 ppm).*

For the uniformly ^{15}N labeled polypeptide it was therefore assumed that amide ^{15}N label of each amino acid has the same CS principal values. The proton-decoupled ^{15}N spectrum of dry powder alamethicin peptide (noisy thin line) and its simulation (thick line) are shown below (Fig. 3.15).

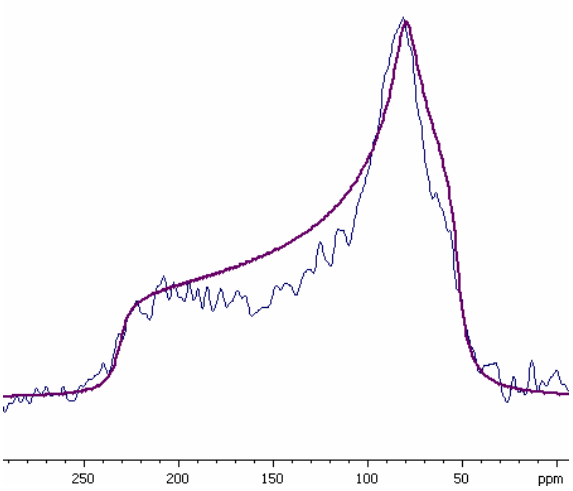

Figure 3.15. *Proton-decoupled ^{15}N solid-state NMR spectrum of dry powder of alamethicin peptide (noisy thin line) and its SIMPSON simulation (thick line) with the CS tensor of (51 ppm, 79 ppm and 230 ppm).*

The values obtained from the simulation of dry alamethicin compound are (51 ppm, 79 ppm and 230 ppm). These static tensor elements were used for the simulations of PISEMA spectra of membrane bound peptides.

Uniaxial rotation of membrane bound peptide around bilayer normal could lead to a remarkable reduction of ^{15}N CSA (North et al., 1995; Yamaguchi et al., 2001; Bechinger and Sizun, 2003; Prongidi-Fix et al., 2007). This question will be discussed in chapter 6.

3.4. *Solid-state NMR of lipid vesicles*

Preparation of MLV samples.

Samples with different lipid compositions: POPC–POPC-d31 (Fig. 3.16B) and POPE–POPG-d31 (Fig. 3.16A), with respective molar ratios of 3:1, were prepared for ^{2}H echo NMR. A total of around 5 mg lipids per sample was dissolved and mixed in chloroform.

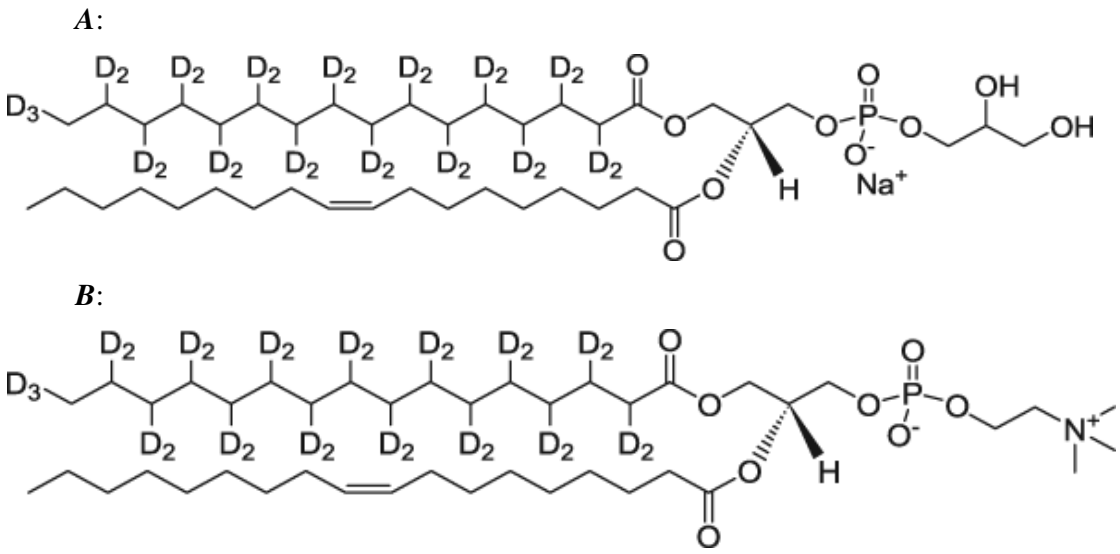

Figure 3.16*. Structure of* ***A****: 1-Palmitoyl(d31)-2-Oleoyl-sn-Glycero-3-[Phospho-rac-(1-glycerol)] (POPG-d31), sodium salt and* ***B****: 1-Palmitoyl(d31)-2-Oleoyl-sn-Glycero-3-Phosphocholine (POPC-d31). Taken from http://avantilipids.com .*

If necessary the solution of alamethicin in chloroform or ampullosporin A peptide in methanol was added to give a final concentration of 2% by mole relative to the lipids. The lipid / peptide mixture were dried under rotor evaporation at room temperature and exposed to a vacuum overnight. Lipid films were then rehydrated with 4 ml of a 0.1 M Tris-0.1 M KCl buffer, pH 7.5, at room temperature. The samples were briefly sonicated in a bath sonicator and subjected to five rapid freeze-thaw cycles and then centrifuged at 21,000 $*$ *g* for 40 min at 4°C. Previous determination of a binding constant of $5.7 * 10^{4}$ M^{-1} (Kropacheva et al., 2005) for ampullosporin A and phosphatidylcholine vesicles at pH 7.5 indicated that very little peptide would be free in solution after this process. The excess buffer was then removed to give final water content of about 50% by weight. The

pellets, containing lipid vesicles with or without associated peptides, were transferred to Bruker 4-mm magic angle spinning (MAS) rotors for NMR measurements.

^{2}H NMR of Labeled Phospholipids

Deuterium is the most versatile nucleus in studies of lipids in model membranes. It is a spin-1 nucleus with a quadrupole moment. The Larmor frequency is only about 15% of that of protons, hence the sensitivity is low. This is in part compensated by the fast quadrupolar relaxation, making it possible to use a relaxation delay between consecutive scans of 100 ms or less.

Since deuterium occurs with a natural abundance of only 0.01%, lipids must be selectively or uniformly labeled. The quadrupole splittings of deuterated acyl chain segments directly reflect the motional order parameters within the hydrophobic region. In the case of an axially symmetric lipid motion, in so-called Pake-powder spectrum (Davis, 1983), the separation between the symmetrical intense horns, denoted as the quadrupolar splitting of the i^{th} C-D bond, is

$$\Delta\nu^i = \frac{3}{4}\frac{e^2qQ}{h}S^i_{C-D} ,$$

where e^2qQ/h is the static quadrupole coupling constant (167 kHz for a C-D bond; Davis, 1983),

The lipid order parameter profile thus reveals any disordering effects of a peptide and indirectly its depth of penetration. The acyl chain order parameter profile shows the mobility of the chain at different position along the acyl chain. When a peptide is inserted in the bilayer surface region, i.e., acting as a spacer between the lipid head groups, this will provide more freedom for the acyl chains to move and consequently decrease their order. If, on the other hand, the peptide is aligned in a transmembrane orientation, the order may increase or decrease depending on the specific interactions between the peptide and the acyl chain segments (de Planque et al., 1998). Furthermore, the main lipid phase transition is readily detected by dramatic changes in the acyl chain spectra. In the gel phase, all resonances are broad and unresolved, but upon chain melting they sharpen to give a typical Pake pattern.

^{2}H NMR experimental parameters. ^{2}H quadrupole echo sequence (Fig. 3.17) were performed at 46.10 MHz on a Bruker Avance 300 NMR spectrometer using a 4-mm MAS probe and a spectral width of 200 KHz with recycle delay, echo delay, acquisition time, and 90° pulse lengths of 0.3 s, 42 μs, 2 ms, and 5 μs, respectively. The temperature was

maintained at 310 K. Between 50,000 and 200,000 transients were acquired to obtain a signal-to-noise ratio greater than 50:1. During processing, the first 32 points were removed in order to start Fourier transformation at the beginning of the echo. Spectra were zero filled to 8,192 points, and 30-Hz exponential line broadening was applied. In fluid lipid bilayers the static splittings of up to 250 kHz are usually motionally averaged down to below 70 kHz for the chains. Smoothed deuterium order parameter profiles were obtained from symmetrized and dePaked ^{2}H NMR powder spectra using published procedures (Schäfer et al., 1995; Seelig and Seelig. 1974; Sternin et al., 1983). Symmetrization and dePaking of experimental ^{2}D spectra were done by A. James Mason.

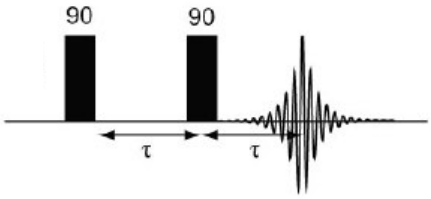

Figure 3.17*. Pulse sequence for quadrupolar echo solid-state NMR experiment.*

Chapter 4

Location of Trichogin GA IV in lipid membrane by ESEEM

The present chapter is a part of the published paper: E.S. Salnikov, D.A. Erilov, A.D. Milov, Yu.D. Tsvetkov, C. Peggion, F. Formaggio, C. Toniolo, J. Raap, S.A. Dzuba "Location and aggregation of the spin-labeled peptide trichogin GA IV in a phospholipid membrane as revealed by pulsed EPR" ***Biophys. J.,*** 2006, **91(4)** 1532–1540
A part of experiments was done together with Denis Erilov.

INTRODUCTION

Trichogin GA IV, isolated from the mold *Trichoderma longibrachiatum* (Auvin-Guette et al., 1992), belongs to the class of peptaibols, characterized by a high percentage of Aib residues and an 1,2-amino alcohol at the C-terminus (Benedetti et al., 1982). The primary structure of this peptaibol is unique due to its lipophilic *n*-octanoyl group at the N-terminus instead of the acetyl group present in most of the other members of this class. Despite the short length of its main chain (11 amino acid residues), trichogin GA IV exhibits remarkable membrane modifying properties (for recent review articles see references (Rebuffat et al., 1999, Toniolo et al., 2001, Peggion et al., 2003).

To elucidate the mechanism by which this short peptide changes the membrane permeability, detailed information is needed on where it is located in the membrane. Orientation and immersion depth of trichogin GA IV were studied using different experimental methods (Monaco et al., 1999a; Mazzuca et al., 2005). Previously, hyperfine interaction (hfi) constants of TOAC spin labeled trichogin analogues in membranes of phosphatidylcholine liposomes were analyzed as a function of environmental polarity (Monaco et al., 1999a). Trichogin was found to be oriented parallel to the membrane surface with the hydrophobic side chains facing towards the

membrane interior. However, this approach (Rebuffat et al., 1999) is based on the questionable procedure of deriving hfi constants, which are not only related to the perpendicular orientation constant, $A_{\perp}$, but also depend on molecular motion. Another approach to assess the degree of insertion of the peptide in the membrane was based on the quenching of fluorescence of 4,4-difluoro-4-bora-3a,4a-diaza-S-indacene (BODIPY) labeled lipids by nitroxide spin labels located at different positions of the peptide chain (Epand et al., 1999, Kaiser and London, 1998). However, as this bulky fluorophoric group attached to phospholipid has a clear tendency to migrate from the hydrocarbon core to the polar head group region of the bilayer (Kaiser and London, 1998), this method is even less reliable.

Recently, Mazzuca et al. (Mazzuca et al., 2005) employed fluorescence quenching measurements to investigate the membrane bound state of trichogin. It was found to depend on the peptide concentration. At low peptide/lipid (P/L) ratios the trichogin molecules are located close to the polar region of lipid head groups. By increasing the peptide concentration until membrane leakage takes place, a cooperative transition occurs and a significant fraction of the peptide becomes buried deeper into the bilayer.

In the present chapter, the peculiarities of trichogin GA IV analogues spin-labeled with TOAC (2,2,6,6-tetramethylpiperidine-1-oxyl-4-amino-4-carboxylic acid) in the presence of multilamellar dipalmitoylphosphatidylcholine (DPPC) membranes (frozen at 77 K) over a broader range of P/L ratios were studied by ESEEM technique. The primary structures of trichogin GA IV and its analogues are shown in chapter 3.1 and also below.

*n*Oct -**TOAC**^{1}-Gly-Leu-Aib^{4}-Gly-Gly-Leu-Aib^{8}-Gly-Ile-Leu-OMe (*n*Oct-TOAC1)

*n*Oct-Aib^{1}-Gly-Leu-**TOAC**^{4}-Gly-Gly-Leu-Aib^{8}-Gly-Ile-Leu-OMe (*n*Oct-TOAC4)

Fmoc-**TOAC**^{1}-Gly-Leu-Aib^{4}-Gly-Gly-Leu-Aib^{8}-Gly-Ile-Leu-OMe (FTOAC1)

Fmoc-Aib^{1}-Gly-Leu-**TOAC**^{4}-Gly-Gly-Leu-Aib^{8}-Gly-Ile-Leu-OMe (FTOAC4)

Fmoc-Aib^{1}-Gly-Leu-Aib^{4}-Gly-Gly-Leu-**TOAC**^{8}-Gly-Ile-Leu-OMe (FTOAC8)

The presence of two CH_3 groups attached to C_{α} in Aib residue makes the replacement of Aib residue by TOAC group very attractive in the way that it is very likely to induce no change on peptide 3D structure. Intensive study of structure and antimicrobial activity of these trichogin GA IV analogs conclude that these replacements do not alter the 3D-structural properties nor the membrane activity of trichogin (Auvin-Guette et al., 1992, Toniolo et al., 2001, Peggion et al., 2003, Toniolo et al., 1996, Venanzi et al., 2006).

RESULTS

An example of the experimental time-domain ESEEM data is shown in Fig. 4.1 for FTOAC1 bound to DPPC bilayers hydrated in D_2O, at two different peptide concentrations. Figs. 4.1a and 4.1c present original data, which were approximated by exponential decays. Figs. 4.1b and 4.1d show the result of their division by these decay functions. It is evident that at high concentration the decay is remarkably faster (compare Figs. 4.1a and 4.1c) which may be readily explained by the concentration dependence of transverse relaxation. Because of the fast decay, at high concentration, and the consequential increase of noise at large T, data in Fig. 4.1d were truncated at $T > 3.5$ μs.

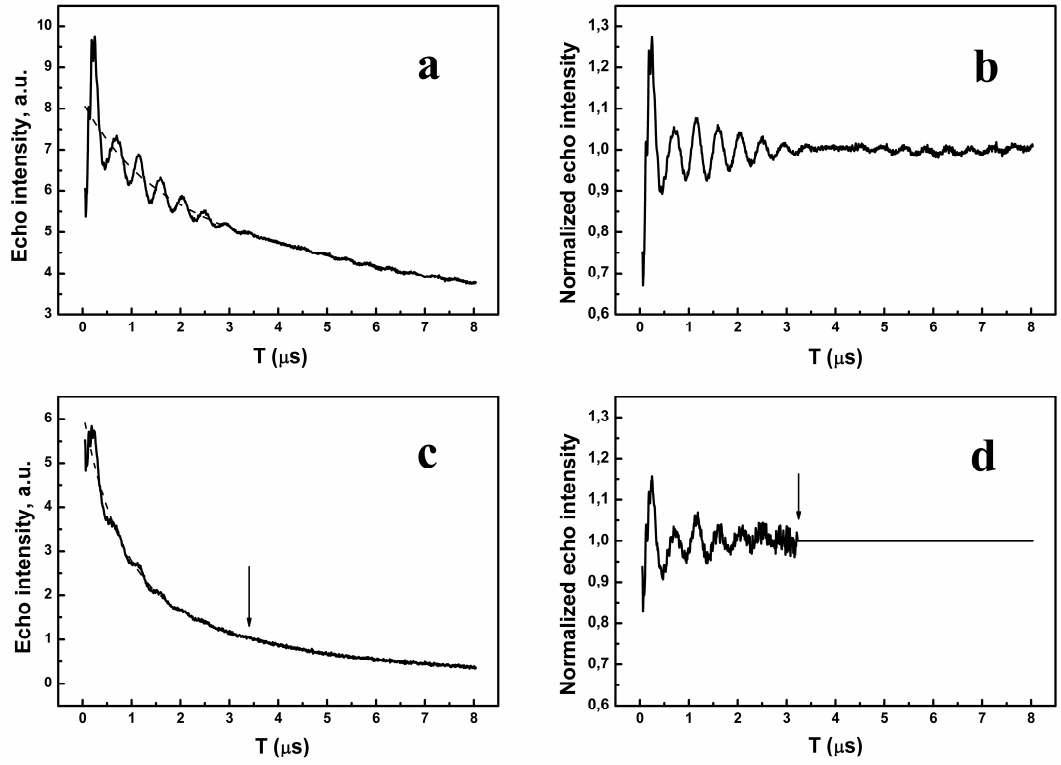

Figure 4.1. *Experimental ESEEM traces obtained for the spin-labeled peptide FTOAC1 in a DPPC membrane, hydrated in D_2O, for P/L molar ratios 1 : 250 (a, b) and 1 : 20 (c, d). Original data, given in (a) and (c), are approximated by a biexponential decay (dashed lines). Data in (b) and (d) are the result of dividing the original data by these decay functions. The arrow marks the point of data truncation to reduce the level of noise.*

Fig. 4.2 shows the modulus Fourier transform spectra for three samples (FTOAC1, FTOAC4, and FTOAC8) at a P/L molar ratio 1 : 250. One can see a narrow doublet at frequency 2.2 MHz, overlapped by a broader line. Since 2.2 MHz is the Larmor frequency of the deuterium nuclei in the magnetic field employed, both of these lines may be readily attributed to the anisotropic hfi between the unpaired electron of the nitroxide label and the deuterium nuclei of water molecules. The narrow doublet, according to the comprehensive analysis performed in reference (Erilov et al., 2005), may be assigned to free water present at the hydrocarbon chain region of the membrane, while the broad line is indicating water molecules bound to the N-O group of the spin label. The doublet is caused by the quadrupolar splitting for the deuterium spin with I = 1.

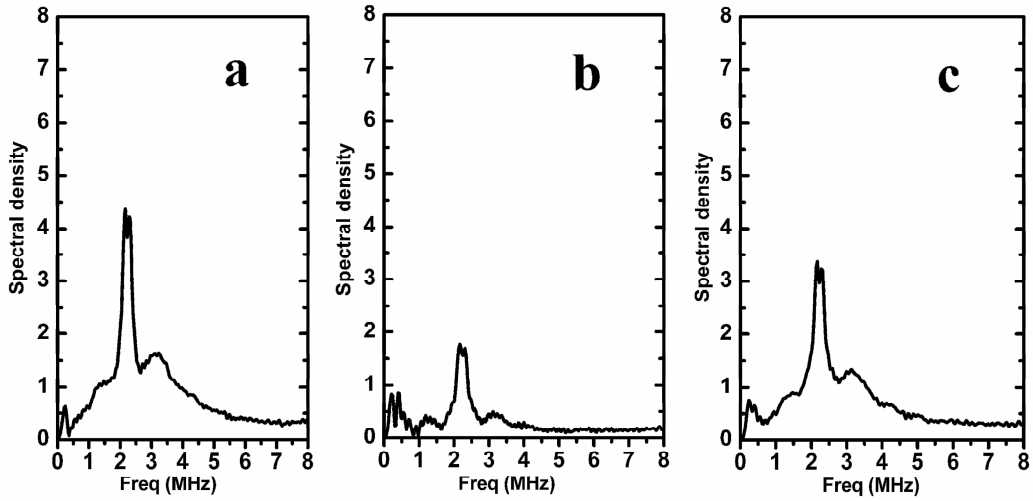

***Figure 4.2**. Modulus Fourier-transform ESEEM spectra obtained for a P/L molar ratio of 1 : 250. (a) FTOAC1, (b) FTOAC4, and (c) FTOAC8.*

The highest amplitude of the deuterium line is observed for the sample containing the membrane bound trichogin analogue labeled at the N-terminus (FTOAC1). Compared to FTOAC1, the sample with the analogue labeled near the C-terminus (FTOAC8) shows a decreased amplitude (by ~ 20 %) for the deuterium line, while in the case of the peptide labeled in the middle of the peptide chain (FTOAC4) the amplitude of the deuterium line is most strongly decreased by ~ 60 %.

Figs. 4.3a and 4.3b show the modulus Fourier transform spectra for membrane bound samples of *n*Oct-TOAC1 and FTOAC1 at a P/L molar ratio 1 : 250 (note that the spectrum shown in Fig. 4.3a coincides with that of Fig. 4.2a). It is clear that both spectra are nearly the same. Fig. 4.3c shows data adapted from ref. (Erilov et al., 2005)

presenting ESEEM amplitudes of nitroxide labels at different positions of the *sn*-2 fatty acyl side chain of DPPC lipid molecules which are incorporated in unlabeled DPPC membranes. As the membrane was obtained under the same experimental conditions as those employed in this work, the data in Fig. 4.3c may serve as a calibration curve for determining the membrane insertion of nitroxide labeled trichogin molecules.

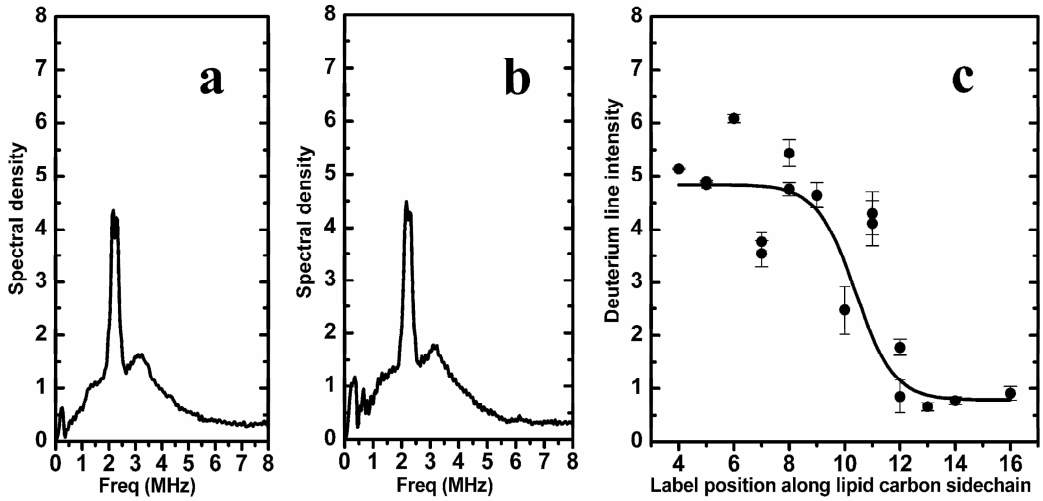

Figure 4.3. *Modulus Fourier-transform ESEEM spectra recorded by using a sample at a P/L molar ratio of 1 : 250 for (a) FTOAC1 (the spectrum is the same as shown in Fig. 4.2a) and (b) nOct-TOAC1. (c) Calibration curve representing ESEEM amplitudes for lipids spin-labeled at different positions along the hydrocarbon side chain (adapted from (Erilov et al., 2005)).*

Figs. 4.4a and 4.4b show the modulus Fourier transform spectra for membrane bound samples of *n*Oct-TOAC4 and FTOAC4 at a P/L molar ratio 1 : 250 (note that the spectrum shown in Fig. 4.4a coincides with that of Fig. 4.2b). It is clear that both spectra are nearly the same.

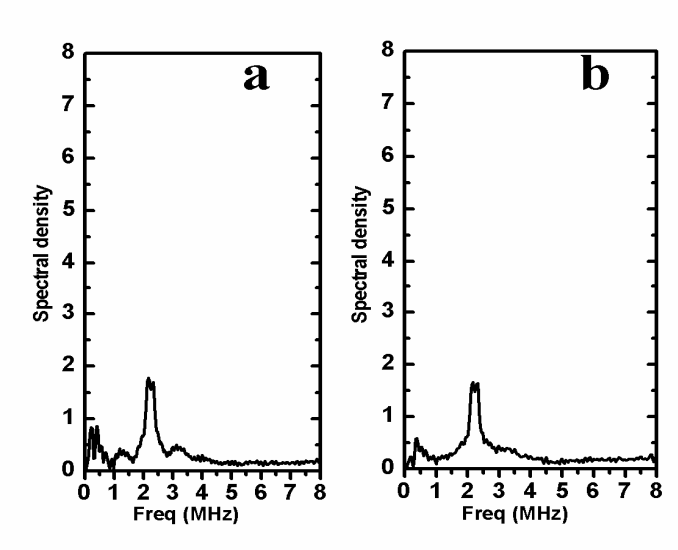

*Figure 4.4. Modulus Fourier-transform ESEEM spectra recorded by using a sample at a P/L molar ratio of 1 : 250 for (**a**) FTOAC4 (the spectrum is the same as shown in Fig. 4.2b) and (**b**) nOct-TOAC4.*

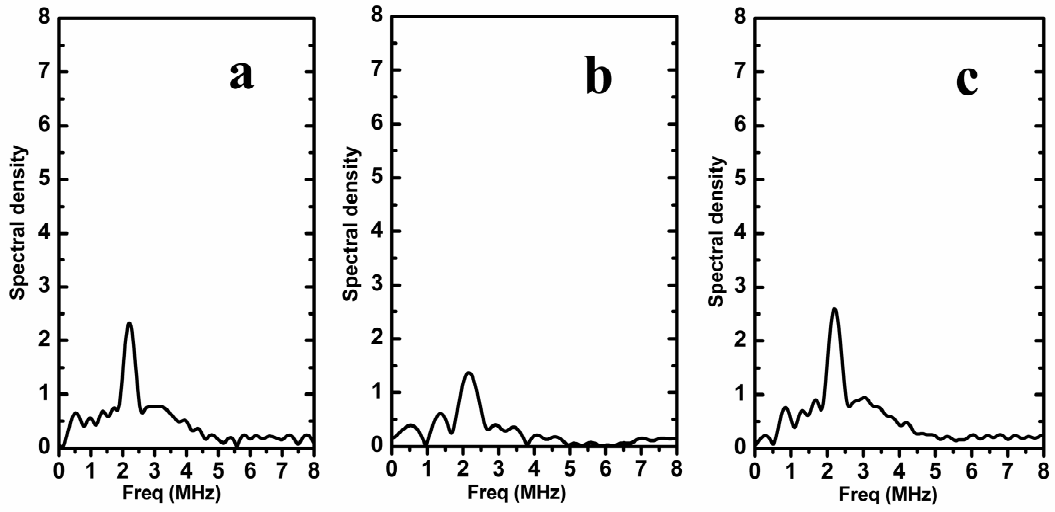

*Figure 4.5. Modulus Fourier-transform ESEEM spectra for a P/L molar ratio 1 : 20 for (**a**) FTOAC1, (**b**) FTOAC4, and (**c**) FTOAC8.*

Fig. 4.5 shows the modulus Fourier transform spectra for three samples, with FTOAC1, FTOAC4 and FTOAC8 analogues at a P/L molar ratio of 1 : 20. In comparison with the data obtained at lower peptide concentration (Fig. 4.2), a remarkable decreased line amplitude is observed for FTOAC1, while those for FTOAC4 and FTOAC8 decrease only slightly. The unresolved doublet at frequency 2.2 MHz may be explained by a broadening due to fast relaxation induced by electron-electron spin-spin interactions at a

high spin-label concentration. Note that this broadening may result also in a slight decrease of intensity, which should be taken into account when comparing with samples of low spin concentration.

All measurements were performed at the liquid nitrogen temperature (77 K). Samples were cooled optionally by shock freezing at the liquid nitrogen temperature, or slowly, at approximately 3°C per minute. Within the experimental accuracy the results were found to be independent on how the sample was cooled.

DISCUSSION

Water concentration profiles obtained for the same model membranes as those used in the present work were previously reported in reference (Erilov et al., 2005), using phospholipids systematically labeled at different locations of the *sn*-2 hydrocarbon chain of the lipid fatty acyl group. Also the experimental ESEEM data were treated in the same way. In this early work the line shapes of the frequency peaks were found similar to those obtained in the present study (Figs. 4.2 – 4.4). Therefore, one may directly compare the peak amplitudes found for the same frequency domain in these two different studies. If it is assumed that trichogin doesn't alter the water concentration profile in the membrane, then the comparison with data from reference (Erilov et al., 2005) (see Fig. 4.3c) will readily provide information on the depth of peptide immersion. Fig. 4.3c shows that the peak amplitude is nearly independent on the label positions of the hydrocarbon chain between the 4^{th} and 9^{th} carbon atoms, thereby forming a plateau with a mean amplitude of about 5 (the value, given in units, scatters between 4 and 6 due to the experimental uncertainty). The amplitude sharply decreases for higher numbers of spin label positions. Taking that into account, one may readily conclude from the data shown in Fig. 4.2 that at a P/L molar ratio 1 : 250 both spin labels in FTOAC1 and FTOAC8 lie above the 9^{th} - 11^{th} positions (closer to the membrane surface), while that in FTOAC4 is located below the 11^{th} position (closer to the hydrocarbon core of the membrane).

Interestingly, the ESEEM spectra for FTOAC1 and *n*Oct-TOAC1 are nearly the same (Fig. 4.3). An analogous result was obtained for FTOAC4 and *n*Oct-TOAC4 (Fig 4.4). Therefore, we conclude that replacement of the *n*Oct-group by Fmoc does not have any effect on the peptide orientation nor on the location in the membrane (at a small P/L molar ratio).

A previous PELDOR study showed that, at low concentration, peptide oligomerization doesn't take place (Milov et al., 2005). It means that the system peptide / membrane is homogeneous and all peptide molecules are equivalent to each other. So, we immediately conclude that at low concentration the peptide chains are located parallel to the membrane surface. Note that in reference (Erilov et al., 2005) it was concluded that the density of the lipid chain packing increases below the level of the 11^{th} carbon. Thus, trichogin GA IV is located above this high-density base.

Increasing the relative molar peptide concentration up to a P/L molar ratio 1 : 20 leads to a dramatic decrease in the peak intensity of FTOAC1, while the spectra of FTOAC4 and FTOAC8 exhibit only a slight decrease of intensities (compare Fig. 4.2 and Fig. 4.5). This result suggests that the N-terminus of trichogin is buried at increased concentration. Note, that we have no information about a possible change of the peptide secondary structure upon changing the peptide concentration. In addition, at this high concentration peptide molecules are in oligomerized form with a mean number of molecules in the oligomers close to two (Salnikov et al., 2006). Distance constraints implie the presence of the two different peptide chains (Salnikov et al., 2006). Assuming that association of the amphipathic molecules leads to dimers with all hydrophobic amino acid side chains oriented to the outside, it is of interest that the present ESEEM results showed that the N-terminal residues of the oligomer are located deeper (as compared to the monomer) into the membrane.

The conclusions of this work are in general agreement with those reported by Mazzuca et al. (Mazzuca et al., 2005). For an egg PC bilayer containing 50 mol % of cholesterol and studied at room temperature, these authors found at low peptide/lipid ratios trichogin binds close to the region of polar headgroups. By increasing the concentration, up to the level of membrane leakage, a strong correlation was found between the fraction of more deeply buried peptide and the fraction of oligomers (Stella et al., 2004). Thus, the monomeric and surface-bound peptide molecules are likely biologically inactive, while the buried, oligomerized peptides are responsible for membrane leakage.

Found two state transition switched by peptide concentration is in agreement with the model, proposed by Huang (Huang, 2006). He suggests in-plane inactive state of membrane-bound peptide at low concentration, which switches to transmembrane pore-forming state over critical concentration. This critical concentration is greatly dependent on membrane composition (Huang, 2006 and reference where). The origin of this process

is referred to membrane-thinning effect, which was found for DPhPC bound alamethicin (Chen et al., 2003) and phosphatidylcholine membrane bound melittin peptide (Lee et al., 2004). However, reported thinning effect has never exceed 3.3 Å limit, which was found for melittin in di-C22:1-PC at a similar high concentration of 1 / 20 P/L ratio, found in the present study. Taking into account relatively small hydrophobic length of short 11mer peptaibol trichogin GA IV 3.3 Å thinning is certainly not enough to produce noticeable amount of transmembrane peptide unless it is in oligomerized form, which extends overall hydrophobic length.

Chapter 5

Alamethicin topology in a phospholipid membrane by Solid State NMR of oriented samples and EPR. Low and cryo temperatures versus room temperature: critical comparative study.

Introduction

Alamethicin is a small 20-residues peptide from the fungus Trichoderma veride that produces a voltage-dependent conductance in bilayer systems (Sansom, 1993). It is of interest both as a model for voltage-gated channels and as a model for the behavior of a membrane-associated helices. Alamethicin is relatively hydrophobic, and it appears to be largely helical (Esposito et al., 1987, Kelsh et al., 1992, Franklin et al., 1994). The single channel behavior and high concentration dependence to the conduction are consistent with an oligomerized form for the channel (Hall et al., 1984).

Alamethicin strongly associates with model membranes and it exhibits a cooperative binding to membranes composed of fluid phase phosphatidylcholines as determined both by CD and by EPR methods (Stankowski and Schwarz, 1989, Archer et al., 1991). The open alamethicin pore has been suggested to consist of “transmembrane helical bundles” or “barrel staves”, a model consistent with the behavior of covalently linked alamethicin dimers (You et al, 1996). However, CW EPR measurement at room temperature of C-terminally labeled alamethicin analog failed to detect the oligomerized state (Archer et al., 1991, Barranger-Mathys and Cafiso, 1994, Marsh et al., 2007).

CD data was obtained for the existence of two forms of membrane bound alamethicin that interconvert as a function of alamethicin concentration (Woolley and Wallace, 1993). As a consequence the two state model has been also proposed by Huang (Huang, 2006) based on the large amount of experimental data from oriented CD, neutron

in-plane scattering and x-ray diffraction techniques (Huang and Wu, 1991, He et al., 1996, Chen et al, 2003, Lee et al., 2004). At low peptide-to-lipid ratios the peptide associates with the surface of a membrane; however, above a threshold concentration the peptide orients in a transmembrane fashion (Huang and Wu, 1991). Correspondingly, a minimal peptide concentration is required in the medium for antibiotic activity. Moreover, well-defined water-filled pores were detected by neutron in-plane scattering in bilayers containing transmembrane alamethicin (He et al., 1996).

On the other hand, direct alamethicin peptide oligomerization has never been detected and the exact molecular structure of the pore is not known. Advanced pulsed EPR (like PELDOR or Double Quantum Coherence (DQC) methods) provides the possibility to access peptide oligomerization. Unfortunately, it is only applicable at cryo-temperatures, where the lipid membranes are in the gel or subgel phase, while at physiological conditions it's certainly in the fluid phase.

In recent studies the influence of gel and subgel phase DPPC, DMPC and DSPC lipids on the conformation and oligomerization of the membrane-modifying peptide gramicidin A was monitored by CW EPR and DQC EPR methods (Dzikovski et al., 2004). A change of the peptide conformation in DPPC and DSPC membranes when switching from the fluid to the gel phase was clearly observed. In contrast, in the case of DMPC the conformation of membrane-bound gramicidin A remains constant in the range 77 K to 333 K which covers all membrane phases. The results were interpreted in terms of match / mismatch between hydrophobic length of the peptide and hydrophobic thickness of bilayers.

Herein we provide a critical analysis for the influence of low and cryo temperatures and lipid membrane phase on the alamethicin peptide orientation when bound to phospholipid membrane.

To check peptide topology at cryo-temperatures the ESEEM technique was chosen (see chapter 3.2). To access peptide topology at biologically relevant temperatures solid-state NMR spectroscopy of macroscopically oriented samples was employed. This technique has already been successfully applied to alamethicin bound to POPC membrane at P/L molar ratio of 1 / 8 (Bechinger et al., 2001). Under these conditions the predominant peptide orientation is transmembrane.

It is reasonable to check peptide orientation in the different membranes. We choose POPC and DPPC lipids: POPC is a major component of phospholipid part of eukariotic membranes, and that's why it is often used. It is in the fluid phase at room temperature.

The gel-to-fluid transition temperature for POPC is 271 K. DPPC is generally accepted to be a ruler for phosphatidylcholine membrane behavior in the gel phase, since it is in the gel phase at room temperature, with fluid to ripple transition temperature at 314.5 K, ripple to gel at 308 K and gel to subgel at 280 K (reviewed in Tristram-Nagle and Nagle, 2004). The phase transition temperatures slightly shift and get broadened upon addition of alamethicin and salt (Oliynyk et al., 2007), but for the present study these effects are of minor importance.

In the present chapter the topological properties of alamethicin are investigated using oriented ^{15}N solid-state NMR spectroscopy and the ESEEM technique. Amino acid sequences of uniformly ^{15}N labeled alamethicin and alamethicin analogs, labeled at three different positions with TOAC, are presented in chapter 3.1 and once again below. In addition, the cases of two different phospholipid membranes (POPC and DPPC) are studied.

In order to allow for the direct comparison of results from both methods the sample preparation was chosen to be similar in the closest way possible. In addition, solid-state NMR spectra are acquired at room temperature and at 248 K, i.e. well-below phase transition temperatures for POPC and DPPC membranes.

Ac-**TOAC^{1}**-Pro-Aib-Ala-*Aib*-Ala-Glu(OMe)-*Aib*-Val-*Aib*-Gly-Leu-*Aib*-Pro-Val-*Aib-Aib*-Glu(OMe)-Glu(OMe)-Phol (Alm1)

Ac-*Aib*-Pro-Aib-Ala-*Aib*-Ala-Glu(OMe)-**TOAC^{8}**-Val-*Aib*-Gly-Leu-*Aib*-Pro-Val-*Aib-Aib*-Glu(OMe)-Glu(OMe)-Phol (Alm8)

Ac-*Aib*-Pro-Aib-Ala-*Aib*-Ala-Glu(OMe)-*Aib*-Val-*Aib*-Gly-Leu-*Aib*-Pro-Val-**TOAC^{16}**-*Aib*-Glu(OMe)-Glu(OMe)-Phol (Alm16)

Ac-*Aib*-Pro-*Aib*-Ala-*Aib-Aib*-Gln-*Aib*-Val-*Aib*-Gly-Leu-*Aib*-Pro-Val-*Aib-Aib*-Gln-Gln-Phol (^{15}N uniformly labelled alamethicin)

Results.

Alamethicin topology by solid-state NMR. Fig. 5.1 shows proton-decoupled ^{15}N CP spectra of uniformly ^{15}N labeled alamethicin bound to oriented POPC (a) and DPPC (b) membranes at a concentration of 1 mol % recorded at room temperature. Insets represent ^{31}P spectra of these samples acquired at room temperature with the normal of the glass

plates parallel to the external magnetic field direction. Note, that the POPC membrane is in the fluid phase at room temperature, while the DPPC bilayers are in the gel phase.

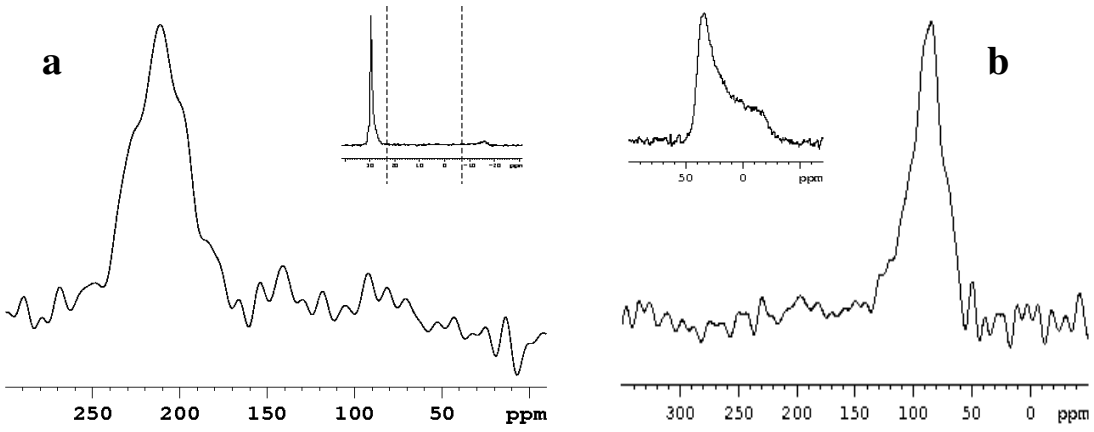

Figure 5.1. *Proton-decoupled solid-state ^{15}N NMR spectra of oriented samples of ^{15}N uniformly labelled alamethicin when bound to POPC (**a**) and DPPC (**b**) membranes at room temperature at P/L ratio equal to 1/100. Insets represent corresponding proton-decoupled ^{31}P NMR spectra.*

The proton-decoupled ^{31}P spectrum of POPC (inset in Fig. 5.1a) exhibits one narrow peak at 28 ppm indicative of highly oriented fluid phase lipid bilayers. The proton-decoupled ^{15}N spectrum acquired of samples oriented with the membrane normal parallel to the B_0 field immediately gives the alignment of peptide helix relative to external magnetic field and subsequently relative to the lipid bilayer. The signal intensity predominantly occurs in the range 190 – 230 ppm (Fig. 5.1a), which corresponds to the "transmembrane" orientation of peptide the helix.

The proton-decoupled ^{31}P spectrum of the DPPC sample at room temperature is line-broadened (which is certainly an effect of gel phase) and shows spectral intensities over the -35–40 ppm region. It means that the alignment of the DPPC headgroups is not as homogenous as it was in the case of POPC sample. The proton-decoupled ^{15}N spectrum of ^{15}N labelled alamethicin when bound to DPPC bilayer (Fig. 5.1b) shows all signal intensity in the region 60 - 120 ppm, which corresponds to in-plane oriented peptide helices. Accompanied by mostly oriented membrane bilayer we should conclude "in-plane" orientation of alamethicin peptide when bound to DPPC bilayer at room temperature.

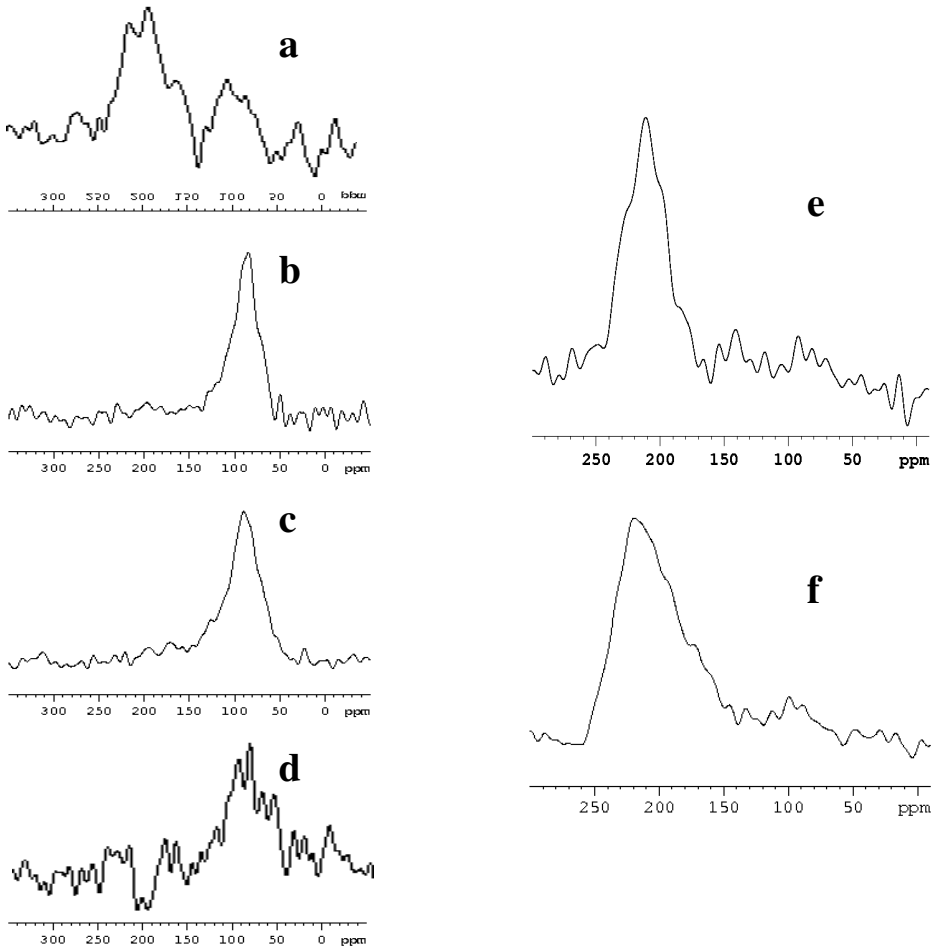

Figure 5.2 *Proton-decoupled solid-state ^{15}N NMR spectra of oriented samples of ^{15}N uniformly labelled alamethicin (**a**-**d**) in DPPC membrane at P/L ratio of 1/100 and a temperature of (**a**) 333 K, (**b**) 294 K (the same as in Fig. 5.1b) (**c**) 248 K, (**d**) 223 K; (**e**, **f**) in POPC membrane at P/L ratio of 1/100 and a temperature of (**e**) 294 K (the same as in Fig. 5.1a) (**f**) 248 K.*

Fig. 5.2(a-d) represents ^{15}N oriented NMR spectra of ^{15}N uniformly labelled alamethicin in DPPC at a P/L ratio 1/100 (the sample in Fig. 5.1b) at different temperatures. Indeed, alamethicin adopts mostly transmembrane orientations in the fluid phase DPPC membrane at 333 K (predominant signal intensity is around 200 ppm in Fig. 5.2a), in line with the results obtained in fluid phase POPC membranes (Fig. 5.1a). At gel phase DPPC bilayer at room temperature alamethicin is in surface (Fig. 5.1b).

Cooling this sample to 248 K and even to 223 K, i.e. well below gel to subgel transition temperature for DPPC, which takes place at 7ºC, results in the spectra shown in Fig. 5.2c-d. Certain broadening is observed when compared to room temperature, but the surface orientation of the peptide is obvious.

Fig. 5.2(e,f) represents the proton-decoupled ^{15}N oriented NMR spectra of ^{15}N uniformly labelled alamethicin in POPC membrane at P/L molar ratio 1/100 (the same sample as shown in Fig. 5.1a). Cooling this sample to 248 K, i.e. below the fluid-to-gel transition temperature of POPC (271 K) leads to the spectra shown in Fig. 5.2f. Certain broadening is observed comparing to room temperature spectrum (Fig. 5.2e), but in contrast to DPPC alamethicin remains transmembrane also in gel phase POPC membranes.

Alamethicin at 77 K by Pulsed EPR.

ESEEM data. Switching to 77 K temperature we can use ESSEM technique to access peptide orientation relative to the membrane surface.

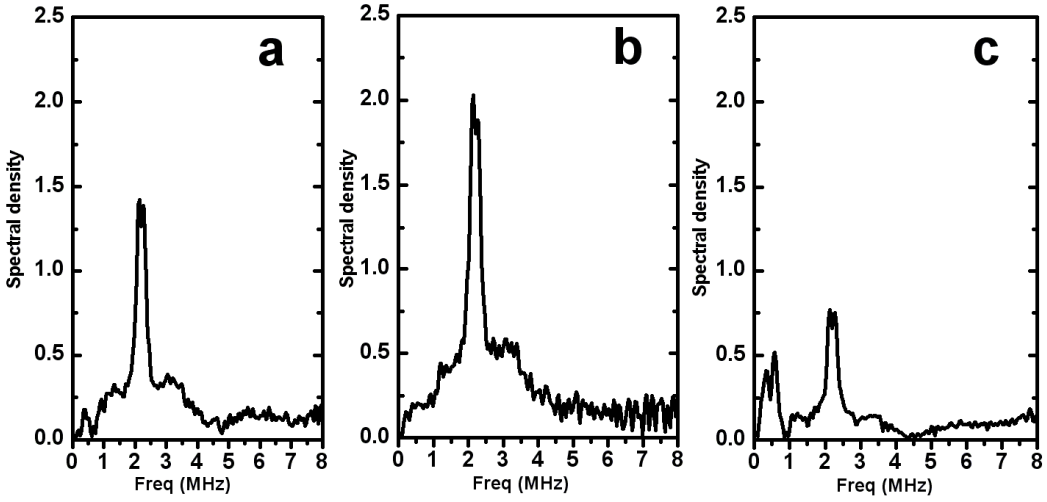

Figure 5.3*. Modulus Fourier-transform ESEEM spectra for TOAC-labelled alamethicin analogs in DPPC membrane at P/L molar ratio 1 : 100. (a) Alm1, (b) Alm8 and (c) Alm16.*

Fig. 5.3 shows modulus Fourier-transform ESEEM spectra for paramagnetically labeled alamethicin analogs in DPPC membrane at P/L molar ratio 1 : 100 (similar data were obtained in the concentration range from 1 : 275 to 1 : 50 P/L ratio). Peak intensity for Alm8 peptide (Fig. 5.3b) is more pronounced than that for other analogs, indicating

that the label at position 8 is the closest to membrane surface, while labels at positions 1 and 16 are buried deeper in the membrane. These results perfectly coincide with "in-plane" oriented peptide molecule, which was supported by solid-state NMR investigations of ^{15}N uniformly labeled alamethicin in subgel phase DPPC (Fig. 5.1b, Fig 5.2b-d).

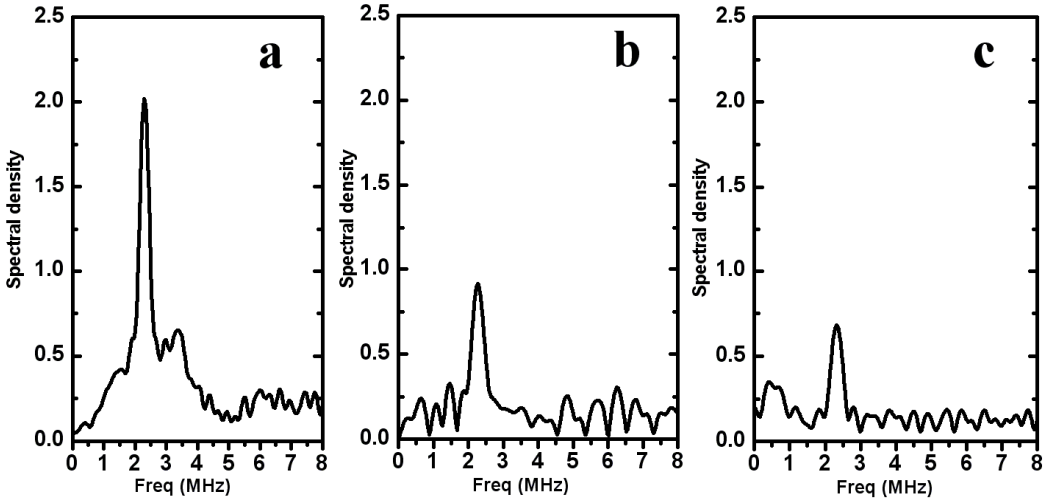

Figure 5.4. *Modulus Fourier-transform ESEEM spectra for TOAC-labelled alamethicin analogs in POPC membrane at P/L molar ratio 1 : 100. (**a**) Alm1, (**b**) Alm8 and (**c**) Alm16.*

When applied to POPC membranes modulus Fourier-transform ESEEM spectra shown in Fig. 5.4 are obtained. In contrast to DPPC membranes the peak intensity is the most pronounced for the label at position 1 (Fig. 5.4a), while labels at position 8 and 16 are averagely buried deeper in the membrane. Please note, that comparison of peak intensity for different membranes (namely, DPPC and POPC) is not straightforward, but peptide orientation in POPC membrane is certainly different of that in DPPC membrane. So, it is clearly not the "in-plane" orientation. On the other hand, ^{15}N NMR study of alamethicin in POPC at 248 K (Fig. 5.2f) indicated "transmembrane" peptide orientation suggesting this topology to persist in POPC membrane at 77 K.

CW EPR study. Immobilised CW spectra at 77 K of TOAC-labelled alamethicin analogs when bound to DPPC membrane at a concentration 1 : 100 P/L ratio are shown in Fig. 5.5. Line widths are quite the same for all peptide analogs. Similar results were found in the concentration range from 1 : 275 to 1 : 50 P/L ratio.

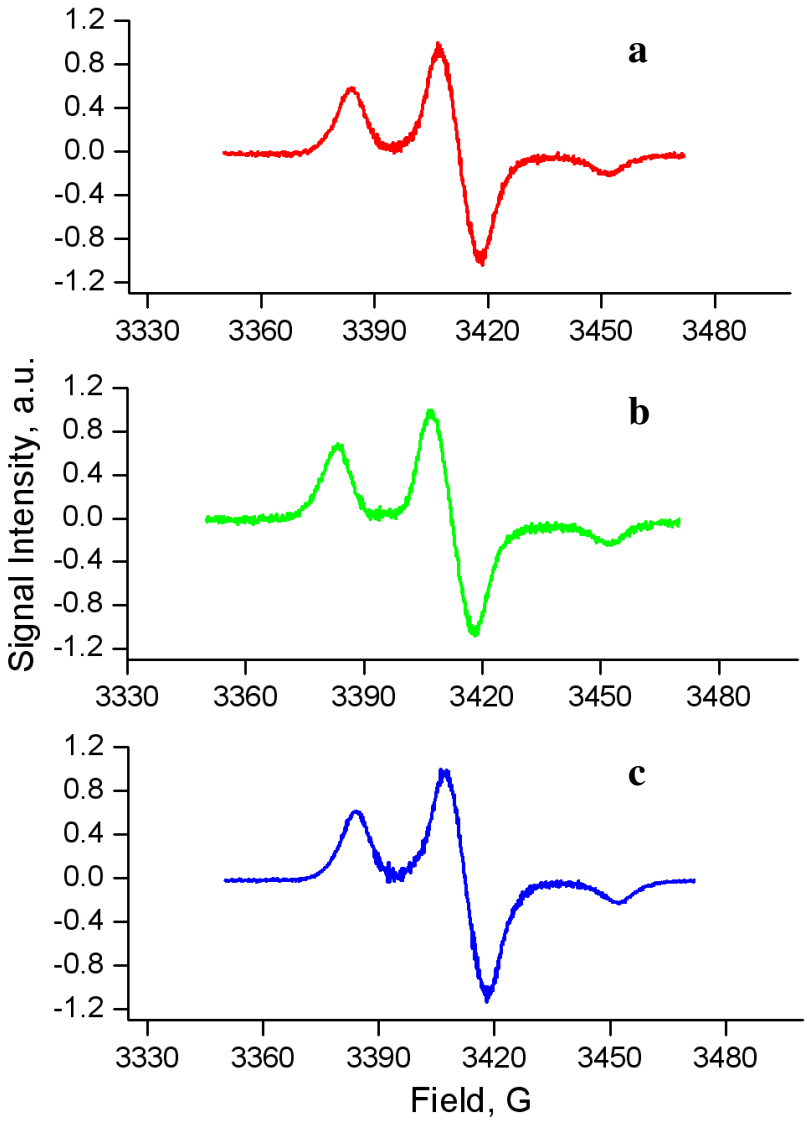

Figure 5.5. *CW EPR of TOAC-labelled alamethicin analogs in DPPC membrane at a P/L ratio 1 : 100 at 77 K. (**a**) Alm1, (**b**) Alm8, (**c**) Alm16.*

Contrary to DPPC membrane, immobilised CW spectra at 77 K of TOAC-labelled alamethicin analogs, when bound to POPC membrane at the same concentration of 1 : 100 P/L molar ratio, demonstrate different line width for the labels at different positions along the peptide backbone chain (see Fig. 5.6). Line-broadening is rather high for the label at position 8, while the label at position 1 doesn't exhibit any additional broadening when compared to the DPPC membrane. The label at position 16 exhibits intermediate CW linewidth. This additional line-broadening could arise from peptide oligomers. On the other hand, different environment, where these labels certainly exist,

when switching from surface peptide orientation in DPPC to transmembrane state in POPC membrane, could also participate to increase the CW EPR line width.

Note, please, that Alm1 peptide was found to be partially degraded (Samoilova and Milov, personal communication), and that's why CW EPR analysis exhibit no additional line broadening for the label in position 1, while oligomerized state is expected there also.

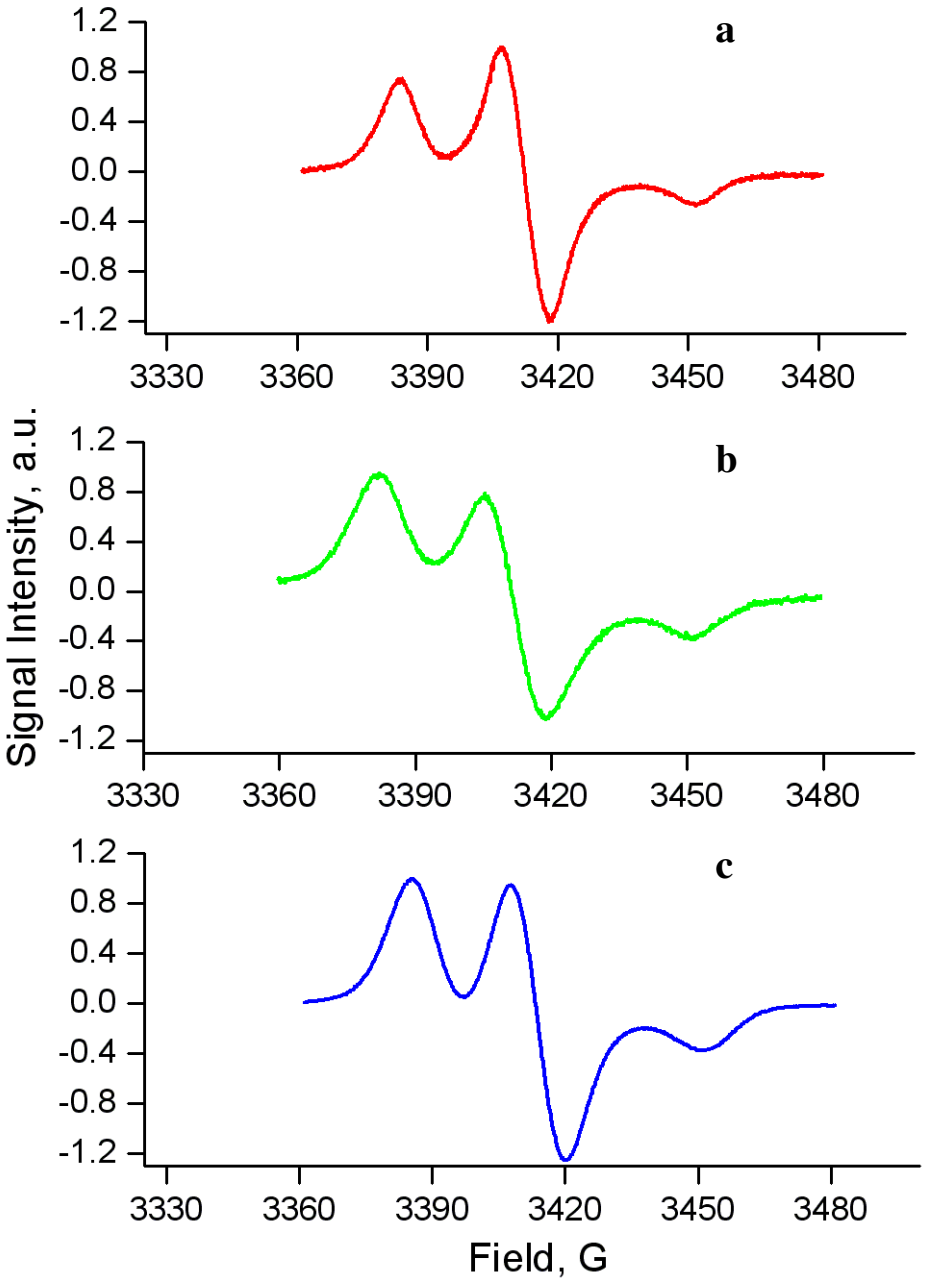

Figure 5.6. *CW EPR of TOAC-labelled alamethicin analogs in POPC membrane at a P/L ratio 1 : 100 at 77 K. (a) Alm1, (b) Alm8, (c) Alm16.*

Concentration effects: two state transition.

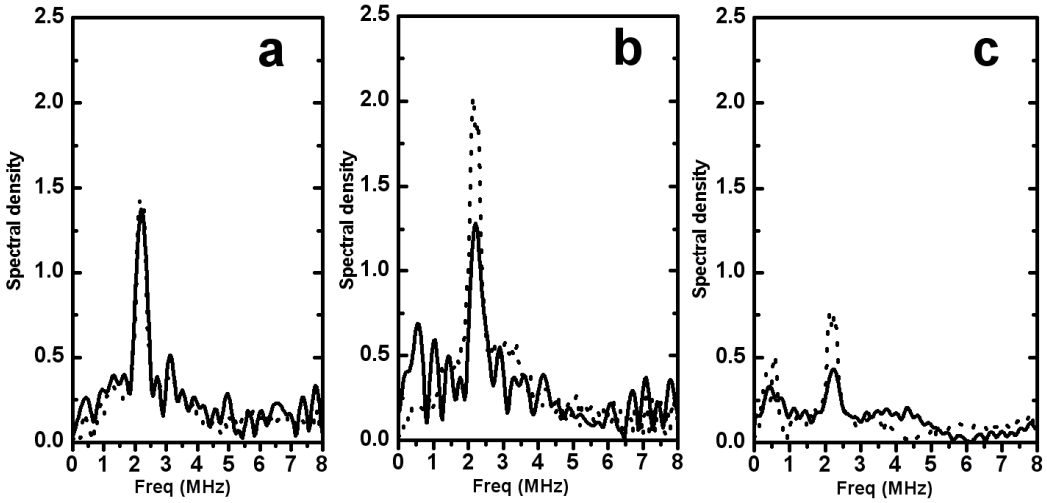

Figure 5.7 *Modulus Fourier-transform ESEEM spectra for TOAC-labelled alamethicin analogs in DPPC membrane at P/L molar ratio 1 : 20. (a) Alm1, (b) Alm8 and (c) Alm16. Modulus Fourier-transform ESEEM spectra for corresponding TOAC-labeled alamethicin analogs at low P/L ratio are figured by dotes.*

No changes in ESEEM spectra at 77 K were found for TOAC-labelled alamethicin analogs when bound to POPC membrane within the concentration range 1 / 100 to 1 / 20 P/L ratio. Solid-state NMR applied to ^{15}N uniformly labelled alamethicin bound to oriented POPC membrane at a P/L molar ratio of 1 / 8 (Bechinger et al., 2001) represents similar transmembrane orientation found here for the concentration 1 / 100.

When bound to DPPC membranes no change in ESEEM spectra was found in the range 1 / 275 to 1 / 50 P/L ratio. Further increasing of peptide concentration to 1 / 20 P/L molar ratio results in a dramatic change in peptide behaviour. ESEEM spectra of peptide bound to DPPC membrane at high concentration 1/20 P/L ratio are present in Fig. 5.7. Alm1 ESEEM spectrum remains unchanged (Fig. 5.7a), while labels at position 8 and 16 start to be buried deeper in the membrane comparing to low concentrated state (Fig. 5.7b,c). Complex behaviour reminds ESEEM spectra obtained for alamethicin bound to POPC membrane, where transmembrane peptide orientation was observed. Note, that direct comparison of modulation amplitudes for two different lipid bilayers is possible only in a qualitative manner.

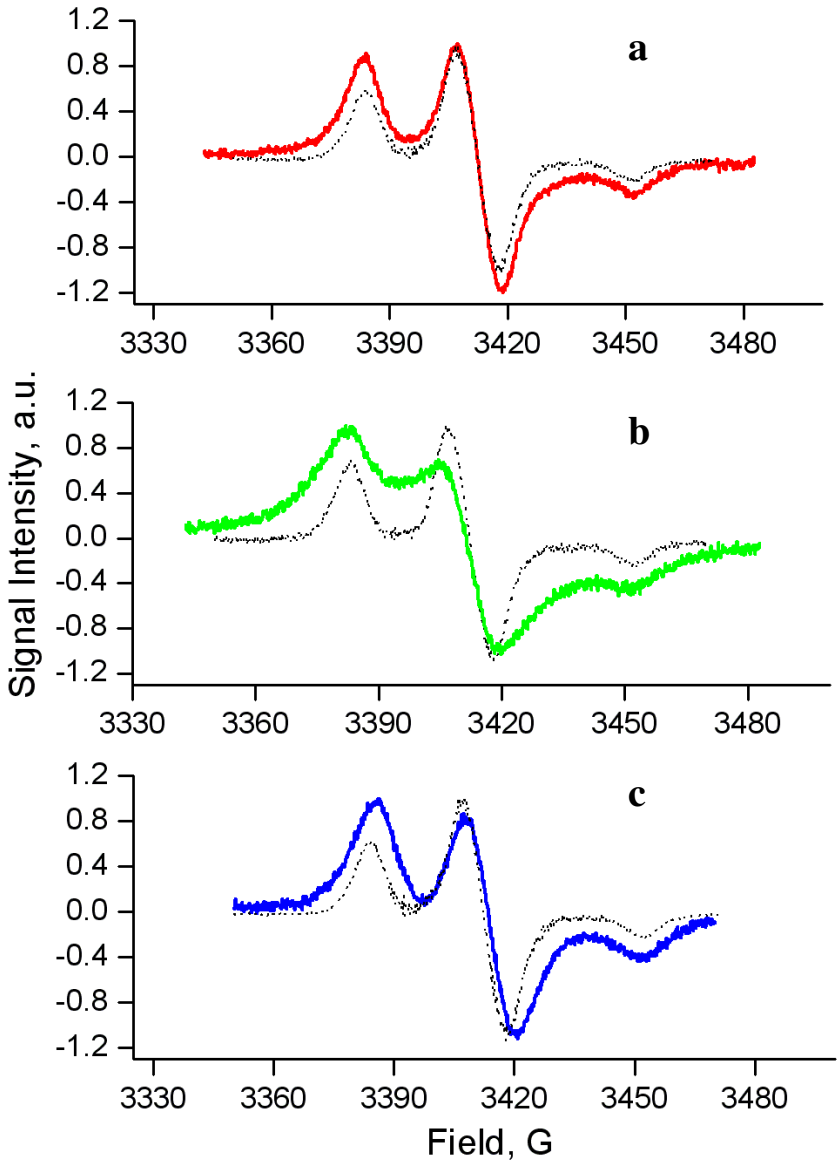

Figure 5.8*. CW EPR of TOAC-labelled alamethicin analogs in DPPC membrane at a P/L molar ratio 1 : 20 at 77 K. (a) Alm1, (b) Alm8 and (c) Alm16. CW spectra for corresponding alamethicin analogs bound to DPPC membrane at low P/L ratio are figured by black doted curves.*

CW EPR spectra at 77 K for TOAC-labeled alamethicin analogs in DPPC at 1/20 P/L molar ratio are shown in Fig. 5.8. Line-broadening is more pronounced for the label at position 8, as it was with alamethicin bound to POPC (Fig. 5.6). For the direct comparison CW spectra of alamethicin in DPPC at P/L molar ratio 1/20 (Fig. 5.8) and alamethicin in POPC at P/L molar ratio 1/100 (Fig. 5.6) were placed in one Fig. 5.9. One can see quite similar line-broadening effects. Quantitative mismatch between these results

could be readily explained by generally higher linewidth in the case of DPPC membrane, coming from 5 times higher label concentration.

These data strongly suggest switching of alamethicin orientation from "in-plane" state at low concentration to POPC-like "transmembrane" state over critical peptide concentration.

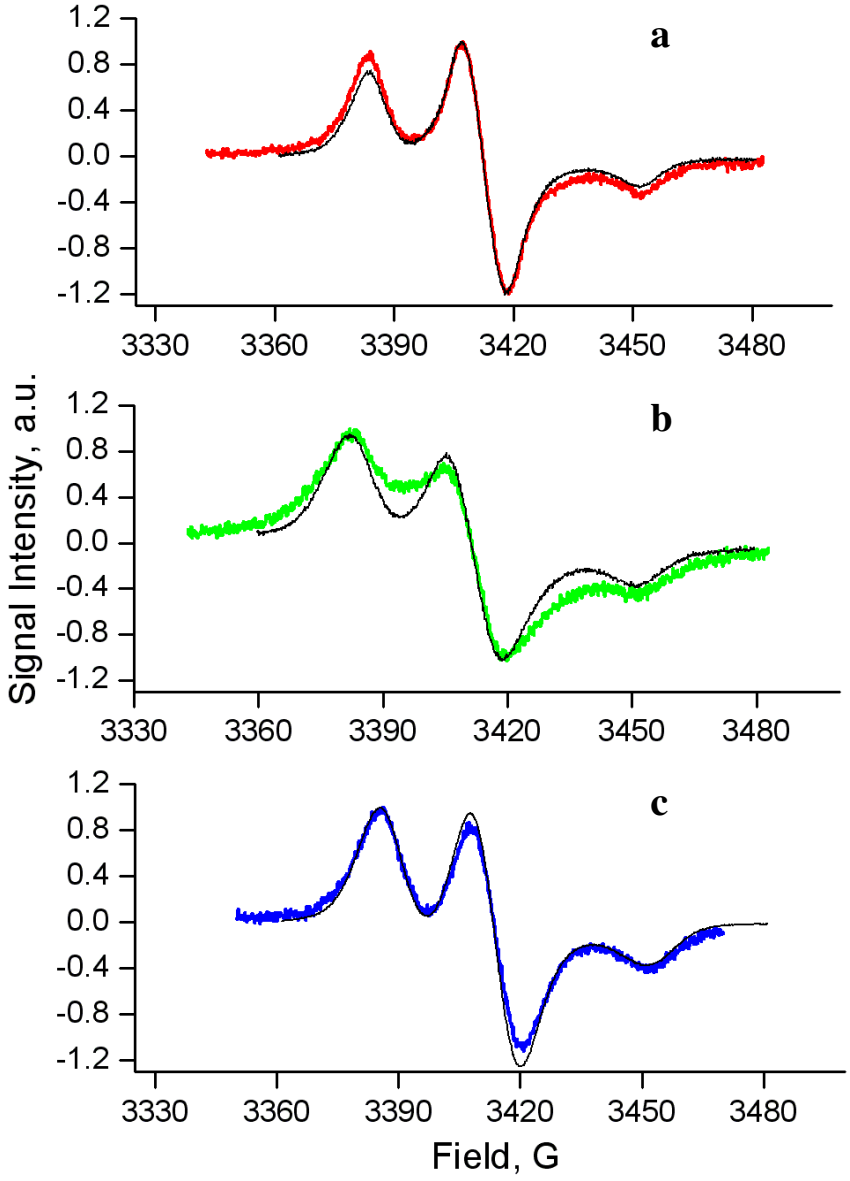

***Figure 5.9**. CW EPR of TOAC-labelled alamethicin analogs in DPPC membrane at a P/L molar ratio 1 : 20 at 77 K are figured by colour noisy lines. (a) Alm1, (b) Alm8 and (c) Alm16. CW spectra for corresponding alamethicin analogs bound to POPC membrane at P/L ratio 1 : 100 are figured by thin black lines.*

In order to support this two state transition found by pulsed EPR techniques an oriented sample with a similar high peptide concentration (1/20) in DPPC was prepared. The results are shown in Fig. 5.10. These ^{15}N spectra are close to the spectrum of disoriented alamethicin and within the noise level reveal no dependence on the orientation of the sample relative to the external magnetic field. In addition, the ^{31}P spectrum reveals poorly oriented DPPC bilayers, due to the high peptide concentration. These data cannot be analysed farther in terms of topology, because of the lack of sample orientation.

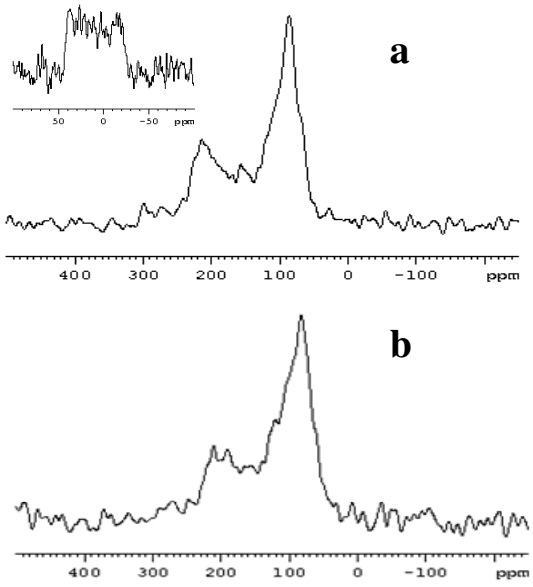

Figure 5.10 *Solid State ^{15}N NMR spectra of oriented samples of ^{15}N uniformly labelled alamethicin bound to DPPC membrane at room temperature at P/L molar ratio 1/20. (**a**) Glass plates normal parallel to external magnetic field, (**b**) perpendicular oriented glass plates. **Inset** represents proton-decoupled ^{31}P spectrum with glass normal aligned with external magnetic field.*

Simulation of CW EPR spectra for monomers

The effect of broadening for the label at position 1 is negligible in all cases. Of course, CW spectra of Alm1 in POPC could be slightly broadened since oligomerization certainly takes place, however quite small broadening effect indicates the distance between interacting spins to be more than 20 Å. This will be used to determine A_{xx}, A_{yy}

and g tensor parameters by simulating all CW spectra of Alm1. A_{zz} is known to be sensitive to environmental polarity and hence was permitted to be free.

Results of simulations are shown in Fig. 5.11. Simulating parameters were found to be g_{xx} = 2.0086, g_{yy} = 2.007, g_{zz} = 2.0023, A_{xx} = 5.2 G, A_{yy} = 2 G, A_{zz} = 33.5 G. One can see rather good agreement with experiment. The line-broadening function is composed of 50% Gaussian and 50% Lorentian. The width is concentration dependent: 4.4 G for the concentration of 1/275 P/L ratio, 5.5 G for the concentration of 1 : 100, 5.3 G for the concentration of 1 : 50 and 6.25 G for the concentration of 1 : 20 P/L ratio. Please note, found linewidth of 5.5 G for Alm1 in POPC at 1/100 seems to exhibit small broadening came from spin-spin interactions, but we have no other ruler of what level linewidth should be at this concentration.

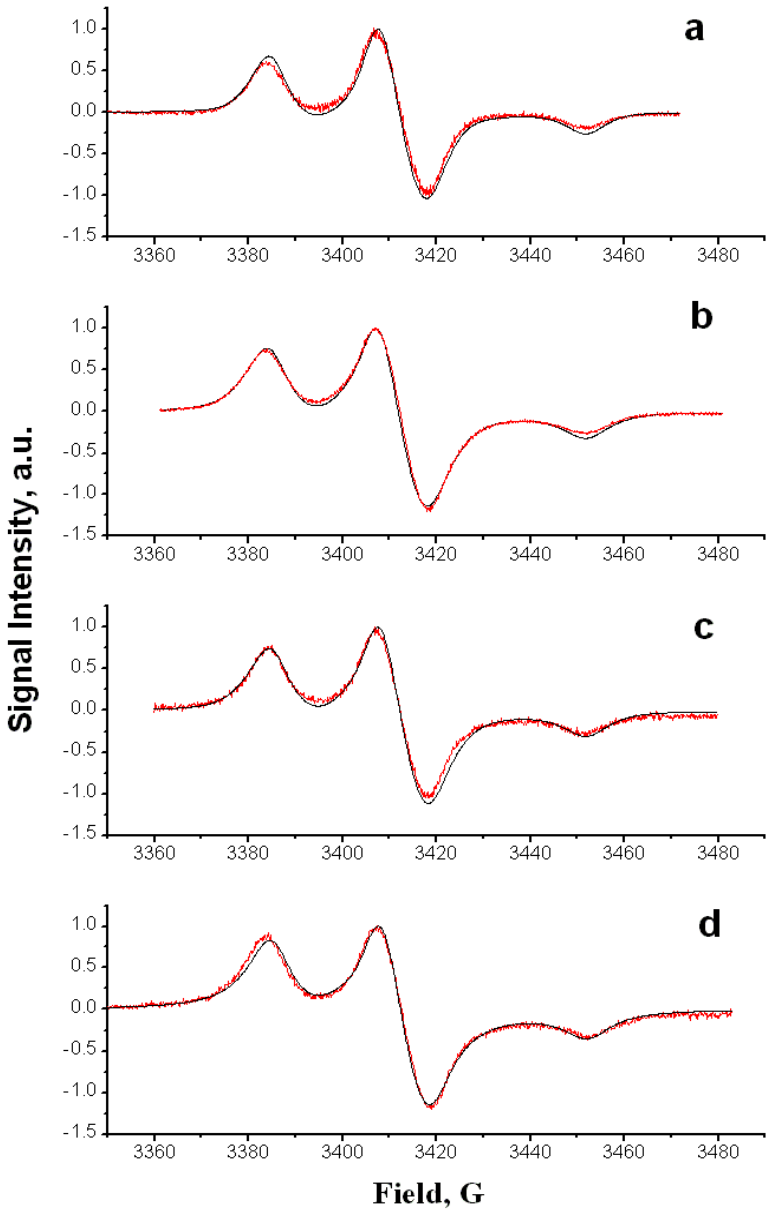

Figure 5.11. *CW EPR spectra at 77 K of Alm1 bound to phospholipid membrane at different concentrations (noisy red lines).* ***A*** *and* ***g*** *tensor parameters were set (5.2 G, 2 G, 33.5 G) and (2.0086, 2.007, 2.0023), correspondingly, for all these simulations (black lines). Line shapes were composed of 50% Gaussian and 50% Lorentian shapes of the same width. (**a**) Alm1 in DPPC at 1/275 molar ratio, fitted linewidth 4.4 G, (**b**) Alm1 in POPC 1/100, fitted linewidth 5.5 G, (**c**) Alm1 in DPPC 1/50, fitted linewidth 5.3 G, (**d**) Alm1 in DPPC 1/20, fitted linewidth 6.25 G.*

Simulation of CW spectra of labeled alamethicin analogs in DPPC at 1 : 275 are shown of Fig. 5.12. Please note that the only varying parameters are A_{zz} and linewidth.

Simulations support the same linewidth parameter of 4.4 G for all labeled alamethicin analogs in DPPC at this low concentration. In addition, similar results were obtained at higher peptide concentration of 1/50 in DPPC (data not shown). In this case linewidth was found to be equal to 5.3 G.

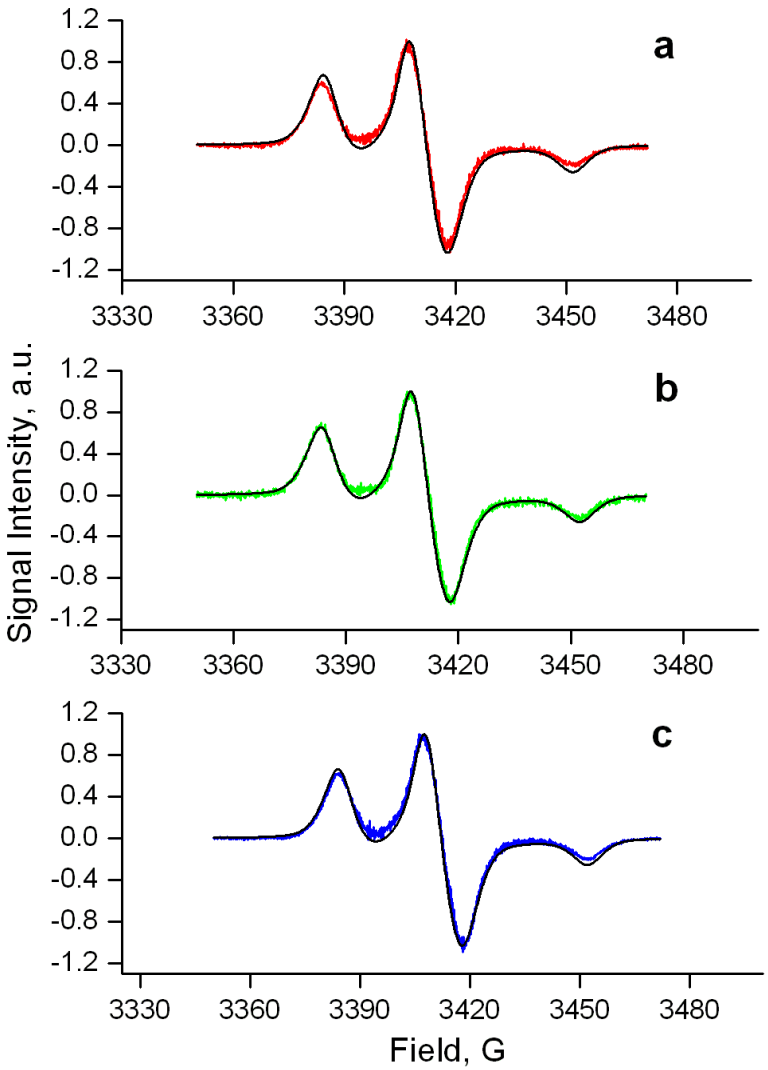

Figure 5.12 *CW EPR spectra at 77 K for TOAC labeled alamethicin analogs bound to DPPC membrane at 1/275 molar ratio (thick colour lines).* A_{xx} *= 5.2 G,* A_{yy} *= 2 G and* ***g*** *tensor parameters (2.0086, 2.007, 2.0023) were set constant for all these simulations (thin black lines).* A_{zz} *was case dependent since it is known to be dependent of polarity. The line-broadening function were composed of 50% Gaussian and 50% Lorentian shapes both of the width 4.4 G. (**a**) Alm1, Azz = 33.5 G, (**b**) Alm8, Azz = 34.3 G, (**a**) Alm16, Azz = 33.8 G.*

Simulation of CW spectra for spin pairs.

At first, to simulate the broadened CW spectra of Alm16 and Alm8 in POPC we used the simplest pair model introduced in (Steinhoff et al, 1997).

Simulating parameters: g_{xx} = 2.0086, g_{yy} = 2.007, g_{zz} = 2.0023, A_{xx} = 5.2 G, A_{yy} = 2 G. The line-broadening function is composed of 50% Gaussian of the width 5.5 G and 50% Lorentian of the width 5.5 G, as it was found for Alm1 at these conditions. A_{zz} was fitted also since it could change with the translocation to transmembrane state.

Closest simulations (black curves) are presented in Fig. 5.13 for Alm16 (blue line) and Alm8 (green line). As you can see, it appears to be impossible to fit experimental spectra within this model.

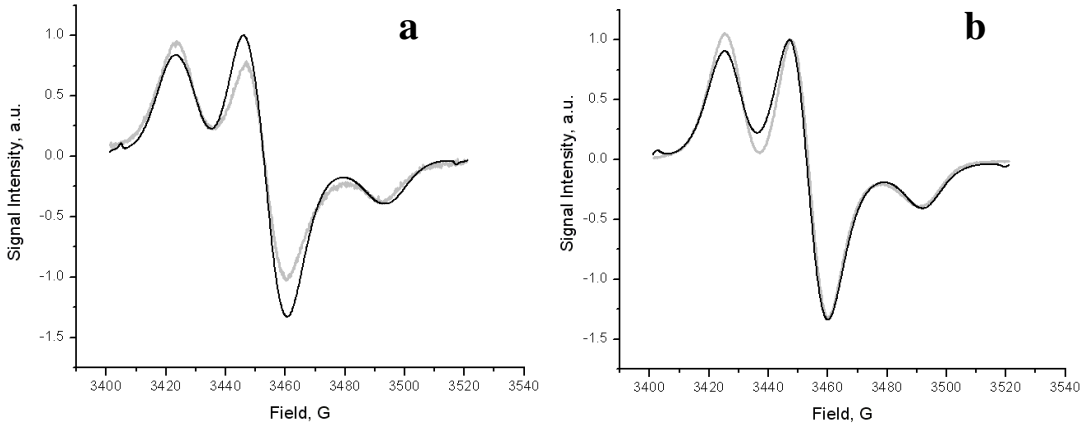

***Figure 5.13**. Simulation with simplest pair model. CW EPR spectra at 77 K for TOAC labeled alamethicin analogs bound to POPC membrane at 1/100 molar ratio (light-gray lines). A_{xx} = 5.2 G, A_{yy} = 2 G and **g** tensor parameters (2.0086, 2.007, 2.0023) were set constant for all these simulations (black lines). The line-broadening function were composed of 50% Gaussian and 50% Lorentian shapes both of the width 5.5 G. (**a**) Alm8, A_{zz} = 34.6 G. Mean distance 1.6 nm and sigma of gaussian distance distribution 0.6 nm. (**b**) Alm16, A_{zz} = 33 G. Mean distance of 1.7 nm and sigma of gaussian distance distribution of 0.3 nm.*

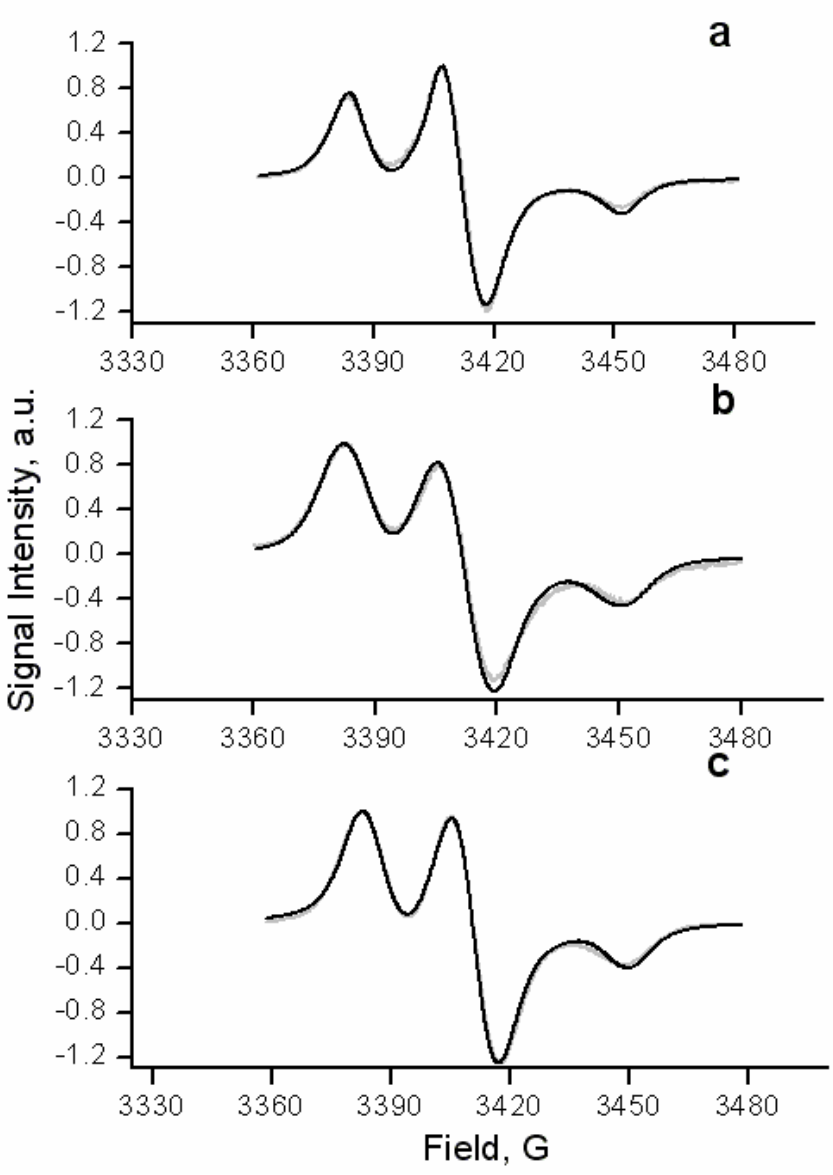

***Figure 5.14**. Simulation CW EPR spectra with biradical model. CW EPR spectra at 77 K for TOAC labeled alamethicin analogs bound to POPC membrane at 1/100 molar ratio (light-gray lines). A_{xx} = 5.2 G, A_{yy} = 2 G and **g** tensor parameters (2.0086, 2.007, 2.0023) were set constant for all these simulations (black lines). The line-broadening function were composed of 50% Gaussian and 50% Lorentian shapes both of the width 5.5 G. (**a**) Alm1, A_{zz} = 33.5 G, (**b**) Alm8, A_{zz} = 33.5 G, alpha1 = 0 rad, beta1 = 1.5 rad, gamma1 = 2.2 rad, alpha2 = -0.3 rad, beta2 = 1.1 rad, gamma2 = 2 rad, distance 1.1 nm (**c**) Alm16, Azz = 33 G, alpha1 = 0 rad, beta1 = 1.5 rad, gamma1 = 2.1 rad, alpha2 = -0.3 rad, beta2 = 1.1 rad, gamma2 = 2 rad, distance 1.4 nm.*

It seems that the relative orientation of the two coupled radical is critical for successful simulations. We therefore used the biradical model to simulate the CW spectra, where relative radical orientation was account on the level of Hamiltonian. For this purpose EasySpin software was used. Simulated spectra are present in Fig. 5.14. One can see quite sufficient agreement of simulated spectra with experimental results. Found distances of 11 Å between labels at position 8 and 14 Å between labels at position 16. Relative orientations of the labels are quite similar for the labels in both positions. Such a good agreement of experimental CW spectra with the simulation based on biradical model means that alamethicin oligomers have very well organized structure.

Discussion

The transmembrane alignment of alamethicin in POPC at 1/8 P/L molar ratio at room temperature has already been reported (Bechinger et al., 2001). Fig. 5.1a shows that this orientation still persists at lower concentration of 1 : 100, indicating that this ratio is below the critical concentration, if there is one, where alamethicin switches its mode of interaction with POPC membrane. For DOPC bilayers, which are about of the same membrane thickness, the reported threshold occurs at ≤ 0.5mol% of alamethicin (Huang and Wu, 1991).

In the fluid phase the hydrophobic thickness of DPPC and POPC membranes are about the same, and alamethicin adopts transmembrane alignments in both systems. Switching to DPPC gel and subgel phases, alamethicin adopts in-plane orientations (Fig. 5.2b-d). This effect is in a perfect agreement with the reported hydrophobic thickness of DPPC gel phase membranes. It switches from 28.5 Å in the fluid phase to 34.4 Å in the gel phase (Nagle and Tristram-Nagle, 2000). Increasing of hydrophobic thickness in the gel phase seems to be common for bilayers composed of saturated chain lipids (Nagle and Tristram-Nagle, 2000, DPPC and DMPC). A similar two state transition when switching from fluid to gel phase has been observed for gramicidin A in DPPC (Dzikovski et al., 2004) and was assigned to hydrophobic mismatch.

Note please, that the lipid chain tilt of around 30° in the gel state of saturated lipid bilayers doesn't affect peptide orientation. It was clearly shown in the study of gramicidin A peptide when bound to DPPC or DMPC in different phase of these bilayers (Dzikovski et al., 2004). It was found that the peptide still forms a channel in the DMPC of gel and subgel phase regardless lipid chain tilt.

The transmembrane orientation of alamethicin still persists in gel phase POPC membranes. Note, that at the moment no information available on the POPC bilayer thickness in the gel phase. However, there is an observation of the constant *d*-spacing parameter of POPC bilayer in the gel phase below 265.6 K and in the fluid phase above 275 K (Wang and Quinn, 2002). Hydrophobic thickness of POPC bilayer is about 27.1 Å, which is reported for DOPC and egg-PC in fluid phases (Nagle and Tristram-Nagle, 2000)).

After freezing to 77 K, the ESEEM data provide evidence for surface-oriented alamethicin when bound to DPPC membrane at low peptide concentrations. It is in a perfect agreement with higher temperature gel phase DPPC experiments. On the other hand, ESEEM data on alamethicin analogs bound to POPC membrane reflect clearly different properties. Therefore, the data are suggestive for a transmembrane orientation of alamethicin in analogy to the observations made at 248 K, i.e. well-below gel-to-fluid transition temperature of POPC bilayers (271 K).

Performing such a critical study we can conclude no influence of the temperature in the range from 77 K to 293 K on the alamethicin topology for both DPPC and POPC membranes studied. In addition, no influence of the membrane phase was observed in the case of POPC membranes, which is consistent with the hydrophobic bilayer thickness being the critical parameter for peptide topology.

CW EPR study at 77 K reveals no dependence of line-width on label position for alamethicin bound to DPPC membrane at low concentrations (from 1/275 to 1/50), see Fig. 5.5. In contrast, CW EPR of TOAC-labeled alamethicin analogs bound to POPC multilamelar vesicles exhibit dramatic dependence of line-width on label position (Fig. 5.6). So differently broadened CW EPR lines are certainly the intrinsic property of transmembrane oriented alamethicin peptide. Such behavior is usually assigned to dipolar coupling between labels (Steinhoff et al., 1997).

Simulation of CW EPR spectra reveals the necessity to fix the relative orientation of the labels in certain positions rather than a random distribution. This is the consequence of the rigid attachment of the TOAC label to the peptide backbone, which gives strictly-shaped oligomerization. However, successful simulation of dipolar broadened CW EPR spectra within the model of rigid biradical doesn't yet mean that thansmembrane peptide molecules form dimers. Dipolar interaction of three or more radicals with higher distances between each other could result in similar CW spectra (Steinhoff et al., 1997). Whereas CW spectra are not able to answer the question of the number of molecules in

the oligomer PELDOR technique is able to do so. Anyway, the model of two coupled radicals gives us the limit for the distances between labels, so that the distance between labels at position 8 is higher then 11 Å and between the labels at position 16 – higher then 14 Å. To the best of our knowledge, it is the first time that oligomerization of transmembrane alamethicin molecules was directly observed.

Recently, self-oligomerization of alamethicin molecules was observed in frozen egg-PC membranes by the PELDOR technique with the number of monomers in the oligomer being 4 (Milov et al., 2007). The distribution function for Alm16 in this case is broad with a maximum at a distance of 2.3 nm. This observation demonstrates the advantages of PELDOR study over conventional CW EPR.

The dependence of alamethicin orientation on peptide concentration has been studied in detail by the group of H.W. Huang using OCD, neutron in-plane scattering and x-ray diffraction techniques (Huang and Wu, 1991, He et al., 1996, Chen et al, 2003, Lee et al., 2004). They found that at low alamethicin concentration peptide molecules are oriented parallel to the membrane surface and produce no stable water-filled pores, whereas at P/L ratios exceeding this threshold, peptide molecules are oriented transmembrane and produce well-defined water-filled pores. The critical concentration was found to be greatly dependent on the lipid composition. The alamethicin orientations, found in this work, and the concentration-dependent switch are in perfect agreement with the two-state model proposed by Huang (Huang, 2006).

Results of the power saturation approach applied to spin-labeled alamethicin in egg-PC reported in (Barranger-Mathys and Cafiso, 1996), suggest water exposed C-terminal end labels at positions 15 and 9 buried at 1 Å and 11.7 Å from the bilayer surface, respectively. So that N-terminal part hardly reaches the opposite bilayer surface and stops about 16 Å inside (Barranger-Mathys and Cafiso, 1996). These data are in contradiction with the present ESEEM study. Possibly, slightly different amino acid sequences used there and in the present study could affect the immersion depth. On the other hand, this power saturation study is also in contradiction with the presence of pores of the transmembrane alamethicin peptide detected in DPhPC and DLPC (He et al., 1996). In addition, egg-PC membrane, which was used in the study of Barranger-Mathys and Cafiso, is a mixture of phosphotidylcholine lipids, so that the alamethicin topology and immersion depth could be different of that in pure POPC.

Atomic force microscopy study of alamethicin bound to DPPC membrane in gel phase at the concentrations 1/20 and 1/100 provides the presence of large pores of 500 Å

in a diameter (Oliynyk et al., 2007). This result is in contradiction with the present study and also such a huge pore size are in general contradiction with barrel-stave model and with results reported by Huang group, who have found pores of 18 Å in diameter in DLPC and 26 Å in DPhPC membrane (He et al., 1996). Possibly, it is the effect of mica surface, on which DPPC monolayers were studied, as they mentioned themselves. However, in this study averaged pore character has changed when increasing the concentration (from relatively small and circular shaped holes to noticeably bigger and irregularly shaped membrane defects). It in some way supports concentration effect found in the present study.

Poorly oriented DPPC membrane upon addition of high amount of alamethicin peptide (1 / 20) made the solid-state oriented sample NMR approach unsuccessful. Possible explanation is the formation of non-bilayer lipid organization, which is consistent with detergent-like action of peptide at high concentration (Bechinger and Lohner, 2006). Contrary, EPR technique still gives valuable information even at these high peptide concentrations. Every method has their own limitations and, as it was shown above, smart combination of different approaches could results in remarkable synergetic progress.

Chapter 6

Structure and alignment of the membrane-associated peptaibols ampullosporin A and alamethicin by oriented ^{15}N and ^{31}P solid-state NMR spectroscopy

Introduction

Ampullosporin A is a 15-mer peptaibol polypeptide that induces pigment formation by the fungus *Phoma destructiva*, forms voltage-dependent ion channels in membranes and exhibits hypothermic effects in mice. The conformation of ampullosporin A, solved by x-ray diffraction, is a largely regular α-helix starting from the acetylated *N*-terminus and a *β*-turn at the *C*-terminus (Kronen et al., 2003). Aminoacid sequence is shown in chapter 3.1 and also below. In similarity to alamethicin, ampullosporin A helices possess a hydrophilic face formed by the polar side chains of Gln^{7}, Gln^{11}, and non hydrogen bonding carbonyl oxygens of Aib^{10} and Gln^{11}, while the hydrophobic face is formed by the bulky side chains of Trp1, Leu^{5}, Leu^{12} and Leu^{15}ol. The length of ampullosporin A in the crystals is only 23 Å, i.e. much shorter than that of antiamoebin (28.3 Å), a 16mer peptaibol (Snook et al., 1998).

Ac-Trp-Ala-*Aib*-*Aib*-Leu-*Aib*-Gln-*Aib*-*Aib*-*Aib*-Gln-Leu-*Aib*-Gln-Lol
(ampullosporin A)

Ac-*Aib*-Pro-*Aib*-Ala-*Aib*-*Aib*-Gln-*Aib*-Val-*Aib*-Gly-Leu-*Aib*-Pro-Val-*Aib*-*Aib*-Gln-Gln-Phol
(alamethicin)

Ion channel activity of ampullosporin A was demonstrated in phosphatidylcholines at P/L ratio as low as 1/3000 (Kropacheva et al., 2005), even in the absence of transmembrane potential. However, in contrast to alamethicin, ampullosporin A displays only a weak antimicrobial effect (Ritzau et al., 1997), but induces pigment formation in the fungus *Phoma destructiva* (Ritzau et al., 1997, Kronen et al., 2001). In addition,

ampullosporin A can also provoke hypothermia and inhibits locomotor activity in mice (Ritzau et al., 1997, Kronen et al., 2001).

Alamethicin was already introduced in the chapter 5, however herein we provide a different aspect of peptide / membrane interaction where conformational aspects are highlighted. Structural analysis by x-ray crystallography (Fox and Richards, 1982), as well as NMR-spectroscopy in methanolic solution (Yee and O'Neil, 1992), and in the presence of SDS micelles (Franklin et al., 1994, Spyracopoulos et al., 1996) all indicate that the conformations of alamethicin are predominantly helical, with a flexible hinge region at the glycine-11 position (North et al., 1994). In the centre of the alamethicin sequence the G-X-X-P motif results in a break of the helix conformation and a less stable C-terminal structure which undergoes considerable conformational averaging (Yee and O'Neil, 1992, Yee et al., 1997, Franklin et al., 1994). These structural findings have been confirmed by molecular dynamics simulations (Tieleman et al., 1999, Tieleman et al., 2001). In addition, FTIR, Raman and CD spectroscopies show that the degree of helicity is dependent on the physical state of the lipid (Vogel, 1987), the lipid-peptide ratio (Cascio and Wallace, 1988) and the presence of transmembrane potentials (Brumfeld and Miller, 1990).

Whereas the biological activities of peptaibols, such as antimicrobial, antimalarial and haemolytic activities (Rebuffat et al., 1999, Chugh and Wallace, 2001) were reported to be generated from their membrane activities, the action mechanisms of the biological activities of ampullosporin A remain unknown although it is suspected that both peptides form channels by related mechanisms.

In addition, despite intensive research our understanding of the detailed mechanism of voltage dependent channel-formation by peptaibols remains incomplete in part because of the paucity of information about the structure of the peptide in biological membranes, which might exhibit different conformational and dynamic properties from the structures in organic solvents or in the crystal. Herein we employ ^{15}N and ^{31}P solid-state NMR spectroscopy of mechanically oriented bilayers to investigate the lipid-dependence of ampullosporin A alignment and the membrane-associated structure of both peptaibols in their transmembrane orientation.

High content of Aib residues promote the formation of 3_{10}-helical structure (reviewed in Crisma et al., 2005). This conformation will be also tested in addition to conventional α-helix.

Results

The high resolution HSQC spectrum of the peptide in CD_3OH is shown in Fig 6.1. The author thanks Dr. Roland Graff and Dr. Lionel Allouche (Service Commun de RMN, Faculté de Chimie, Université Louis Pasteur, Strasbourg, France) for acquiring this spectrum. 15 ^{15}N resonances are observed within the isotropic chemical shift positions of the amides (between 102 - 121 ppm for ^{15}N and 6.7 - 7.6 ppm for ^{1}H). Additional resonances at a 10.4 ppm ^{1}H chemical shift position were assigned to the tryptophan side chain. Three glutamine side chains exhibit ^{15}N isotropic chemical shift values around 97 ppm. The data therefore indicate that all sites were consistently labeled with ^{15}N.

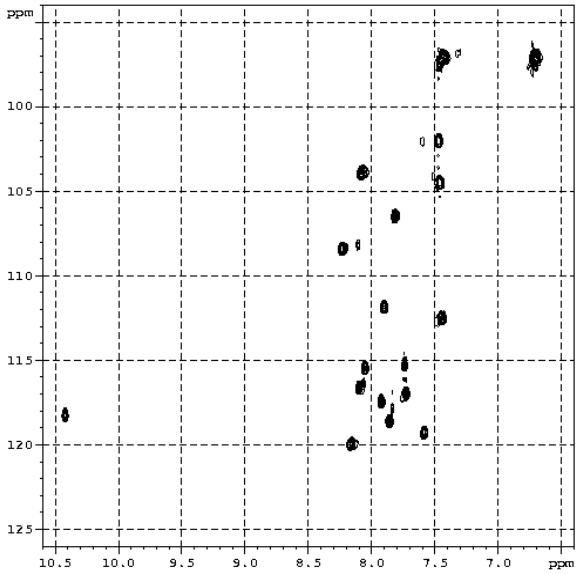

Figure 6.1. *HSQC spectrum of uniformly ^{15}N labeled ampullosporin A in CD_3OH.*

Experimental spectra of ^{15}N uniformly labeled ampullosporin A in different length carbon tail PC at pH = 4.5 and peptide/lipid molar ratio 1/100 are shown in Figs. 6.2A-D. The ^{31}P NMR signals of same samples monitoring the order of phospholipid head groups indicate that the membranes are well oriented (Fig. 6.3A). One can see clear signal in the region 65-120 ppm for thick membranes of POPC and di-C14:1-PC, which is indicative of in-plane peptide helix alignment. In contrast the peptide switches to a tilted transmembrane orientation when bound to thinner bilayers of di-C12:0-PC and di-C10:0-PC. Note, that chemical shift values are slightly less for di-C10:0-PC than that in di-C12:0-PC, indicating that the average helix tilt angle is larger for thinner membranes. The peptides adopt higher tilt angles for thinner bilayers to hide a larger fraction of hydrophobic residues inside the membrane core. When the sample orientation of

ampullosporin A in POPC is tilted by 90 degrees resonances were observed in the regions 100-110 ppm and 120-150 ppm (Fig. 6.2E). The absence of powder pattern line shapes at this alignment is indicative of motional averaging and fast rotational diffusion around the bilayer normal of the in-plane oriented peptides (Aisenbrey and Bechinger, 2004; Prongidi-Fix et al., 2007).

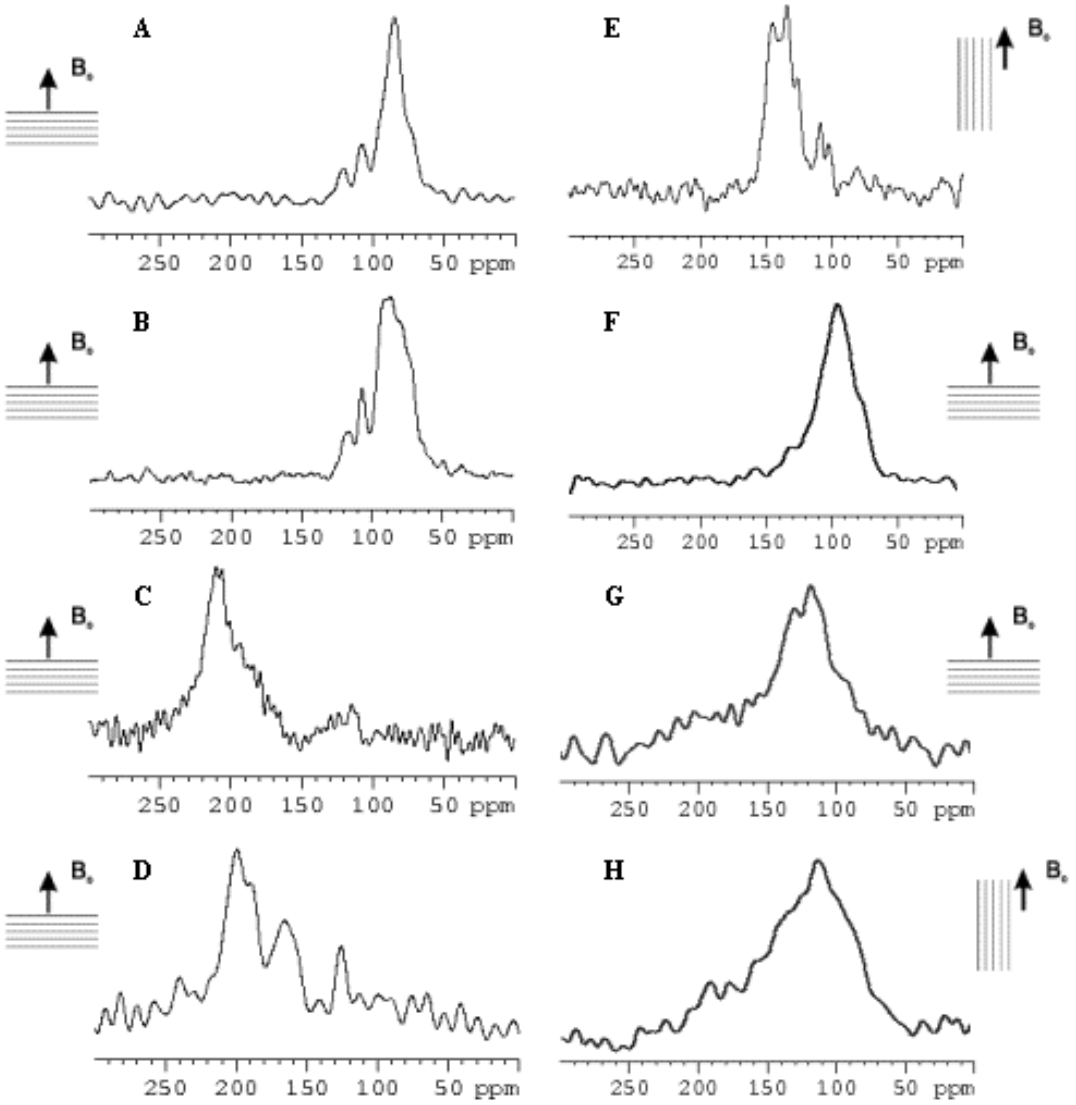

Figure 6.2. *Proton-decoupled ^{15}N solid-state NMR spectra of ampullosporin A labeled uniformly with ^{15}N and reconstituted into phosphatidylcholine oriented membranes: (**A**) POPC (C16:0-C18:1-PC), (**B**) di-C14:1-PC, (**C**) di-C12:0-PC, (**D**) di-C10: 0-PC. (**E**) POPC. The molar peptide-to-lipid ratio of these (A-E) samples is 1:100 and pH = 4.5. (**F**) POPC, P/L ratio is 1:100 and pH is adjusted to 7.5. (**G**) and (**H**): POPC, pH 7.5, P/L ratio 1:10. The bilayer normal is parallel to the external magnetic field for **A-D, F** and **G.** And the bilayer normal is perpendicular to the external magnetic field for **E** and **H**.*

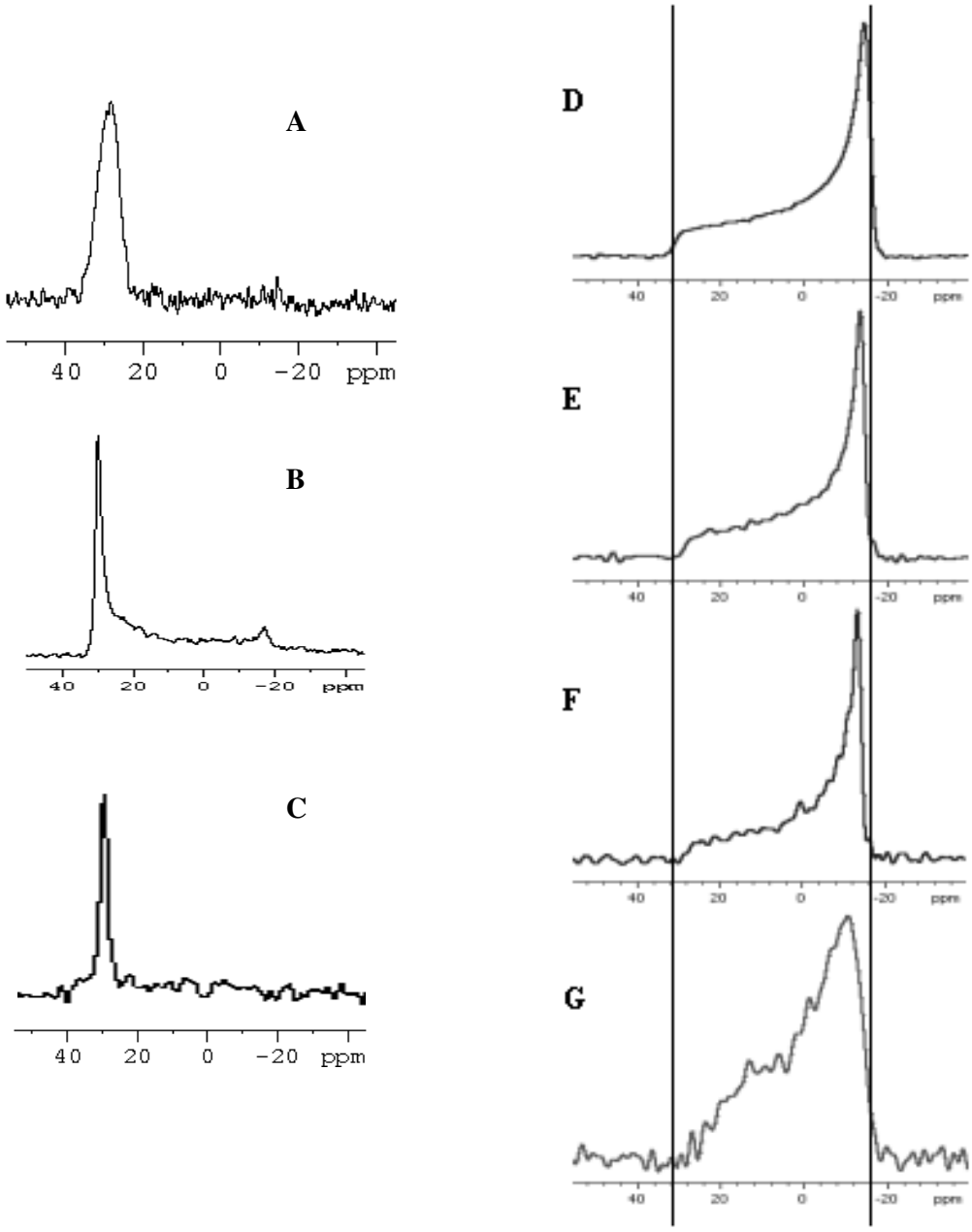

Figure 6.3. *Proton-decoupled ^{31}P spectra of oriented (**A-C**) and non-oriented (**D-G**) samples of ampullosporin A bound to different PC membranes at different concentrations. (**A**) di-C10:0-PC (1/100), (**B**) POPC, pH 7.5 (1/100), (**C**) POPC, pH 7.5 (1/10) (**D**) pure POPC vesicles (**E**) POPC (1/100), (**F**) POPC (1/20), (**G**) POPC (1/10).*

It has been observed before that the presence of salt and buffer solutions makes the preparation of oriented phospholipid bilayers more difficult. Therefore, an ampullosporin A sample was prepared that is identical to that of Fig. 6.2A (POPC, P/L 1:100), except

that the pH was adjusted and stabilized at pH 7.5 by the addition of small amounts of NaOH and 100 µl of 10 mM Tris buffer during the preparation procedure. The proton-decoupled ^{31}P solid-state NMR spectrum indicates a predominant peak at 30 ppm indicative of well-oriented lipid bilayers. However, the signal intensities in the region from < 30 ppm are increased (Fig. 6.3B) and indicative of some additional disorder, possibly arises from the presence of salt. The proton-decoupled ^{15}N spectrum of this sample when aligned with the bilayer normal parallel to the external magnetic field looks rather similar to the one in the absence of salt and at pH 4.5 (cf. Figs 6.2A, F). In order to optimize sample alignment and resolution for the structural analysis by two-dimensional NMR, the samples shown in Figures 6.2A-E were therefore prepared without buffer addition.

In order to increase the signal-to-noise ratio during the structural analysis of polypeptides reconstituted into oriented membranes by solid-state NMR it is advantageous to work with high peptide concentrations. However, due to the limited coil volume this also requires an increase in the peptide-to-lipid ratio. A sample with P/L = 1:10 and pH 7.5 was prepared and its proton-decoupled ^{15}N spectra were recorded. The spectrum obtained with bilayer normal perpendicular to external magnetic field (Fig. 6.2G) shows signal intensities in the range 200-60 ppm when at the same time the ^{31}P NMR spectrum of this preparation is indicative of well-oriented membranes (Fig. 6.3 C). When the sample is tilted by 90 degrees (Fig. 6.2H) the changes in the spectral line shape are much less pronounced when compared to the situation at P/L 1/100 (Fig. 6.2 E). Notably, a pronounced signal intensity is observed at 110-150 ppm indicative of isotropic realignment of amide resonances or helical tilt angles close to the magic angle. The ensemble of spectra indicates a more heterogeneous alignment of the peptides and an important contribution of tilted helix arrangements or conformations undergoing isotropic averaging.

^{31}P spectra of POPC vesicles with and without unlabeled ampullosporin A are shown in Fig. 6.3 (D-G). It's worthwhile noting that the pH of these samples is 6.5. Upon peptide addition the characteristic bilayer lineshape of the ^{31}P NMR spectra persists up to a relatively high peptide concentration of P/L = 1 : 20. Although at this ratio the CSA is reduced by 4 ppm these results indicate overall persistence of bilayer lipid organization with a slight influence of bound ampullosporin A to POPC headgroups, inducing a change in a headgroup orientation which leads to reduced ^{31}P CSA tensor values.

Reaching P/L = 1 : 10 concentration, ampullosporin A strongly disturbs the POPC membrane. Analysis of ^{31}P spectra of this kind suggests the induction of different lipid organization.

In order to get insight to the structure of the peptide when bound to lipid bilayer 2D ^{15}N -^{1}H dipolar coupling ^{15}N chemical shift correlation spectra were recorded. PISEMA spectrum for ^{15}N uniformly labeled ampullosporin A in di-C10:0-PC is present in Fig. 6.4A. Peaks with CS more than 150 ppm should be mostly assigned to transmembrane amid ^{15}N. Note that no peak appears in the range 170-185 ppm. Peak at 120 ppm could be possibly assigned to isotropic chemical shift of four side chain ^{15}N labels presented in ampullosporin A (3 Gln and Trp residues), since it appears at all spectra of ampullosporin A bound to different width PC membranes (Fig. 6.2).

PISEMA spectra were simulated for a series of models that are likely to represent the structure of the peptide in its membrane-associated state using the SIMMOL and SIMPSON software (Bak, Rasmussen and Nielsen, 2000).

The crystal structure ampullosporin A (Kronen et al., 2003) exhibits a more-or-less regular α-helix at the N-terminus (the first 10 residues), ending with kinked less regular structure with a possible interpretation as 3_{10}-helix. It appears to be impossible to fulfill the experimental restrictions with crystal structure. The best simulation of PISEMA experiment for ^{15}N backbone labeled crystal structure ampullosporin A (pdb: AMPA) with the regular helix (N-terminal end) tilted by 32º in the way to partially compensate the bent of C-terminal end is shown in Fig. 6.4C.

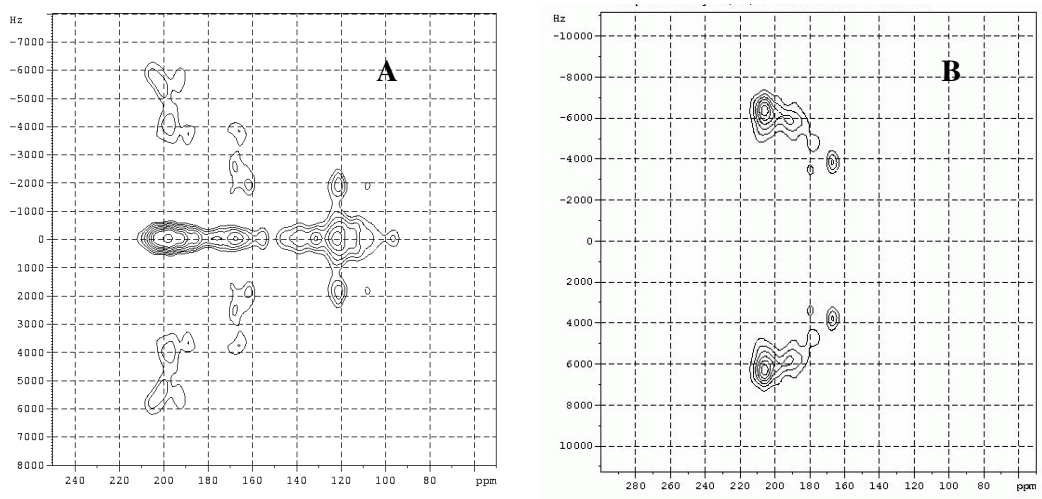

Figure 6.4 A,B *Experimental 2D PISEMA spectrum of ^{15}N uniformly labeled ampullosporin A associated with perpendicular oriented (**A**) di-C10:0-PC bilayers and (**B**) di-C12:0-PC bilayers*

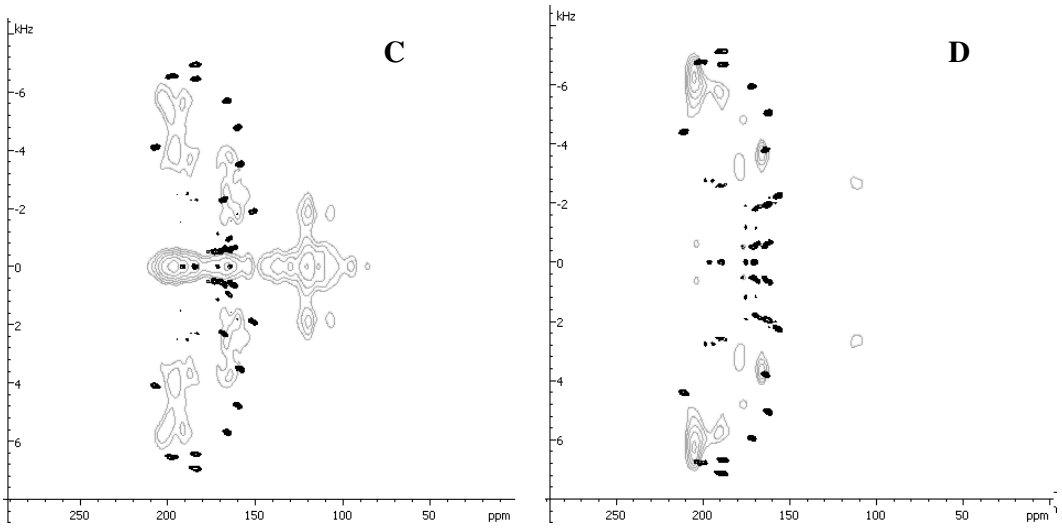

Figure 6.4 C,D *SIMMOL calculated PISEMA spectrum for ^{15}N uniformly labeled crystal ampullosporin A structure (pdb: AMPA) superimposed on the corresponding experimental spectrum obtained in di-C10:0-PC (**C**) or di-C12:0-PC (**D**). N-terminal end (the first 10 residues) tilted (**C**) 32° or (**D**) 30° relative to external magnetic field*

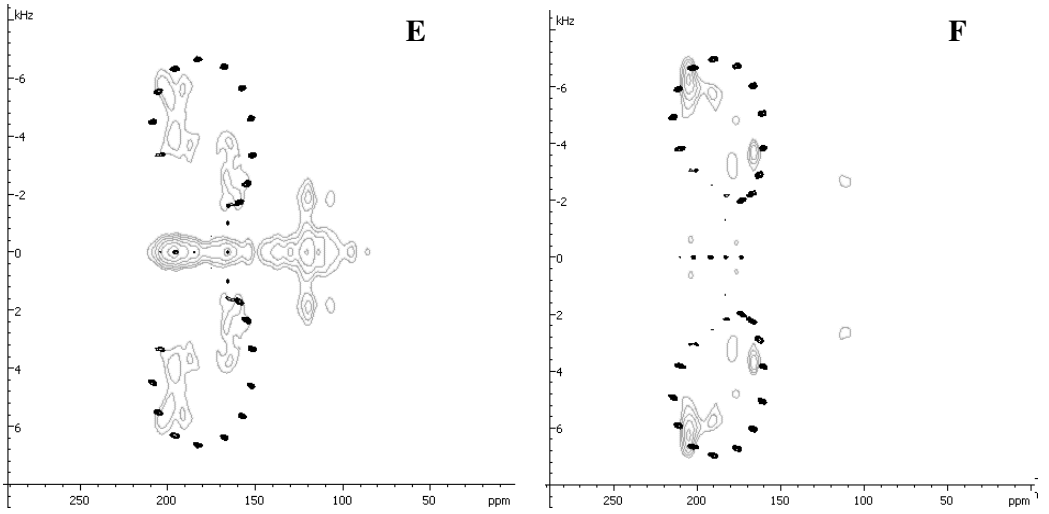

Figure 6.4 E,F *SIMMOL calculated PISEMA spectra for ^{15}N uniformly labeled alpha-helical (φ = -65°, ψ = -45°) polyalanine peptide tilted (**E**) 33° and (**F**) 30° relative to external magnetic field. Shown superimposed on the corresponding experimental spectrum obtained in di-C10:0-PC (**E**) or di-C12:0-PC (**F**)*

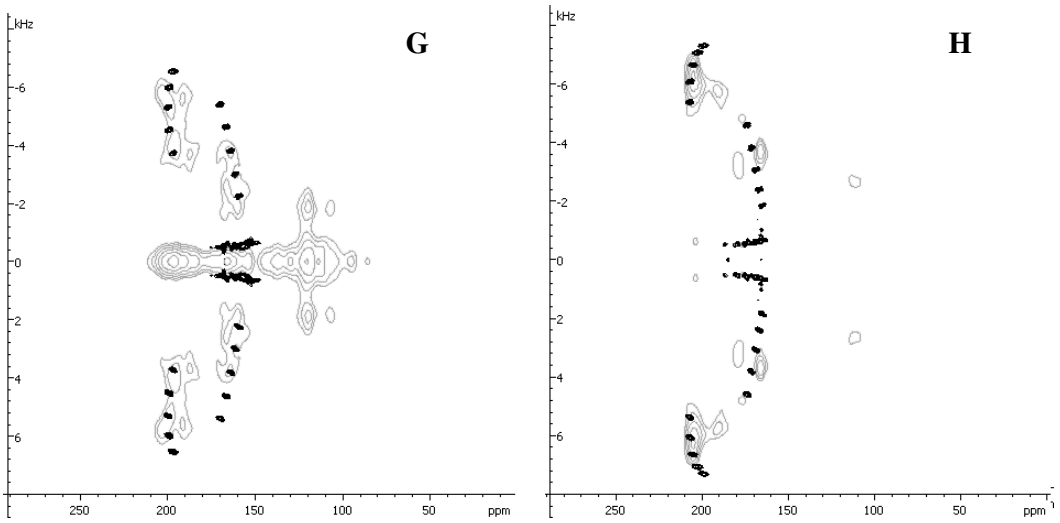

Figure 6.4 G,H *SIMMOL calculated PISEMA spectrum for ^{15}N uniformly labeled 3_{10}-helical (φ = -50°, ψ = -31°) model peptide, tilted (**G**) 35° and (**H**) 32º relative to external magnetic field. In the case of di-C12:0-PC (**H**) the rotational pitch angle was adjusted to 340° to fit better the experimental spectrum. Shown superimposed on the corresponding experimental spectrum obtained in di-C10:0-PC (**E**) or di-C12:0-PC (**F**)*

In a next step the PISEMA spectrum of an ideal α-helix labeled uniformly with ^{15}N at its backbone was considered (φ = -65°, ψ = -45°). An α -helix with a tilt angle of 33° results in an "helical wheel" shown in Fig. 6.4E. Although this alignment of all α-helical

simulations best fits the experimental spectrum, this model does not explain the total absence of experimental signal intensities in the region 170-185 ppm. In a third step the PISEMA spectrum of a 3_{10}-helix labeled at its backbone (φ = -50°, ψ = -31°) an exhibiting a tilt angle of 35° was calculated (Fig. 6.4G). Indeed this structural model is consistent with the absence of intensities in the region 170-185 ppm, as observed in the experimental spectrum. Our and others' simulations (Kim and Cross, 2004) show that gaps in the 'helical wheel' are characteristic for the 3_{10} helical structure and their position dependent on the helical pitch angle characterizing the positioning of residues around the helix long axis.

Since the spectrum was recorded using cross-polarization, it remains possible that the efficiency of the magnetization transfer from ^{1}H to ^{15}N is dependent on the resonance position. "Holes" in the spectra around the chemical shift position of the magic angle have been observed previously in cross-polarized ^{15}N or ^{31}P solid-state NMR spectra of membranes (Frye et al., 1985, Prongidi-Fix et al., 2007, Yamaguchi et al., 2001). However, similar experiments performed with ampullosporin A reconstituted into oriented di-C12:0-PC exhibits clear signal intensities in this chemical shift region (Fig. 6.4B) indicating that magnetization transfer works well. Notably, the upper and lower limits of the ^{15}N chemical shift range observed for ampullosporin A in di-C12:0-PC or di-C10:0-PC bilayer closely match each other suggesting a similar tilt angle of the peptides. Again, the experimental spectrum (Fig. 6.4B) was compared to spectral simulations for structural models representing either the crystal structure, a perfect α-helix (φ = -65º, ψ = -45º) or a perfect 3_{10}-helix (φ = -50º, ψ = -31º). A helix tilt of 30º for the crystal structure, a perfect α-helix and of 32º for a perfect 3_{10}-helix matches well the chemical shift range. And spectral simulations of a perfect 3_{10}-helix were performed with variable pitch angles around the helix long axis. The best results are shown in Fig. 6.4 D,F,H, indicating that for the spectrum of ampullosporin in di-C12:0-PC all these structures fit at the same level of reliability.

As our data are suggestive that the 15-residue ampullosporin A adopts a high degree of 3_{10} helical structure in di-C10:0-PC we decided to more closely investigate the structure of alamethicin in membrane environments. The membrane alignment of alamethicin has been characterized as a function of lipid composition and hydration using OCD techniques (Huang and Wu, 1991) and the membrane interactions of this peptaibol have been intensely studied by a variety of techniques including oriented solid-state NMR spectroscopy. Using this latter approach transmembrane alignments have been observed

in POPC using 1D ^{15}N solid-state NMR spectroscopy or uniformly labeled alamethicin at P/L ratios of 1:15 and 1:237 (Bechinger et al., 2001), or in DMPC at P/L ratio of 1:8 were four peptides each labeled at a single-site have been studied using PISEMA (Bak et al., 2001), In both cases it was assumed that alamethicin adopts an α-helical conformation and the data were analyzed accordingly.

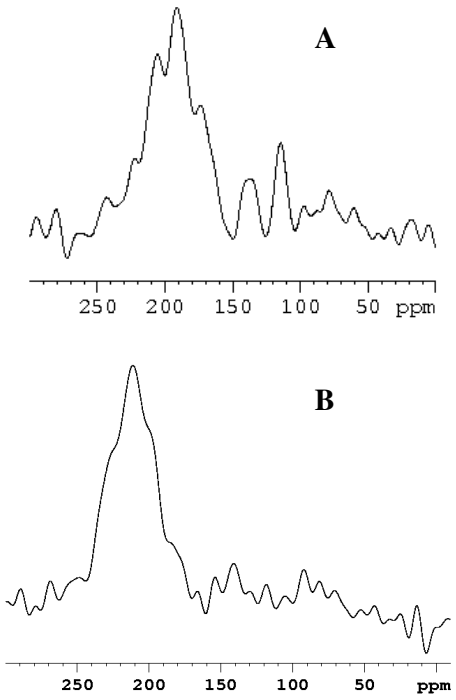

Figure 6.5. *1D proton-decoupled ^{15}N spectra of ^{15}N uniformly labeled alamethicin in (**A**) oriented DMPC (1/8), 37°C, (**B**) POPC (1/100), 21°C*

In order to better compare with the PISEMA spectra recorded for single ^{15}N labeled alamethicin in fluid phase DMPC (Bak et al., 2001), a proton-decoupled ^{15}N spectrum of alamethicin in the liquid crystalline DMPC bilayer at P/L ratio of 1:8 was recorded under similar conditions than used here for POPC membranes (Fig. 6.5). Although both spectra are indicative of transmembrane alignments the chemical shift range observed for alamethicin in DMPC (Fig. 6.5A) suggested a more tilted helix arrangement when compared to POPC (Fig. 6.5B).

In order to get insight to the structure of alamethicin bind to lipid bilayer 2D ^{15}N -^{1}H dipolar coupling ^{15}N chemical shift correlation spectra were recorded. PISEMA spectrum for ^{15}N uniformly labeled alamethicin in POPC at room temperature with the bilayer normal parallel to external magnetic field is shown in Fig. 6.6A. The spectrum is characterized by high signal intensities in the ^{15}N chemical shift range of 200-235 ppm,

which correlate with ^{15}N-^{1}H dipolar couplings of 8 - 16 kHz. Weak additional intensities are observed at 107 ppm / 2 kHz, which is close to the isotropic ^{15}N chemical shift of glutamine side chains, of which the peptide carries three.

Simulation of PISEMA experiment using SIMMOL and SIMPSON software (Bak et al., 2002) for the uniformly labelled backbone amides are shown in Fig. 6.6B. We first compared how the known crystal structure at various alignments relative to the membrane normal fits the experimental spectrum. The alamethicin crystal structure found by (Fox and Richards, 1982) contains three units. In all of them the N-terminus is alpha-helical which is followed by a less well-ordered secondary structure at the C-terminus. Units A and B exhibit a 25°-35° bent around Pro^{14}. The closest SIMMOL simulation of PISEMA experiment for ^{15}N backbone labeled units A and B are shown in Fig. 6.6B. This model produces noticeable peaks in the region < 200 ppm, which is inconsistent with experimental result. Apparently, the tilt angle of 14° in not sufficient to compensate for the strong bent present in unit A and B of crystal structure, resulting in the additional signals in this region. Unit C has a more complex structure, but even the simulation with an alignment that matches best the experimental spectrum (Fig. 6.6C), is inconsistent with experimental result.

In a next step a uniformly ^{15}N labeled ideal α-helix of 20 residues (φ = -65°, ψ = -45°) tilted by 14° gives the "helical wheel" shown in Fig. 6.6 D. One can see that this simulation does not explain the experimental peak at 210 ppm ^{15}N chemical shift and 8 kHz dipolar splitting.

Finally, the simulation of the PISEMA experiment for a 3_{10} helical model peptide (φ = -50°, ψ = -31°) with all backbone nitrogens labeled with ^{15}N and arranged at a 14° tilt angle relative to external magnetic field is shown superimposed on the experimental spectrum in Fig. 6.6 E. Note, that the peak at 210 ppm and 8 kHz dipolar splitting, which was not possible to explain with α-helical conformation, is nicely reproduced this time.

From these simulations, a combination of two helices: α-helix and 3_{10}-helix is likely to reproduce experimental spectrum. As an example, model 20 residues peptide of α-helix in N-terminus (the first 10 residues) and 3_{10}-helix in C-terminus (the last 10 residues) results in a PISEMA spectrum, shown in Fig. 6.6F. Of all the models tested this structure shows the best agreement with the experimental restrictions.

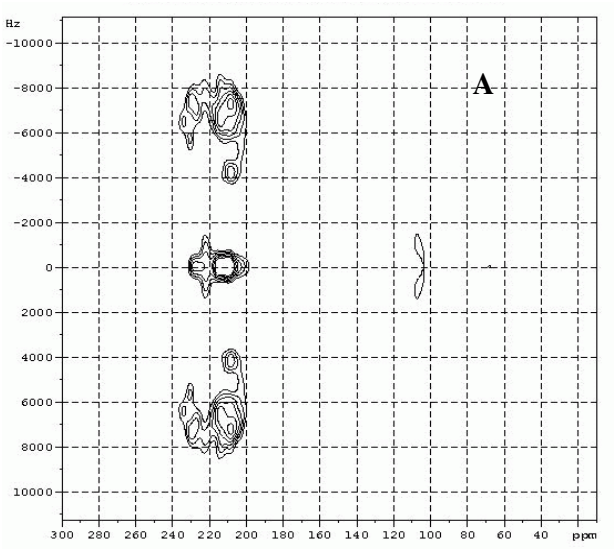

Figure 6.6 A. *Experimental 2D PISEMA spectrum of ^{15}N uniformly labeled alamethicin associated with perpendicular oriented POPC bilayers*

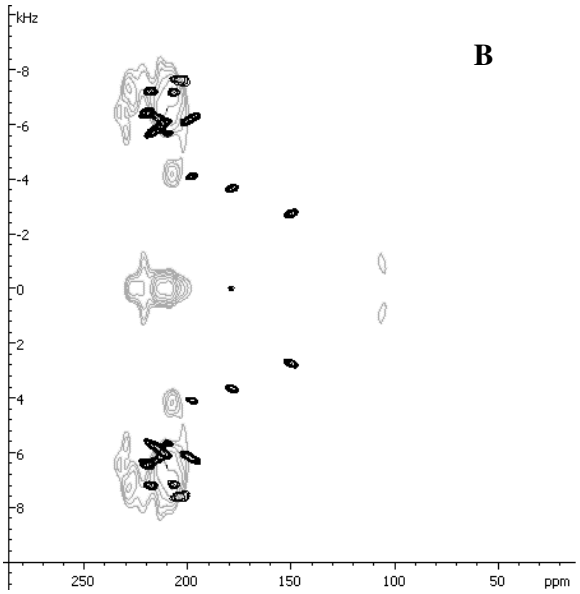

Figure 6.6 B. *SIMMOL calculated PISEMA spectrum for ^{15}N uniformly labeled XRD alamethicin structure (pdb: 1AMT), unit A, N-terminal end (the first 11 residues) tilted 10° relative to external magnetic field (black) superimposed on the experimental spectrum (light gray)*

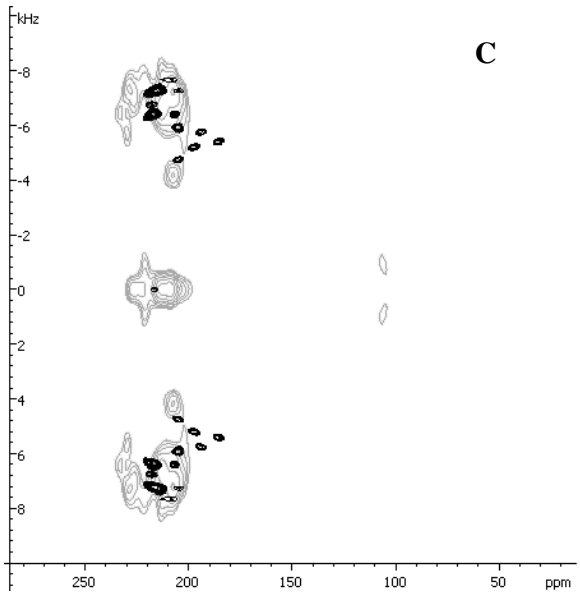

Figure 6.6C *SIMMOL calculated PISEMA spectrum for ^{15}N uniformly labeled XRD alamethicin structure (pdb: 1AMT), unit C, N-terminal end (the first 8 residues) tilted 10° relative to external magnetic field (black) superimposed on the experimental spectrum (light gray)*

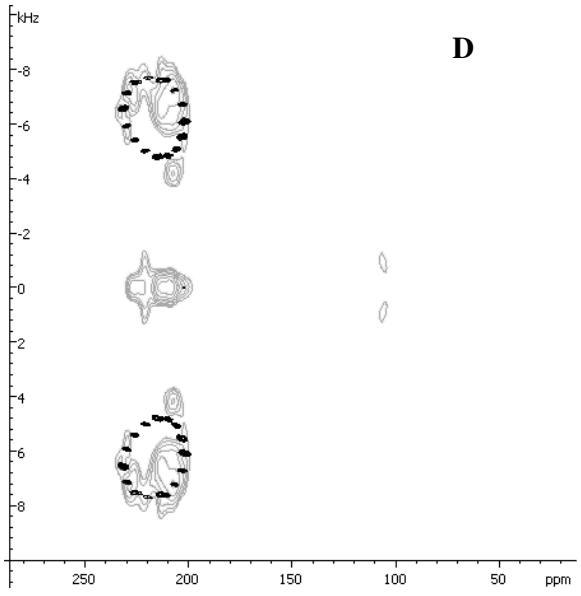

Figure 6.6D *SIMMOL calculated PISEMA spectrum for ^{15}N uniformly labeled model alpha-helical (φ = -65°, ψ = -45°) peptide tilted 14° relative to external magnetic field (black) superimposed on the experimental spectrum (light gray).*

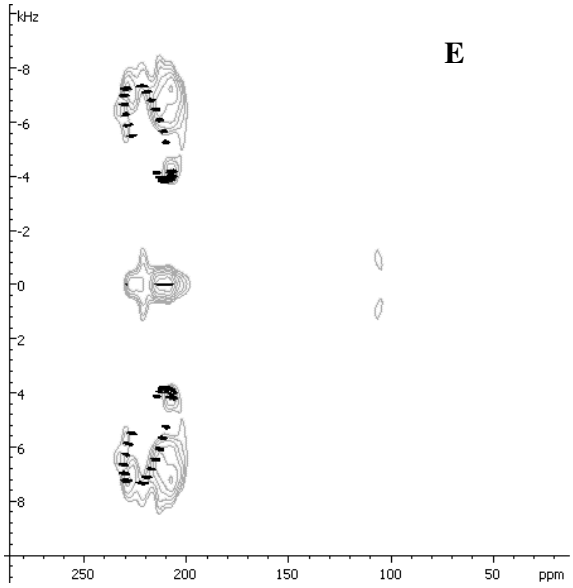

Figure 6.6E *SIMMOL calculated PISEMA spectrum for ^{15}N uniformly labeled 3_{10}-helical (φ = -50°, ψ = -31°) model peptide, tilted 14° relative to external magnetic field (black) superimposed on the experimental spectrum (light gray).*

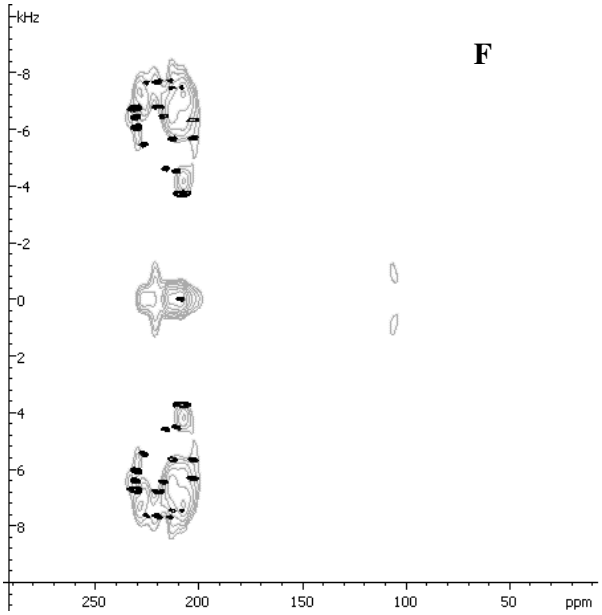

Figure 6.6F *SIMMOL calculated PISEMA spectrum for ^{15}N uniformly labeled mixed $\alpha / 3_{10}$-helical model peptide, tilted 14° relative to external magnetic field (black) superimposed on the experimental spectrum (light gray).*

When the sample used to obtain the spectrum shown in Fig. 6.6A is tilted by 90 degrees, the 2D PISEMA spectrum shown in Fig. 6.7A is obtained. The 3_{10}-helical structure tilted 104 degrees (Fig. 6.7 C) matches better the experimental spectrum when

compared to an ideal α-helix or the alamethicin crystal structures tilted by 104 degrees relative to the external magnetic field direction (Fig. 6.7 B). However, since the spectral resolution at this orientation is considerably reduced, the differences between the two simulations are less pronounced.

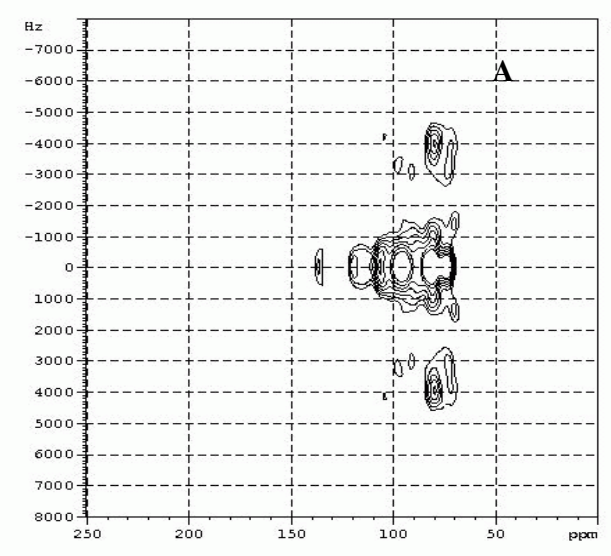

Figure 6.7A. *Experimental PISEMA spectrum for ^{15}N uniformly labeled alamethicin in POPC (the same sample as in Fig 6.6) with the membrane alignment parallel to external magnetic field.*

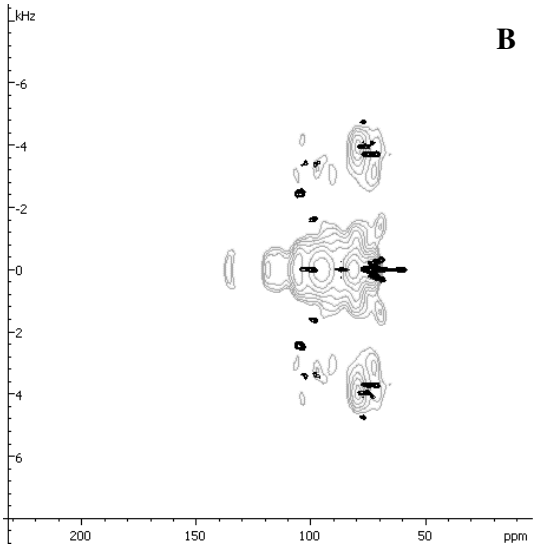

Figure 6.7B. *SIMMOL calculated PISEMA spectrum for ^{15}N uniformly labeled α-helical (φ = -65°, ψ = -45°) model peptide, tilted 104° relative to external magnetic field (black) superimposed on the experimental spectrum (light gray).*

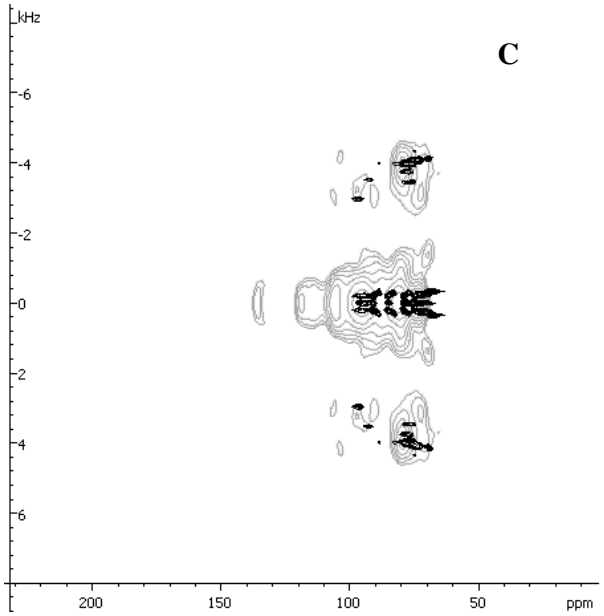

***Figure 6.7C**. SIMMOL calculated PISEMA spectrum for ^{15}N uniformly labeled 3_{10}-helical (φ = -50°, ψ = -31°) model peptide, tilted 104° relative to external magnetic field (black) superimposed on the experimental spectrum (light gray).*

Discussion

Ampullosporin A is composed of predominantly hydrophobic amino acids; only about one-quarter are polar, and none of them are charged. The peptide, therefore, strongly interacts with phospholipid membranes. In di-C10:0-PC bilayers transmembrane alignment is observed at P/L = 1/100 (Fig. 6.2A). Whereas ampullosporin A adopts transmembrane alignments in di-C10:0-PC, it is oriented parallel to the sample surface when the fatty acyl chains of the bilayer phosphatidylcholines exceed 12 carbon atoms (Figs 6.2A-D).

Slightly different chemical shift for ampullosporin A bound to di-C12:0-PC and di-C10:0-PC indicate a higher tilt angle of the peptide in thinner membrane (Fig. 6.2 C and D). Similar observations were made with alamethicin when bound to fluid DMPC and POPC membranes (Fig. 6.5). The increase in tilt is one of the possible mechanisms for the peptide to compensate for mismatch conditions, when the hydrophobic part of a peptide is too long to span the membrane (Killian, 1998).

In the presence of phosphatidylcholine bilayers of a thickness commonly observed in biological membranes, ampullosporin A orients parallel to the membrane surface (Figs

6.2A,B). Similarly in the absence of transmembrane potentials, in-plane alignments have been observed at low P/L ratios for zervamicin II (Bechinger et al., 2001) and alamethicin (Huang and Wu, 1991). It is believed that peptaibols are inactive in their in-plane orientation (Huang, 2006). Interestingly the permeability of POPC vesicles is increased in the presence of peptaibols ampullosporin A, zervamicin IIB and antiamoebin I at P/L ratios similar to and lower than those used in this study even in the absence of transmembrane potentials (Kropacheva et al., 2005). ^{15}N solid-state NMR data are consistent with zervamicin II and ampullosporin A exhibiting partial transmembrane helical alignments albeit at different concentrations. Therefore, it remains possible that transmembrane helical bundle formation and pore formation occur also in the absence of voltage-gating.

On the other hand, increases in membrane permeability induced by amphipathic peptide helices, which exhibit stable in-plane alignments, have also been observed (Bechinger, 1999). To explain these observations, various models, some of them based on peptaibol interactions with phospholipid bilayers others on the detergent-like properties of amphiphiles, have been suggested (Bechinger, 1999; Bechinger and Lohner, 2006). Detergent-like properties were also used as an explanation for the increased release of fluorescent dyes from large unilamellar vesicles at high P/L ratios and in the absence of transmembrane potentials (Kropacheva et al., 2005, Snook et al., 1998). However, formation of non-bilayer lipid conformations was observed upon ampullosporin A incorporation to membrane at much higher P/L ratios of 1/10 (Fig. 6.3G).

The in-plane membrane-bound ampullosporin A is not a static molecule. Rather, the entire helix undergoes uniaxial rotational diffusion around the bilayer normal, perpendicular to the helix axis, on a timescale shorter than ~150 ms. This is unambiguously shown by the averaging observed in the perpendicular oriented ^{15}N spectrum (Fig. 6.2E). Similarly fast rotation around the bilayer normal was reported for the in-plane POPC bound ovispirin peptide (Yamaguchi et al., 2001) and in-plane fluid DMPC bound KL14 model peptide (Aisenbrey and Bechinger, 2004). Note that this uniaxial rotational diffusion does not contradict the amphipathicity of the peptide, because the motional axis is not the helix axis but rather the bilayer normal. Thus, the hydrophobic face of the peptide remains in contact with the hydrophobic lipid bilayer, and the hydrophilic residues face the water molecules even during rotational diffusion.

Uniaxial rotation is known to occur in several transmembrane oriented peptides of similar sizes, such as gramicidin (Cornell et al., 1988; Lee et al., 1993), melittin (Smith et

al., 1994), alamethicin (North et al., 1995) and even in transmembrane domain of the M2 protein from the influenza A virus, which was found to have a significant tilt angle of 32°–38° with respect to the bilayer normal (Song et al., 2000). It also undergoes fast uniaxial rotation around the bilayer normal, as shown by the motionally averaged ^{15}N lineshape (Fig. 4 *B* in Song et al., 2000) when the bilayer normal was perpendicular to the magnetic field.

The 3_{10}-helix is more tightly packed and more elongated than the α-helix. The sets of φ,ψ torsion angles of the α- and 3_{10}-helices do not differ much, falling within the same region of the Ramachandran map (termed "helical" region). However, the C=O ··H–N intramolecular H-bonding schemes are different, $i \leftarrow i+3$ for the 3_{10}-helix, and $i \leftarrow i+4$ for the α-helix. Thus, the α -helix may be gradually transformed into a 3_{10}-helix (and vice versa) maintaining a nearly helical conformation of the chain throughout. Further, if one of the conformations should turn out to be impossible (e.g., as a result of side-chain interactions), the main chain may slip into the other conformation. In fact, the 3_{10}-helix appears to derive its importance mainly from its proximity in the conformational energy map to the more stable α -helix. Thus, the role of the 3_{10}-helix as an important intermediate in the mechanism of folding of α-helical proteins may be envisaged. (Bolin and Millhauser, 1999).

The 3_{10}-helix has been initially associated with peptides containing Aib. Indeed, tri-, tetra- and pentapeptides containing at least one Aib residue fold into a 3_{10}-helical structure. However, longer Aib-containing peptides have α-helical or mixed 3_{10}/α-helical geometries (Karle and Balaram, 1990).

Molecular dynamics studies of isolated transmembrane peptides in di-C14:0-PC bilayers showed that the length of an α-helix may fluctuate significantly due to local variations in backbone structure (Shen et al., 1997, Belchorcova et al., 1997). Among the possibly more stable configurations that might occur in α-helical peptides are (partial) transitions to a 3_{10}-helix, which has a smaller helical pitch than an α-helix, and therefore would increase peptide length, or to a π-helix, which has a wider helical pitch. Both these transitions were observed at least locally and temporarily by molecular dynamics in a transmembrane polyalanine helix (Shen et al., 1997).

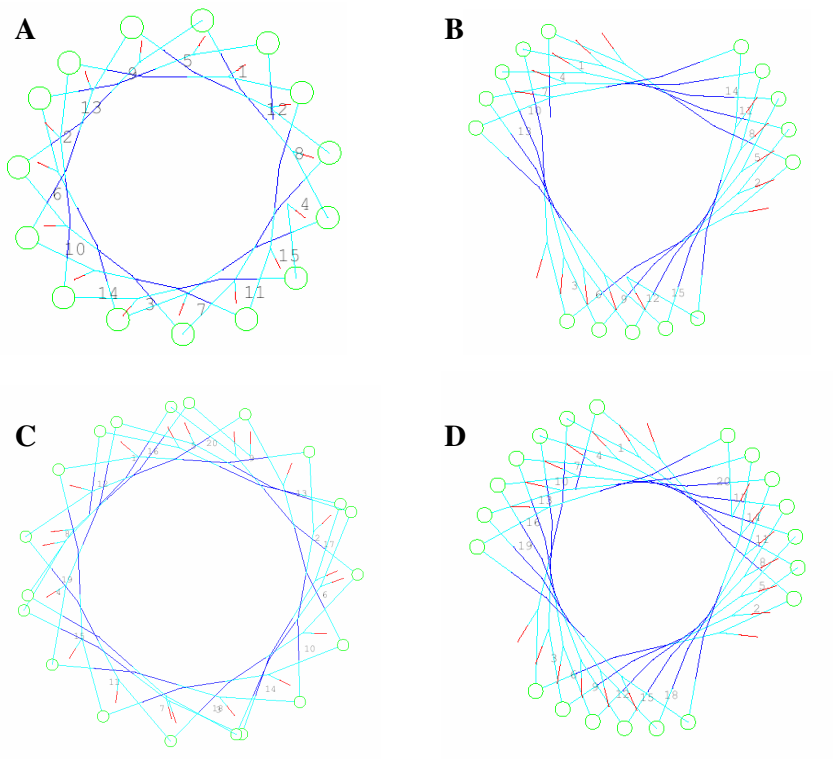

***Figure 6.8**. Helical wheel projections for α-helix (A, C) and 3_{10}-helix (B, D) of 15 and 20 amino acids.*

To get access to the structure of transmembrane peptides 2D PISEMA experiments were performed. For the simulation of these spectra crystallographic structure and 2 model peptide structures of 3_{10}- and α-helixes were compared.

Alamethicin crystal structure (obtained by Fox and Richards, 1982, pdb: 1AMT) has strong 25° - 35° bent and doesn't represent well the POPC-bound peptide conformation. In the same way the simulation of PISEMA experiments using the crystal structure of ampullosporin A (Kronen et al., 2003, pdb: AMPA) was not successful to fit experimental spectra.

The amid ^{15}N tensor orientation was measured in molecular frame, relative to so-called peptide plane – the plane created by C-O and N-H of mutual amino acids connected by peptide bond. This is only possible when ω-angle is equal to 180°. Taking into account up to 17° deviation of ω-angle from 180° (see Table 3 from Kronen et al., 2003) could result in a deviation in ^{15}N CS resonances on the order of 10 ppm. On this basis the found inconsistence of crystal structure with membrane bound ampullosporin A state is not so evident. However, CD analysis on Ampullosporin A (Nguyen et al., 2003) gives that: in micellar detergents, the CD spectra were characteristic of helical association

with less helicity accompanied with higher content of 3_{10} or β structure then that found in crystal.

According to simulation with model peptide at different secondary structure, perfect α-helix (Figs 6.4E, 6.6G) is not sufficient to match experimental data (Figs 6.4 A, 6.6 A), while 3_{10}-helix quite reasonably describes the experiment (Figs 6.4 G, 6.6 I). Experimental PISEMA constraints strongly support the existence of 3_{10}-helix peptaibols when bound to PC membranes, at least in part.

Similar results were found in (Bak et al., 2001). Three single ^{15}N labeled alamethicin analogs were reconstituted to DMPC membrane and ^{15}N-^{1}H versus ^{15}N chemical shift spectra were recorded. Simulation of these spectra using X-ray diffraction alamethicin structure (obtained by Fox and Richards, 1982, pdb: 1AMT) and ideal α-helix was not sufficient to fulfill experimental constrains, while simulation with ideal 3_{10}-helix nicely coincides with experimental results. Indeed, perfect 3_{10}-helix conformation of alamethicin doesn't exhibit amphipathic properties, which supposed to be necessary to self-assemble to transmembrane channel. Taking this into account they came up with mixed secondary structure, namely α-helix at N-terminus with the tilt angle of 17° switching to somewhat close to 3_{10}-helix structure around the Pro^{14} residue with the tilt angle of 11°.

Chapter 7

Lipid membrane disturbance by the presence of alamethicin and ampullosporin A peptides. Perspective.

Introduction

Whereas the mode of binding to the lipid bilayer is an important aspect in understanding the mechanism of action of peptaibols, measuring the effects on the structure and dynamics of lipid bilayers upon peptide binding provide additional useful insights into the antimicrobial functions. ^{2}H NMR is a widely used probe of the conformational order of liquid-crystalline lipid bilayers (Koenig et al., 1999; Seelig and Seelig, 1980). Experiments, made so far, were concentrated on PC membranes, where peptaibols were shown to be active (Duclohier and Wroblewski, 2001, Kropacheva et al., 2005, Mazzuca et al., 2005). On the other hand, the peptide behavior is membrane dependent (Kropacheva et al., 2005, Huang and Wu, 1991). And it would be of interest to study model membranes of different composition. In the present chapter we provide a study with POPC and POPE–POPG 3/1 membranes. The last one is considered the mimetic of the composition of *E.coli* membranes We compared the ^{2}H quadrupolar splittings of POPC-d31 in the absence and presence of alamethicin or ampullosporin A peptides. Also, the ^{2}H quadrupolar splittings of deuterated POPG in the mixed POPE/POPG membrane in the presence and absence of alamethicin and ampullosporin A peptides were compared. ^{15}N solid state NMR spectroscopy was taken as a complementary technique.

The de-Paking of ^{2}H spectra was done by A. James Mason.

Results

The ^{2}H spectra of POPC/POPC-d31 lipid vesicles without the peptide (Fig. 7.1*A*) exhibits well resolved splittings, which can be converted to an order parameter profile that decreases along the acyl chain with increasing depth (Bloom et al., 1991). The largest quadrupolar splitting is 24 kHz, which corresponds to an order parameter of 0.19, and can be assigned to the relatively rigid CD_2 groups closest to the glycerol backbone. The smallest splitting is 5 kHz and corresponds to the mobile methyl groups at the end of the acyl chains in the core of the bilayer.

Upon the addition of ampullosporin A to POPC lipid at 2mol%, a reduction of some of the ^{2}H quadrupolar splittings is observed (Fig. 7.1*A*). Simulation of spectrum yields a reduction of the order parameters of 0.01 units for CH_2 groups deeper then position 9 (Fig. 7.1*B*). This increased disorder of the acyl chains in the hydrophobic core of the bilayer is understandable taking into account predominant surface orientation of the peptide (chapter 6, Fig. 6.2). Binding of ampullosporin A at the membrane-water interface increases the area of the membrane at the level of lipid headgroup, thereby allowing more spatial freedom for motion in the acyl chains. Such an increase in the bilayer disorder and fluidity has also been reported recently for other membrane peptides and proteins that possess a predominantly surface component (Huster et al., 2001; Koenig et al., 1999).

Upon the addition of alamethicin to POPC membranes at 2mol%, no influence on the ^{2}H quadrupolar splittings was observed (Fig. 7.1*A*). DePaking of the spectra yielded a similar order parameters for the entire lipid chain length when compared to pure POPC/POPC-d31 membranes (Fig. 7.1*B*). The difference on the influence of these two peptides on the POPC membrane may be readily explained by the different mode of peptide binding. No visible effect on bilayer lipid chain ^{2}H quadrupolar splittings is in agreement with the transmembrane orientation of alamethicin (chapter 5).

Similar experiments were performed with POPE-POPG-d31 membrane (fig. 7.1C). In this case the ^{2}H spectra of lipid vesicles without the peptide exhibits quadrupolar splittings that are larger then that obtained for POPC vesicles. The largest quadrupolar splitting is now 30 kHz, which corresponds to an order parameter of 0.23, and can be assigned to the relatively rigid CD_2 groups closest to the glycerol backbone. The smallest splitting is 3 kHz and corresponds to the mobile methyl groups at the end of the acyl

chains in the core of the bilayer. Subsequently in this case a reduction of ^{2}H quadrupolar splittings upon 2mol% peptide addition is clearly more pronounced. Surprisingly, a significant reduction of the ^{2}H quadrupolar splittings and a broadening of most peaks upon peptide addition were found to be similar for both peptides studied (Fig. 7.1C). DePaking of these spectra yielded reduced order parameters for the entire lipid chain length, ranging from 0.22 to 0.03 (Fig. 7.1D). Such a reduction is consistent with the surface peptide orientation.

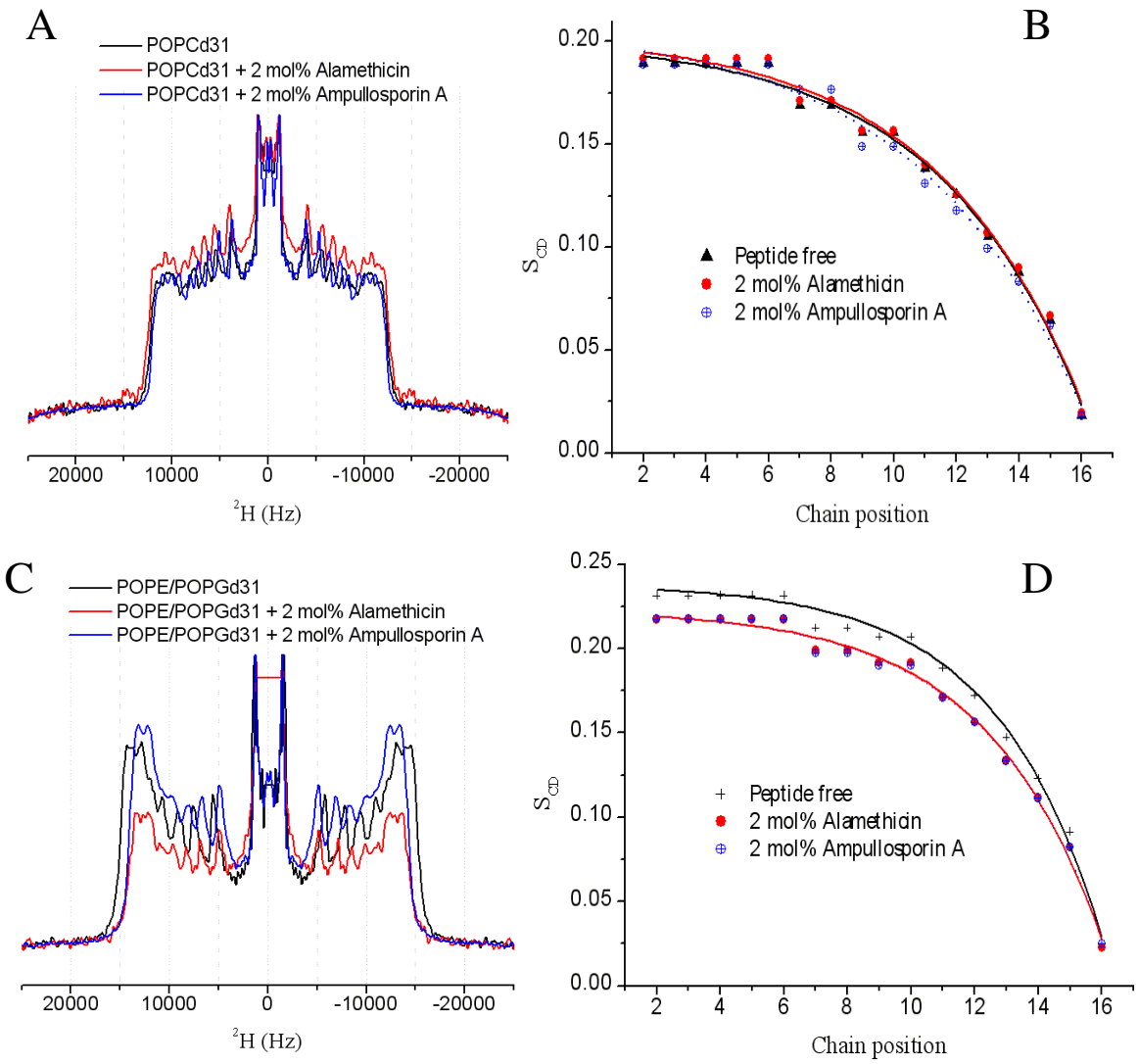

Figure 7.1. *Comparison of ^2H echo spectra acquired for lipid vesicles containing either POPC/POPCd31 (3:1) (**A**) or POPE/POPGd31 (**C**) either alone or with 2 mol% peptide added and their respective smoothed order parameter (S_{CD}) profiles (**B**, **D**). The presence of peptide reduces lipid acyl chain order in POPE/POPGd31 vesicles but not in POPC/POPCd31 vesicles.*

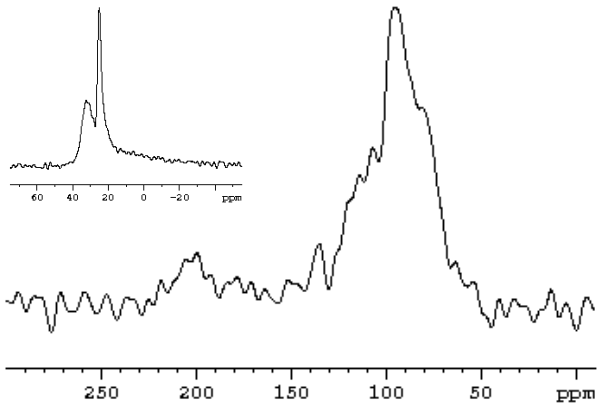

Figure 7.2. *Proton-decoupled oriented solid-state ^{15}N NMR spectrum of alamethicin in POPE/POPG 3/1 bilayers at a concentration of 2 mol %. pH 7.5 was set by addition of 1 mM Tris buffer solution. Temperature was maintained at 37°C. Bilayer normal was aligned with external magnetic field.* ***Inset*** *represents corresponding proton-decoupled ^{31}P NMR oriented spectrum.*

In order to check the orientation of alamethicin peptide proton-decoupled ^{15}N CP spectrum of uniformly ^{15}N labeled alamethicin and reconstituted into fully hydrated POPE/POPG membrane at 2mol% at pH 7.5 was recorded at the temperature 310 K (Fig. 7.2). Major peak in the region less then 120 ppm reveals indeed a predominant surface orientation of this helical peptide. The proton-decoupled ^{31}P solid-state NMR spectrum of the same sample (inset in Fig. 7.2) indicates a homogenous alignment of the lipid headgroups.

Discussion

Membrane perturbation by surface bound peptide molecules is well known (Yamaguchi et al., 2001, de Planque et al., 1998) and not surprising. No influence of transmembrane bound peptide to the membrane has been also reported for WALP peptide under conditions of matching between peptide hydrophobic length and membrane hydrophobic thickness (de Planque et al., 1998).

Similar disturbance of POPE/POPG lipid bilayer for both alamethicin and ampullosporin A indicates similar surface binding of these peptides. Interestingly,

alamethicin adopts a transmembrane orientation when bound to POPC membrane and switches to an in-planar mode in POPE/POPG bilayers. There could be two possible reasons. First of all, the most obvious difference between these membranes is the negative charge of PG headgroup, while PE and PC are zwitterionic. Indeed, Aguilella and Bezrukov (Aguilella and Bezrukov, 2001) report that conductance level of alamethicin in negatively charged POPS membrane is lower than that in neutral POPE membrane. Note, that according to barrel-stave model active peptide molecules adopt transmembrane orientation.

Another explanation could be related to the different order profiles of POPC and POPE/POPG membranes (Fig. 7.1), which reveals a difference in the packing of these membranes. Whereas POPE/POPG bilayers have much more ordered structure where the motions of the hydrocarbon tails are reduced, POPC membrane shows a high degree of motional freedom in its core. This is certainly the consequence of different headgroups, which occupy a different volume and the subsequent differences in hydrophobic thickness of these two lipid bilayers. Data are available for the thickness of DLPC and DLPE bilayers. Indeed, the DLPE thickness is 25.8 Å (Nagle and Tristram-Nagle, 2000), whereas the DLPC hydrophobic core reaches only 19.5 Å (Lewis and Engelman, 1983), and difference of similar order of magnitude should be present for POPE and POPC membranes in their fluid phase. PG headgroup has even less volume (if the mutual repulsion between neighbor's negatively charged headgroups of PG could be neglected, as it is in mixed PE/PG membranes with high enough content of neutral PE component), suggestive that mixed POPE/POPG membranes exhibit a higher hydrophobic thickness when compared to POPC membranes.

For the moment the question of the key-parameter (the negative charge of PG headgroup or extended hydrophobic thickness of POPE/POPG membrane), which is responsible for surface bounding of alamethicin, remains open. Further experiments are needed to refine this question.

Chapter 8

Summary

The aim of the thesis was the characterization of the structure, dynamics and topology of selected peptaibols when associated with model biological membranes. Investigations were focused on the three members: trichogin GA IV, ampullosporin A and alamethicin, which are different in length and vary in their intensity of biological activity.

The studies suggest the hydrophobic (mis)match between peptide hydrophobic length and membrane apolar core plays a key role for peptide topology. Indeed, the 20meric alamethicin adopts a transmembrane orientation in POPC and in fluid phase DPPC membranes (chapter 5), while the increase in membrane thickness of DPPC when reaching the gel phase forces alamethicin into an in-plane alignment (chapter 5). A similar behaviour was observed for 15-mer ampullosporin A, studied in chapter 6. It adopts transmembrane orientations in thin membranes of diC10:0PC and diC12:0PC, but switches to the in-plane mode with increasing membrane thickness. In a similar manner the 11-mer trichogin GA IV is obviously too short to completely span DPPC membrane and, indeed, it adopts an in-plane orientation, as described in chapter 4.

Using hydrophobic (mis)match as a key-player on peptide topology, it is possible to explain the concentration effect, found for alamethicin in gel phase DPPC (chapter 5), for ampullosporin A in fluid POPC (chapter 6) and even for trichogin GA IV in gel phase DPPC (chapter 4). In all these cases at low peptide-to-lipid ratios the peptide adopts in-plane orientations; however, above a threshold concentration the peptide orients in a transmembrane fashion. This behaviour is in perfect agreement with the two state model, proposed by Huang (Huang, 2006). The in-plane oriented peptides partition into the surface of the membrane at the level of the lipid headgroups and produce a membrane-thinning effect, which depends on peptide concentration (Chen et al., 2003; Lee et al., 2004). This effect is also reflected by a decrease in the order parameter profiles of lipid hydrocarbon chains in the presence of in-plane oriented peptides (see chapter 7). At

critical peptide concentrations membrane thickness reaches the level, which is sufficient to better match the hydrophobic length of the peptide and subsequently makes the transmembrane peptide orientation energetically more favourable.

Interestingly, transmembrane oriented alamethicin was unambiguously observed in their oligomerized form (chapter 5). These data are in line with "barrel-stave" model as the formation of transmembrane pores was suggested. Indeed, well-defined water-filled pores were detected by neutron in-plane scattering in bilayers containing transmembrane alamethicin (He et al., 1996). In addition, similar oligomerized state of alamethicin was observed in gel phase DPPC at high concentrations, which also suggests the presence of transmembrane peptide alignments.

Similar concentration effect was found for trichogin GA IV in gel phase DPPC membranes. Whereas at low peptide concentrations trichogin is bound to the DPPC membrane surface as a monomer (Milov et al., 2005), at high peptide concentration oligomers tend to appear (Salnikov et al., 2006). These observations are in general agreement with those reported by Mazzuca et al., 2005. For an egg PC bilayer containing 50 mol % cholesterol and studied at room temperature, these authors found that at low peptide/lipid ratios trichogin binds close to the region of polar headgroups. By increasing the concentration, up to the level of membrane leakage, a strong correlation was found between the fraction of more deeply buried peptide and the fraction of oligomers (Stella et al., 2004). Thus, the monomeric and surface-bound peptide molecules are likely to be biologically inactive, while the buried, oligomerized peptides are responsible for membrane leakage.

Detection of a high 3_{10} helical content in both alamethicin and ampullosporin A peptides when in a transmembrane state makes the similarity of these peptaibols even more pronounced (chapter 6). Similarly a mixed $\alpha/3_{10}$ helix conformation was also reported for trichogin GA IV in different organic solvents and in a membrane-mimetic environment (Monaco et al., 1999b). Possibly such behavior is the consequence of high content of unusual Aib aminoacids, which are known to favour 3_{10} helical peptide conformations (reviewed in Crisma et al., 2006). As the 3_{10} helix is more elongated when compared to α-helical conformation, the ability to adopt a high degree of this secondary structure could play an important role in membrane permeation by peptaibols.

Our studies therefore suggest some common properties for the peptaibols when bound to membrane. Hydrophobic (mis)match between peptide hydrophobic length and membrane apolar core was shown to play a key role on peptide orientation. The data

suggest similar modes of action for all peptaibols with their biological activity dependent on their hydrophobic length. This supposition is well consistent with the order of their antimicrobial activity: Alm >> AmpA >> Trichogin GA IV. However, it could be that the right mode of action is the detergent-like model, where different complementary models of action might occur depending on the detailed conditions. In this case the extensive plasticity of peptide/detergent–lipid complexes opens up the possibility that a peptide induces a certain macromolecular structure when interacting with the membranes of one organism, but a different one when interacting with another species (Bechinger and Lohner, 2006).

Another important aspect of this thesis work was the investigation of exactly the same peptaibol molecule, e.g. alamethicin, when bound to membranes using EPR and oriented solid-state NMR to obtain information on both the alignment and the oligomerization of the peptides in membranes. This approach using two complementary techniques allows not only the gathering of more information about peptide/membrane interactions but also the direct comparison of these different magnetic resonance methods.

Pulsed EPR applied to peptides in membranes needs the introduction of relatively bulky spin labels and to be performed at low temperatures in order to decrease the rate of relaxation processes. Both these restrictions could dramatically affect the native peptide-membrane interactions. Solid-state NMR is free of these particular restrictions, but relatively insensitive to peptide oligomerization. The critical comparative study (chapter 5) proofs no influence of the temperature in the range from 77 K to 295 K and introduction of bulky spin label on the alamethicin topology. In addition, no influence of the membrane phase was observed in the case of POPC membranes, which is consistent with the hydrophobic bilayer thickness being the critical parameter for peptide topology.

On the other hand, solid-state NMR of oriented samples requires macroscopically oriented membranes. Preparation of well-aligned samples is of particular importance for deducing peptide helix orientation, which immediately moves these experiments to the field of the art. For example, poorly oriented DPPC membrane upon addition of high amount of alamethicin peptide (1 / 20) made the solid-state oriented sample NMR approach unsuccessful. Possible explanation is the formation of non-bilayer lipid organization, which is consistent with detergent-like action of peptide at high concentration (Bechinger and Lohner, 2006). Contrary, EPR technique still gives valuable information even at these high peptide concentrations.

Every method has their own limitations and, as it was shown in this thesis, smart combination of different approaches could results in remarkable synergetic progress.

Appendix

Preparation of ^{15}N uniformly labelled ampullosporin A.

Preparation of ^{15}N uniformly labelled ampullosporin A was done by Herdis Friedrich, Jena.

^{15}N-ampullosporin A was isolated from cultures of *Sepedonium ampullosporum* HKI-053 grown on ^{15}N enriched medium. The strain was cultivated as a surface culture (25 l) at 23 °C in 500 ml Erlenmeyer flasks containing 100 ml medium composed as follows (g/l): maltose 5, ^{15}N-Celtone-Powder 2, KH_2PO_4 2, $MgSO_4$ x 7 H_2O 0.5, $ZnSO_4$ x 7 H_2O 0.008, pH 5.8 ... 6.2. After 34 days of cultivation the culture broth was dispersed and extracted with ethyl acetate. The residue (924 mg) was subjected to silica gel chromatography (silica gel 60, Merck, 0.063-0.1 mm, gradient: 100 % $CHCl_3$, 9:1, 8:2, 7:3, 6:4, 5:5, 4:6, 3:7, 100 % MeOH). Fractions containing ^{15}N-ampullosporin A were checked by analytical HPLC. The combined fractions were subjected to exclusion chromatography (Sephadex LH-20, MeOH). The fractions were checked by analytical HPLC. Final purification was achieved by preparative HPLC.

analytical HPLC: SPD-M10AVP Diode array detector
Nucleosil 100 C18, 5 µm, 100 Å pore size, 3 mm x 125 mm
A: 0.1 % TFA in water
B: acetonitrile
gradient: 0,5 % - 99,5 % B in 12 min
99,5 % B for 5 min
99,5 % - 0,5 % B in 4 min
0,5 % B for 1 min
flow: 1 ml/min
detection: 220 nm

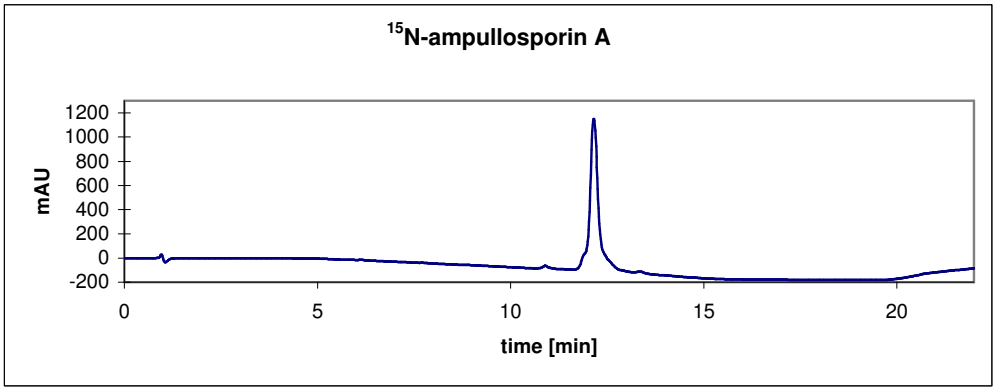

chromatographic profile of ^{15}N-ampullosporin A

preparative HPLC: Shimadzu LC 8A

Eurospher 100-Säule C8, 5 µm, 250 x 32,5 mm

A: 0,1 % TFA in H_2O

B: 0,1 % TFA in 90 % Acetonitril/H_2O

gradient: 50 % bis 100 % B in 120 min

flow: 9 ml/min

detection: 220 nm

The MS-Measurements were done with the LCQ Benchtop Massenspektrometer (Thermoelectron, Bremen). The eluent was MeOH/H_2O (99:1) and the flow 80 µl/min.

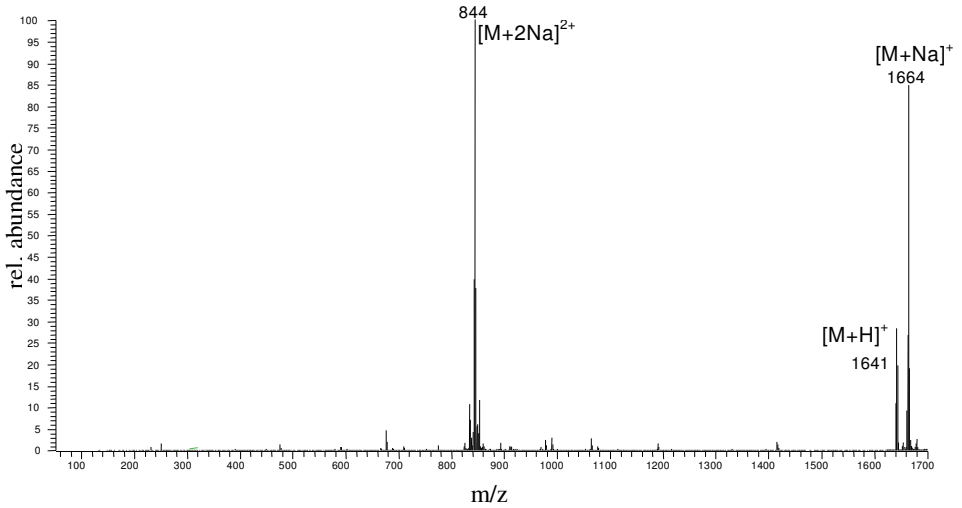

MS spectrum of ^{15}N-ampullosporin A

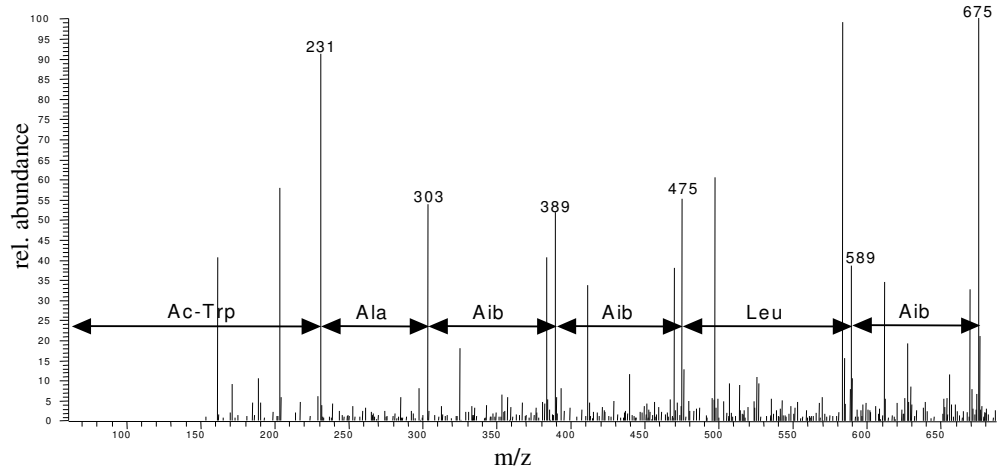

MS spectrum of *N*-terminal amino acid sequence of ^{15}N-ampullosporin A

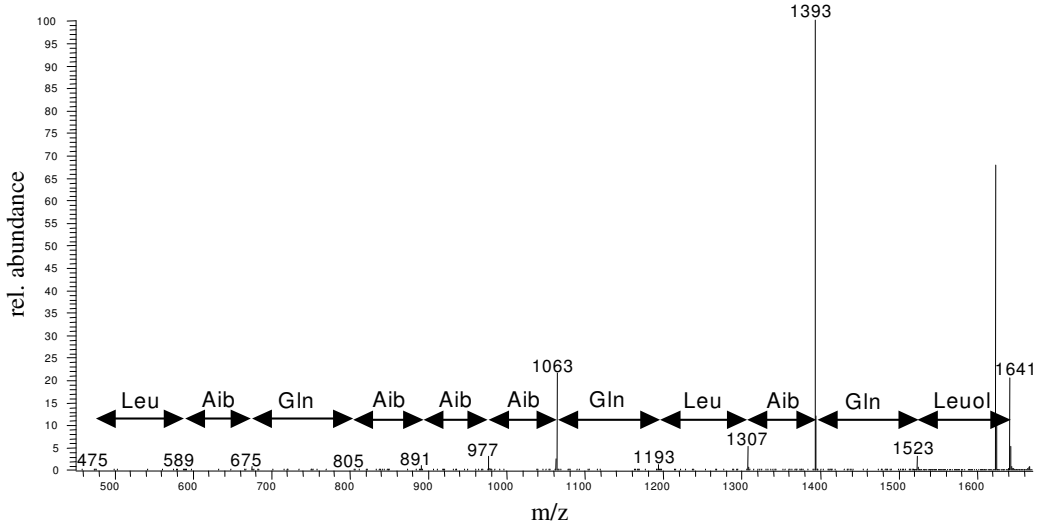

MS spectrum of *C*-terminal amino acid sequence of ^{15}N-ampullosporin A

Bibliography

Aguilella, V.M., and S.M. Bezrukov. 2001. Alamethicin channel conductance modified by lipid charge. *Eur. Biophys. J.* 30:233-241.

Aisenbrey, C., and B. Bechinger. 2004. Investigations of Polypeptide Rotational Diffusion in Aligned Membranes by ^{2}H and ^{15}N Solid-State NMR Spectroscopy. *J. Am. Chem. Soc*. 126:16676-16683.

Auvin-Guette, C., S. Rebuffat, Y. Prigent, and B. Bodo. 1992. Trichogin GA IV, an 11-residue lipopeptaibol from Trichoderma longibrachiatum. *J. Am. Chem. Soc.* 114:2170–2174.

Bak, M., R.P. Bywater, M. Hohwy, J.K. Thomsen, K. Adelhorst, H.J. Jakobsen, O.W. Sørensen, and N.C. Nielsen. 2001. Conformation of Alamethicin in Oriented Phospholipid Bilayers Determined by ^{15}N Solid-State Nuclear Magnetic Resonance. *Biophys. J.* 81:1684–1698.

Bak, M., R. Schultz, Th. Vosegaard, and N.Chr. Nielsen. 2002. Specification and Visualization of Anisotropic Interaction Tensors in Polypeptides and Numerical Simulations in Biological Solid-State NMR. *J. Magn. Reson.* 154:28–45.

Barranger-Mathys, M., and David S. Cafiso. 1996. Membrane Structure of Voltage-Gated Channel Forming Peptides by Site-Directed Spin-Labeling. *Biochemistry* 35:498-505.

Bechinger, B., and S.J. Opella. 1991. Flat-coil probe for NMR spectroscopy of oriented membrane samples. *J. Magn. Reson.* 95:585–588.

Bechinger, B. 1997. Structure and Functions of Channel-Forming Polypeptides: Magainins, Cecropins, Melittin and Alamethicin. *J. Membrane Biol.* 156:197-211.

Bechinger, B. 1999. The structure, dynamics and orientation of antimicrobial peptides in membranes by multidimensional solid-state NMR spectroscopy. *Biochim. Biophys. Acta*(1462):157-183.

Bechinger, B., Dmitry A. Skladnev, Andrey Ogrel, Xing Li, Elena V. Rogozhkina, Tatyana V. Ovchinnikova, Joe D. J. O'Neil, and Jan Raap. 2001. ^{15}N and ^{31}P Solid-State NMR Investigations on the Orientation of Zervamicin II and Alamethicin in Phosphatidylcholine Membranes. *Biochemistry* 40:9428-9437.

Bechinger, B., and C. Sizun. 2003. Alignment and Structural Analysis of Membrane

Polypeptides by ^{15}N and ^{31}P solid state NMR Spectroscopy. *Concepts in Magnetics Resonance* 18:130-145.

Bechinger, B., and K. Lohner. 2006. Detergent-like actions of linear amphipathic cationic antimicrobial peptides. *Biochimica et Biophysica Acta* 1758:1529–1539.

Belchorcova, K., J.H. Davis, T.B. Woolf, B. Roux. 1997. Structure and dynamics of an amphiphilic peptide in a lipid bilayer: a molecular dynamics study. *Biophys. J.* 73:3039-3055.

Benedetti, E., A. Bavoso, B. Di Blasio, V. Pavone, C. Pedone, C. Toniolo, and G. M. Bonora. 1982. Peptaibol antibiotics: A study on the helical structures of the 2-9 sequence of emerimicins III and IV. *Proc. Natl. Acad. Sci. USA* 79:7951–7954.

Bloom, M., E. Evans, and O. G. Mouritsen. 1991. Physical properties of the fluid lipid-bilayer component of cell membranes: a perspective. *Q. Rev. Biophys.* 24:293–397.

Boheim, G. 1974. Statistical analysis of alamethicin channels in black lipid membranes. *J. Membrane Biol.* 19:277-303.

Bolin, K.A., and G.L. Millhauser. 1999. α and 3_{10}: the split personality of polypeptide helices. *Acc. Chem. Res.* 32:1027-1033.

Brogden, K.A. 2005. Antimicrobial peptides: pore formers or metabolic inhibitors in bacteria? *Nature Reviews. Microbiology* 3:238-250.

Brumfeld, V., and I. R. Miller. 1990. Electric field dependence of alamethicin channels. *Biochim. Biophys. Acta* 1024:49-53.

Caffrey, M., and G.W. Feigenson. 1981. Fluorescence quenching in model membranes: The relationship between Ca2+-ATPase enzyme activity and the affinity of the protein for phosphatidylcholines with different acyl chain characteristics. *Biochemistry* 20:1949-1961.

Cascio, M., and B. A. Wallace. 1988. Conformation of alamethicin in phospholipid vesicles: implications for insertion models. *Proteins* 4:89-98.

Chen, F.Y., M.T. Lee, H.W. Huang. 2003. Evidence for membrane thinning effect as the mechanism for peptide-induced pore formation. *Biophys. J.* 84:3751–3758.

Chugh, J.K., and B. A. Wallace. 2001. Peptaibols: models for ion channels. *Biochem. Soc. Trans.* 29:565-571.

Ciecierska-Tworek, Z., S. P. Van, and O. H. Griffith. 1973. Electronelectron dipolar splitting anisotropy of a dinitroxide oriented in a crystalline matrix. *J. Mol. Struct.* 16:139-148.

Closs, G.L., M. D. E. Forbes, and P. Piotrowiak. 1992. Spin and reaction dynamics in flexible polymethylene biradicals as studied by EPR, NMR, and optical spectroscopy and magnetic field effects: measurements and mechanisms of scalar electron spin-spin coupling. *J. Am. Chem. Soc.* 114:3285-3294.

Cornell, B.A., F. Separovic, A. J. Baldassi, and R. Smith. 1988. Conformation and orientation of gramicidin A in oriented lipid bilayers measured by solid-state carbon-^{13}C NMR. *Biophys. J.* 53:67–76.

Crisma, M., F. Formaggio, A. Moretto, C. Toniolo. 2006. Peptide Helices Based on α-Amino Acids. *Biopolymers (Peptide Science)* 84:3–12.

Dathe, M., and T. Wieprecht. 1999. Structural features of helical antimicrobial peptides: their potential to modulate activity on model membranes and biological cells. *Biochim. Biophys. Acta* 1462:71–87.

Davis, J.H. 1983. The description of membrane lipid conformation, order and dynamics by ^{2}H-NMR. *Biochim. Biophys. Acta* 737:117–171.

de Planque, M.R.R., D.V. Greathouse, R.E. Koeppe, H. Schäfer, D. Marsh, and J.A. Killian. 1998. Influence of Lipid/Peptide Hydrophobic Mismatch on the Thickness of Diacylphosphatidylcholine Bilayers. A ^{2}H NMR and ESR Study Using Designed Transmembrane R-Helical Peptides and Gramicidin A *Biochemistry* 37:9333-9345.

Dikanov, S.A., and Yu.D. Tsvetkov. 1992. *In* Electron Spin Echo Envelope Modulation (ESEEM) Spectroscopy. CRC Press, Boca Raton FL. 1-412.

Duclohier, H., and H. Wroblewski. 2001. Voltage-dependent pore formation and antimicrobial activity by alamethicin and analogues. *J Membr Biol* 184:1–12.

Dzikovski, B.G., Petr P. Borbat, and Jack H. Freed. 2004. Spin-Labeled Gramicidin A: Channel Formation and Dissociation. *Biophys. J.* 87:3504-3517.

Epand, R.F., R.M. Epand, V. Monaco, S. Stoia, F. Formaggio, M. Crisma, and C. Toniolo. 1999. The antimicrobial peptide trichogin and its interaction with phospholipid membranes. *Eur. J. Biochem.* 266:1021-1028.

Erilov, D.A., R. Bartucci, R. Guzzi, A. A. Shubin, A. G. Maryasov, D. Marsh, S. A. Dzuba, and L. Sportelli. 2005. Water concentration profiles in membranes measured by ESEEM of spin-labeled lipids. *J. Phys. Chem. B.* 109:12003–12013.

Esposito, G., J. A. Carver, J. Boyd, and I. D. Campbell. 1987. High resolution ^{1}H NMR study of the solution structure of alamethicin. *Biochemistry* 26:1043–1050.

Fox, O.R., and M.F. Richard. 1982. A voltage-gated ion channel model inferred from the

crystal structure of alamethicin at 1.5-Å resolution. *Nature* 300:325–330.

Franklin, J.C., J. F. Ellena, S. Jayasinghe, L. P. Kelsh, and D. S. Cafiso. 1994. The structure of micelle associated alamethicin from ^{1}H NMR. Evidence for conformational heterogeneity in a voltage-gated peptide. *Biochemistry* 33:4036-4045.

Frye, J., A.D. Albert, B.S. Selinsky, and Ph.L. Yeagle. 1985. Cross polarization P-31 nuclear magnetic resonance of phospholipids. *Biophys. J.* 48:547-552.

Fu, R., and T.A. Cross. 1999. Solid-State Nuclear Magnetic Resonance Investigation of Protein and Polypeptide Structure. *Annu. Rev. Biophys. Biomol. Struct.* 28:235–268.

Gazit, E., Boman, A., Boman, H. G. and Y. Shai. 1995. Interaction of the mammalian antibacterial peptide cecropin P1 with phospholipid vesicles. *Biochemistry* 34:11479-11488.

Gennis, R.B. 1989. Biomembranes, Molecular Structure and Function. Springer, New York.

Gordon, L.G., and D. A. Haydon. 1972. The unit conductance channel of alamethicin. *Biochim. Biophys. Acta* 255:1014-1018.

Hahn, E.L. 1950. Spin Echoes. *Phys. Rev.* 80:580 - 594.

Hall, J.E., I. Vodyanoy, T. M. Balasubramanian, and G. R. Marshall. 1984. Alamethicin: a rich model for channel behavior. *Biophys. J.* 45:233-247.

Hallock, K.J., D.K. Lee, and A. Ramamoorthy. 2003. MSI-78, an analogue of the magainin antimicrobial peptides, disrupts lipid bilayer structure via positive curvature strain. *Biophys. J.* 84:3052-3060.

Harzer, U., and B. Bechinger. 2000. The alignment of lysine-anchored membrane peptides under conditions of hydrophobic mismatch: A CD, ^{15}N and ^{31}P solid-state NMR spectroscopy investigation. *Biochemistry* 39:13106-13114.

He, K., S.J. Ludtke, D.L.Worcester, H.W. Huang. 1996. Neutron scattering in the plane of membrane: structure of alamethicin pores. *Biophys. J.* 70:2659–2666.

Hicks, A., M. Dinda, and M.A. Singer. 1987. The ripple phase of phosphatidylcholines: effect of chain length and cholesterol. *Biochimica et Biophysica Acta* 903:177-185.

Huang, C., Z.Q. Wang, H.N. Lin, E.E. Brumbaugh, and S. Li. 1994. Interconversion of bilayer phase transition temperatures between phosphatidylethanolamines and phosphatidylcholines. *Biochim. Biophys. Acta* 1189:7-12.

Huang, H.W., Y. Wu. 1991. Lipid-alamethicin interactions influence alamethicin orientation. *Biophys. J.* 60:1079–1087.

Huang, H.W. 2006. Molecular mechanism of antimicrobial peptides: The origin of cooperativity. *Biochim. Biophys. Acta* 1758:1292-1302.

Huster, D., X. Yao, K. Jakes, and M. Hong. 2001. Conformational changes of colicin Ia channel-forming domain upon membrane binding: a solidstate NMR study. *Biochimica et Biophysica Acta* 1561:159-170.

Kaiser, R.D., and E. London. 1998. Determination of the depth of BODIPY probes in model membranes by parallax analysis of fluorescence quenching. *Biochim. Biophys. Acta* 1375:13-22.

Karle, I., and P. Balaram. 1990. Structural characteristics of a-helical peptide molecules containing Aib residues. *Biochemistry* 29:6747-6755.

Kelsh, L.P., J. F. Ellena, and D. S. Cafiso. 1992. Determination of the molecular dynamics of alamethicin using ^{13}C NMR: implications for the mechanism of gating of a voltage-dependent channel. *Biochemistry.* 31:5136 –5144.

Ketchem, R.R., K.-C. Lee, S. Huo, and T.A. Cross. 1996. Macromolecular structural elucidation with solid-state NMR-derived orientational constraints. *Journal of Biomolecular NMR* 8:1-14.

Killian, J.A. 1998. Hydrophobic mismatch between proteins and lipids in membranes. *Biochim. Biophys. Acta* 1376:401–415.

Kim, A., and T.A. Cross. 2004. 2D solid state NMR spectral simulation of 3_{10}, □, and □-helices. *J. Magn. Reson.* 168:187–193.

Kim, Y., Valentine K., Opella S.J., Schendel S.L., Cramer, W.A. 1998. Solid-state NMR studies of membrane-bound closed state of the colicin E1 channel domain in lipid bilayers. *Protein Sci.* 7:342–348.

Koenig, B.W., H.H. Strey, K. Gawrisch. 1997. Membrane lateral compressibility determined by NMR and x-ray diffraction: Effect of acyl chain polyunsaturation. *Biophys. J.* 73:1954-1966.

Koenig, B.W., J. A. Ferretti, and K. Gawrisch. 1999. Site-specific deuterium order parameters and membrane-bound behavior of a peptide fragment from the intracellular domain of HIV-1 gp41. *Biochemistry* 38:6327– 6334.

Korzhnev, D.M., M. Billeter, A.S. Arseniev, V.Y. Orekhov. 2001. NMR studies of Brownian tumbling and internal motions in proteins. *Progress in Nuclear Magnetic Resonance Spectroscopy* 38:197-266.

Kronen, M., Kleinwächter P., Schlegel B, Härtl A, Gräfe U. 2001. Ampullosporins B, C, D, E1, E2, E3 and E4 from Sepedonium ampullosporum HKI-0053: structures and biological activities. *J. Antibiotics* 54:175–178.

Kronen, M., Görls H., Nguyen H.H., Reissmann S., Bohl M., Sühnel J., Gräfe U. 2003. Crystal structure and conformational analysis of ampullosporin A. *J. Pept. Sci.* 9:729–744.

Kropacheva, T.N., E.S. Salnikov, H.-H. Nguyen, S. Reissmann, Z.A. Yakimenko, A.A. Tagaev, T.V. Ovchinnikova, J. Raap. 2005. Membrane association and activity of 15/16-membered peptide antibiotics: Zervamicin IIB, ampullosporin A and antiamoebin I. *Biochim. Biophys. Acta* 1715:6-18.

Kurshev, V.V., and L. Kevan. 1995. Electron spin echo modulation studies of doxylstearic acid spin probes in frozen vesicle solutions: interaction of the spin probe with ^{31}P in the surfactant headgroups. *J. Phys. Chem.* 99:10616-10620.

Lakey, J.H., D. Massotte, F. Heitz, J.L. Dasseux, J.F. Faucon, M.W. Parker, and F. Pattus. 1991. Membrane insertion of the pore-forming domain of colicin A. A spectroscopic study. *European Journal of Biochemistry* 196:599-607.

Lee, D.-K., Yu. Wei, and A. Ramamoorthy. 2001. A Two-Dimensional Magic-Angle Decoupling and Magic-Angle Turning Solid-State NMR Method: An Application to Study Chemical Shift Tensors from Peptides That Are Nonselectively Labeled with ^{15}N Isotope. *J. Phys. Chem. B* 105:4752-4762.

Lee, K.-C., W. Hu, and T. A. Cross. 1993. ^{2}H NMR determination of the global correlation time of the gramicidin channel in a lipid bilayer. *Biophys. J.* 65:1162–1167.

Lee, M., and W. Goldburg. 1965. Nuclear magnetic resonance line narrowing by a rotating RF field. *Phys. Rev.* 140:1261–1271.

Lee, M.T., F.Y. Chen, H.W. Huang. 2004. Energetics of pore formation induced by antimicrobial peptides. *Biochemistry* 43:3590–3599.

Levitt, M.H., D. Suter, and R. R. Ernst. 1986. Spin dynamics and thermodynamics in solid-state nmr cross polarization. *J. Chem. Phys.* 84(8):4243–4255.

Lewis, B.A., and D. M. Engelman. 1983. Lipid bilayer thickness varies linearly with acyl chain length in fluid phosphatidylcholine vesicles. *J. Mol. Biol.* 166:211-217.

Libertini, L.J., and 0. H. Griffith. 1970. Orientation dependence of the electron spin resonance spectrum of di-t-butyl nitroxide. *J. Chem. Phys.* 53:1359-1367.

Likhtenshtein, G.I. 1976. Spin Labeling Methods in Molecular Biology. John Wiley, New

York.

Marassi, F.M., A. Ramamoorthy, and S. J. Opella. 1997. Complete resolution of the solid-stateNMRspectrum of a uniformly ^{15}N-labeled membrane protein in phospholipid bilayers. *Proc. Natl. Acad. Sci. USA* 94:8551–8556.

Marassi, F.M., and S. J. Opella. 1998. NMR structural studies of membrane proteins. *Curr. Opin. Struct. Biol.* 8:640–648.

Marassi, F.M. 2002. NMR of Peptides and Proteins in Oriented Membranes. *Concepts Magn. Reson.* 14:212–224.

Marsh, D., Micha Jost, Cristina Peggion, and Claudio Toniolo. 2007. TOAC Spin Labels in the Backbone of Alamethicin: EPR Studies in Lipid Membranes. *Biophys. J.* 92:473-481.

Matsuzaki, K., O. Murase, N. Fujii, and K. Miyajima. 1996. An antimicrobial peptide, magainin 2, induced rapid flip-flop of phospholipids coupled with pore formation and peptide translocation. *Biochemistry* 35 11361–11368.

Matsuzaki, K. 2001. Molecular mechanisms of membrane perturbation by antimicrobial peptides. *In* Development of Novel Antimicrobial Agents:Emerging Strategies. Lohner K, editor. Horizon Scientific Press, Wymondham. 167-181.

Mazzuca, C., L. Stella, M. Venanzi, F. Formaggio, C. Toniolo and B. Pispisa. 2005. Mechanism of membrane activity of the antibiotic trichogin GA IV: A two-state transition controlled by peptide concentration. *Biophys. J.* 88:3411–3421.

Milov, A.D., D. A. Erilov, E. S. Salnikov, Yu. D. Tsvetkov, F. Formaggio, C. Toniolo, and J. Raap. 2005. Structure and spatial distribution of the spin-labelled lipopeptide trichogin GA IV in a phospholipid membrane studied by pulsed electron-electron resonance (PELDOR). *Phys. Chem. Chem.Phys.* 7:1794-1799.

Milov, A.D., R.I. Samoilova, Yu.D. Tsvetkov, F. Formaggio, C. Toniolo, and J. Raap. 2007. Self-Aggregation of Spin-Labeled Alamethicin in ePC Vesicles Studied by Pulsed Electron-Electron Double Resonance. *J. Am. Chem. Soc.* 129:9260-9261.

Monaco, V., F. Formaggio, M. Crisma, C. Toniolo, P. Hanson, and G.L. Millhauser. 1999a. Orientation and immersion depth of a helical lipopeptaibol in membranes using TOAC as an ESR probe. *Biopolymers* 50:239-253.

Monaco, V., F. Formaggio, M. Crisma, C. Toniolo, P. Hanson, G. Millhauser, C. George, J.R. Deschamps, J.L. Flippen-Anderson. 1999b. Determining the occurrence of a 3_{10}-helix and an α-helix in two different segments of a lipopeptaibol antibiotic using TOAC, a nitroxide spin-labeled C^{α}-tetrasubstituted α-aminoacid.

Bioorganic and Medicinal Chemistry, 7(13):119-131

Nagle, J.F., and S. Tristram-Nagle. 2000. Structure of lipid bilayers. *Biochim. et Biophys. Acta* 1469:159-195.

Nguyen, H.H., D. Imhof, M. Kronen, U. Gräfe, and S. Reissmann. 2003. Circular Dichroism Studies of Ampullosporin-A Analogues. *J. Peptide Sci.* 9:714–728.

North, C.L., J. C. Franklin, R. G. Bryant, and D. S. Cafiso. 1994. Molecular flexibility demonstrated by paramagnetic enhancements of nuclear relaxation. Application to alamethicin: a voltage-gated peptide channel. *Biophys. J.* 67:1861-1866.

Oliynyk, V., Udo Kaatze, and Thomas Heimburg. 2007. Defect formation of lytic peptides in lipid membranes and their influence on the thermodynamic properties of the pore environment. *Biochim. Biophys. Acta* 1768(2):236-245.

Peggion, C., F. Formaggio, M. Crisma, R. F. Epand, R. M. Epand, and C. Toniolo. 2003. Trichogin: a paradigm for lipopeptaibols. *J. Pept. Sci.* 9:679-689.

Peggion, C., I. Coin, C. Toniolo. 2004. Total Synthesis in Solution of Alamethicin F50/5 by an Easily Tunable Segment Condensation Approach. *Biopolymers (Peptide Science)* 76:485–493.

Pispisa, B., L. Stella, M. Venanzi, A. Palleschi, F. Marchiori, A. Polese and C. Toniolo. 2000a. A spectroscopic and molecular mechanics investigation on a series of Aib-based linear peptides and a peptide template, both containing tryptophan and a nitroxide derivatives as probes. *Biopolymers* 53:169-181.

Pispisa, B., L. Stella, M. Venanzi, A. Palleschi, C. Viappiani, A. Polese, F. Formaggio, and C. Toniolo. 2000b. Quenching mechanisms in bichromophoric, 3_{10}-helical Aib-based peptides, modulated by chain-length dependent topologies. *Macromolecules* 33:906-915.

Prongidi-Fix, L., Ph. Bertani, and B. Bechinger. 2007. The Membrane Alignment of Helical Peptides from Non-oriented ^{15}N Chemical Shift Solid-State NMR Spectroscopy. *J. Am. Chem. Soc.* 129:8430-8431.

Rebuffat, S., Goulard, C., Bodo, B., and M. Roquebert. 1999. The peptaibol antibiotics from Trichoderma soil fungi: structural diversity and membrane properties. *Recent Res. Devel. Org. & Bioorg. Chem.* 3:65-91.

Ritzau, M., Heinze S., Dornberger K., Berg A., Fleck W., Schlegel B., Härtl A., Gräfe U. 1997. Ampullosporin, a new peptaibol-type antibiotic from Sepedonium ampullosporum HKI-0053 with neuroleptic activity in mice. . *J. Antibiotics* 50:722–728.

Sackmann, E. 1995. Physics of vesicles. *In* Handbook of Biological Physics. Lipowsy R, and E. Sackmann, editor. Elsevier Science B.V. 210-232.

Salnikov, E.S., D. A. Erilov, A. D. Milov, Yu. D. Tsvetkov, C. Peggion, F. Formaggio, C. Toniolo, J. Raap, and S. A. Dzuba. 2006. Location and Aggregation of the Spin-Labeled Peptide Trichogin GA IV in a Phospholipid Membrane as Revealed by Pulsed EPR. *Biophys. J.* 91:1532-1540.

Sansom, M.S. 1993. Alamethicin and related peptaibols - model ion channels. *Eur. Biophys. J.* 22:105-124.

Schäfer, H., B. Mädler, and F. Volke. 1995. De-PAKE-ing of NMR powder spectra by nonnegative least-squares analysis with Tikhonov regularization. *J. Magn. Reson.* 116:145–149.

Schweiger, A., and G. Jeschke. 2001. Principles of Pulsed EPR. Oxford University Press, Oxford, U.K.

Seelig, A., and J. Seelig. 1974. Dynamic structure of fatty acyl chains in a phospholipid bilayer measured by deuterium magnetic-resonance. *Biochemistry* 13:4839–4845.

Seelig, J., and A. Seelig. 1980. Lipid conformation in model membranes and biological membranes. *Q. Rev. Biophys.* 13:19–61.

Sharon, J.A., Jeffrey F. Ellena, and David S. Cafiso. 1991. Dynamics and aggregation of the peptide ion channel alamethicin. Measurements using spin-labeled peptides. *Biophys. J.* 60:389-398.

Shen, L., D. Bassolino, T. Stouch. 1997. Transmembrane helix structure, dynamics and interactions: multi-nanosecond molecular dynamics simulation. *Biophys. J.* 73:3-20.

Silvius, J.R. 1982. Thermotropic Phase Transitions of Pure Lipids in Model Membranes and Their Modifications by Membrane Proteins. John Wiley and Sons, New York.

Smith, R., F. Separovic, T. J. Miller, A. Whittaker, F. M. Bennett, B. A. Cornell, and A. Makriyannis. 1994. Structure and orientation of the pore-forming peptide, melittin, in lipid bilayers. *J. Mol. Biol.* 241:456–466.

Snook, C.F., Wooley G.A., Oliva G., Pattabhi V., Wood S.P., Blundell T.L., Wallace B.A. 1998. The structure and function of antioamoebin I, a proline-rich membrane-active polypeptide. *Structure* 6:783–792.

Song, Z., F. A. Kovacs, J. Wang, J. K. Denny, S. C. Shekar, J. R. Quine, and T. A. Cross. 2000. Transmembrane domain of M2 protein from influenza A virus studied by solid-state ^{15}N polarization inversion spin exchange at magic angle NMR.

Biophys. J. 79:767–775.

Spyracopoulos, L., A. A. Yee, and J. D. J. O'Neil. 1996. Backbone dynamics of an alamethicin in methanol and aqueous detergent solution determined by heteronuclear ^{1}H-^{15}N NMR spectrsocopy. *Journal of Biomolecular NMR* 7:283-294.

Stankowski, S., and G. Schwarz. 1989. Lipid dependence of peptidemembrane interactions. Bilayer affinity and aggregation of the peptide alamethicin. *FEBS (Fed. Eur. Biochem. Soc.) Lett.* 250:556-560.

Steinhoff, H.-J., Nicole Radzwill, Wilhelm Thevis, Volker Lenz, Dietrich Brandenburg, Alfred Antson, Guy Dodson, and Axel Wollmer. 1997. Determination of Interspin Distances between Spin Labels Attached to Insulin: Comparison of Electron Paramagnetic Resonance Data with the X-Ray Structure. *Biophys. J.* 73:3287-3298.

Stella, L., C. Mazzuca, M. Venanzi, A. Palleschi, M. Didonè, F. Formaggio, C. Toniolo, and B. Pispisa. 2004. Aggregation and water membrane partion as major determinants of the activity of the antibiotic peptide trichogin GA IV. *Biophys. J.* 86:936–945.

Sternin, E., M. Bloom, and A. L. MacKay. 1983. De-PAKE-ing of NMR Spectra. *J. Magn. Reson.* 55:274–282.

Stoll, S., and A. Schweiger. 2006. EasySpin, a comprehensive software package for spectral simulation and analysis in EPR. *J. Magn. Reson.* 178(1):42-55.

Szoka, F.J., and D. Papahadjopoulos. 1980. Comparative properties and methods of preparation of lipid vesicles (liposomes). *Ann. Rev. Bioeng.* 9:468-508.

Tieleman, D.P., M. S. P. Sansom, and H. J. C. Berendsen. 1999. Alamethicin helices in a bilayer and in solution: Molecular dynamics simulations. *Biophys. J.* 74:40-49.

Tieleman, D.P., H. J. C. Berendsen, and M. S. P. Sansom. 2001. Voltage-dependent insertion of alamethicin at phospholipid / water and octane / water interfaces. *Biophys. J.* 80:331-336.

Toniolo, C., M. Crisma, F. Formaggio, C. Peggion, V. Monaco, C. Goulard, S. Rebuffat, and B. Bodo. 1996. Effect of N^{a} -acyl chain length on the membrane-modifying properties of synthetic analogs of the lipopeptaibol trichogin GA IV. *J. Am. Chem. Soc.* 118:4952-4958.

Toniolo, C., M. Crisma, F. Formaggio, C. Peggion, R. F. Epand, and R. M. Epand. 2001. Lipopeptaibols, a novel family of membrane active, antimicrobial peptides. *Cell.*

Mol. Life Sci. 58:1179-1188.

Tristram-Nagle, S., Yu. Liu, J. Legleiter, and J.F. Nagle. 2002. Structure of Gel Phase DMPC Determined by X-Ray Diffraction. *Biophys. J.* 83(6):3324–3335.

Tristram-Nagle, S., and J.F. Nagle. 2004. Lipid bilayers: thermodynamics, structure, fluctuations, and interactions. *Chemistry and Physics of Lipids* 127:3–14.

Venanzi, M., E. Gatto, G. Bocchinfuso, A. Palleschi, L. Stella, F. Formaggio, and C. Toniolo. 2006. Dynamics of formation of a helix-turn-helix structure in a membrane active peptide: a time-resolved spectroscopy study. *ChemBioChem.* 7:43-45.

Vogel, H. 1987. Comparison of the conformation and orientation of alamethicin and melittin in lipid membranes. *Biochemistry* 26:4562-4572.

Wang, X., and Peter J. Quinn. 2002. The interaction of α-tocopherol with bilayers of 1-palmitoyl-2-oleoyl-phosphatidylcholine. *Biochim. Biophys. Acta* 1567:6–12.

Whitmore, L., J.K. Chugh, C.F. Snook, B.A. Wallace. 2003. The peptaibol database: a sequence and structure resource. *J Pept Sci*.

Woolley, G.A., Wallace, B.A. 1992. Model ion channels: gramicidin and alamethicin. *J Membr Biol* 129:109–136.

Woolley, G.A., and B. A. Wallace. 1993. Temperature Dependence of the Interaction of Alamethicin Helices in Membrane. *Biochemistry* 32:9819-9825.

Wu, C.H., A. Ramamoorthy, and S. J. Opella. 1994. High-resolution heteronuclear dipolar solid-state NMR spectroscopy. *J. Magn. Reson. A* 109:270-272.

Yamaguchi, S., Daniel Huster, Alan Waring, Robert I. Lehrer, William Kearney, Brian F. Tack, and Mei Hong. 2001. Orientation and Dynamics of an Antimicrobial Peptide in the Lipid Bilayer by Solid-State NMR Spectroscopy. *Biophys. J.* 81:2203–2214.

Yang, L., T.A. Harroun, T.M. Weiss, L. Ding, and H.W. Huang. 2001. Barrel-stave model or toroidal model? A case study on melittin pores. . *Biophys. J.* 81:1475–1485.

Yee, A.A., and O'Neil, J. D. 1992. Uniform labelling of a fungal peptide:the structure and dynamics of an alamethicin by ^{15}N and ^{1}H NMR spectroscopy. *Biochemistry* 31:3135-3143.

Yee, A.A., K. Marat, and J. D. J. O'Neil. 1997. The interactions with solvent, heat stability, and C-13 labelling of alamethicin, an ion-channel-forming peptide. *Eur. J. Biochem.* 243:283-291.

You, S., S. Peng, L. Lien, J. Breed, M.S.P. Sansom, G.A. Woolley. 1996. Engineering stabilized ion channels: covalent dimers of alamethicin. *Biochemistry* 35(20):6225– 6232.

Zakharov, S.D., J.B. Heymann, Y.L. Zhang, and W.A. Cramer. 1996. Membrane binding of the colicin E1 channel: activity requires an electrostatic interaction of intermediate magnitude. *Biophys. J.* 70:2774-2783.

Publications and Conference Abstracts

Publications:

- E.S. Salnikov, D.A. Erilov, A.D. Milov, Yu.D. Tsvetkov, C. Peggion, F. Formaggio, C. Toniolo, J. Raap, S.A. Dzuba "Location and aggregation of the spin-labeled peptide trichogin GA IV in a phospholipid membrane as revealed by pulsed EPR" ***Biophys. J.,*** **2006**, 91(4) 1532–1540
- S.A. Dzuba, E.S. Salnikov, L.V. Kulik, CW EPR, echo-detected EPR, and field-step ELDOR study of molecular motions of nitroxides in o-terphenyl glass: dynamical transition, dynamical heterogeneity and β relaxation, **Appl. Magn. Reson.**, 30, 637-650 (**2006**).
- S.A. Dzuba, E.P. Kirilina, and E.S. Salnikov, "On the possible manifestation of harmonic-anharmonic dynamical transition in glassy media in electron paramagnetic resonance of nitroxide spin probes"` ***J. Chem. Phys.*** 125, 054502 (**2006**), 5 pages.
- T.N. Kropacheva, E.S. Salnikov, H.-H. Nguyen, S. Reissmann, Z.A. Yakimenko, A.A. Tagaev, T.V. Ovchinnikova, J. Raap, "Membrane association and activity of 15/16-membered peptide antibiotics: Zervamicin IIB, ampullosporin A and antiamoebin I " ***Biochim. Biophys. Acta*** 1715 (**2005**), 6 - 18
- A. D. Milov , D. A. Erilov , E. S. Salnikov , Yu. D. Tsvetkov , F. Formaggio , C. Toniolo and J. Raap "Structure and spatial distribution of the spin-labelled lipopeptide trichogin GA IV in a phospholipid membrane studied by pulsed electron–electron double resonance (PELDOR)" ***Phys. Chem. Chem. Phys.,*** **2005**, 7 (8), 1794 – 1799
- S. A. Dzuba, E. P. Kirilina, E. S. Salnikov, and L. V. Kulik "Restricted orientational motion of nitroxides in molecular glasses: Direct estimation of the motional time scale basing on the comparative study of primary and stimulated electron spin echo decays" ***J. Chem. Phys.*** 122, 094702 (**2005**) (7 pages)
- L.V. Kulik, E.S. Salnikov, S.A. Dzuba, Nuclear spin relaxation in free radicals as revealed in a stimulated electron spin echo experiment, ***Appl. Magn. Reson.*** 28 (**2005**), 1-11.
- L.V. Kulik, I.A. Grigor'ev, E.S. Salnikov, S.A. Dzuba, and Yu.D. Tsvetkov "Electron Spin-Echo Envelope Modulation Induced by Slow Intramolecular Motion" ***J. Phys. Chem. A*** **2003**, 107, 3692-3695

Conference Abstracts:

- Evgeniy S. Salnikov, Philippe Bertani, Burkhard Bechinger "Membrane-modifying Peptides Alamethicin and Ampullosporin A by Solid State NMR of Oriented Samples" Worshop on NMR & Soft Matter/Atelier RMN & Matière Molle – Arcachon, France, June 3-5, **2007**, p.36
- Lydia Prongidi, Christopher Aisenbray, A.James Mason, Evgeniy Salnikov, Claire Gasnier, Antoine Kichler, Gilles Prevost, Marie-Helene Metz-Boutigue and Burkhard Bechinger "A New Family of Peptidic Vectors with Potent Transfection and Antibiotic Activities" International Summer School "Supramolecular Systems in Chemistry and Biology" September 25-29, **2006**, Tuapse, Russia, p. 27
- E.S. Salnikov, P. Bertani, H. Friedrich, S. Reissmann, B. Bechinger, J. Raap **"**Orientation and Dynamics of an Antimicrobial Peptide in the Lipid Bilayer by

Solid-State NMR Spectroscopy**”** International Summer School “Supramolecular Systems in Chemistry and Biology” Seprember 25-29, **2006**, Tuapse, Russia, p. 89

- XVIII symposium ”*Modern Chemical Physics*”, 22 September – 3 October **2006**, Tuapse, Russia. Book of Abstracts (in russian)
- Evgeniy S. Salnikov, Burkhard Bechinger, Jan Raap, Sergey A. Dzuba “Membrane Composition Influences Topology of Membrane-Modifying Peptaibol Alamethicin: Pulsed EPR and Solid State NMR Study” Sendai-Berlin-Novosibirsk 2006, 28-31 August **2006**, Novosibirsk, Russia, p.33
- Evgeniy S. Salnikov, Jan Raap, Yuri D. Tsvetkov, Sergey A. Dzuba “Location of Spin-Labeled Alamethicin in a Model Phospholipid Membrane as Revealed with Electron Spin Echo Envelope Modulation (ESEEM)” The Asia Pacific EPR/ESR Symposium 2006. August 24-27, **2006**. Novosibirsk, Russia, p.149
- Evgeniy S. Salnikov, Denis A. Erilov*, Sergey A. Dzuba, Jan Raap “Location of Spin-Labeled Trichogin GA IV in a Model Phospholipid Membrane as Revealed with Electron Spin Echo Envelope Modulation (ESEEM)” 4th International Conference on Nitroxide Radicals: Synthesis, Properties and Implication of Nitroxides. (SPIN-2005) September 20-24, **2005** Novosibirsk, Russia, p.93
- Vadim K. Khlestkin, Tatyana A. Duda, Evgenii S. Salnikov, Larisa L. Sveshnikova, Olga I Semenova, Sergey A. Dzuba “LB Film of Nitronyl Nitroxide With Long-Chain Alkyl Group” 4th International Conference on Nitroxide Radicals: Synthesis, Properties and Implication of Nitroxides. (SPIN-2005) September 20-24, **2005** Novosibirsk, Russia, p.72
- XV symposium ”*Modern Chemical Physics*”, 18-29 September **2003** , Tuapse, Russia. Book of Abstracts (in russian).
- E. Kirilina, E. Salnikov, S. Dzuba “Orientational molecular motion in glasses by means of pulse EPR: comparison of different glasses” 5th Meeting of the European Federation of EPR Groups Lisbon, 7-11 September **2003**, Portugal.
- Thesis in Books of Abstracts of International Scientific Student’s Conferences “*Student and scientific-technical progress”*, Novosibirsk, Russia, April **2003** (in russian).
- Russian scientific school for young scientists “*New aspects of applied magnetic resonance*”, 20-22 november **2002**, Kazan, Russia. Book of Abstracts (in russian).
- Kulik L.V., Salnikov E.S., Dzuba S.A., Tsvetkov Yu.D. “Stimulated electron spin echo modulation induced by slow methyl group reorientation” VI Voevodsky Conference ‘Physics and Chemistry of Elementary Chemical Processes’ July 21-25, **2002**, Novosibirsk, Russia, p.166.